Universität Stuttgart

technische universiteit eindhoven

Universiteit Utrecht

TU Delft Technische Universiteit Delft

WAGENINGEN UNIVERSITY WAGENINGEN UR

International Research Training Group nupus

“Non-linearities and upscaling in porous media“

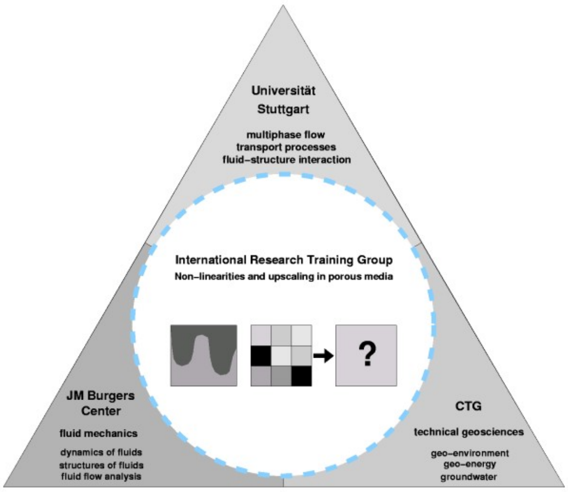

Master Thesis (Diplomarbeit)

Comparison of Mathematical and Numerical Models for Twophase Flow in Porous Media

Markus Wolff

Supervisors:
Bernd Flemisch
Rainer Helmig

Preprint 2008/10

GRK 1398/1 (DFG)
DN 81-754 (NWO)
- Geschäftsstelle -
Pfaffenwaldring 61
70569 Stuttgart

Telefon: 0711/685-60399
Telefax: 0711/685-60430
E-Mail: maria.costa@iws.uni-stuttgart.de
http://www.nupus.uni-stuttgart.de

Abstract

This thesis compares a fully coupled twophase flow formulation and two different kinds of fractional flow formulations. The fully coupled formulation is directly described by two mass balance equations - one equation for each phase. The governing equations of the fractional flow formulations are one saturation equation and one pressure equation. The pressure equation is formulated in terms of a global pressure where the saturation equation shows an advection diffusion form, as well as in terms of a phase pressure where the saturation equation is purely advective. Different numerical schemes are applied for the discretisation of the fully coupled formulation and the discretisation of the fractional flow formulations. The solution behaviour of the numerical models according to the mathematical formulations is investigated concerning accuracy and efficiency. Depending on the physical process, a superior scheme is tried to be determined which can be used for more complex applications. Therefore, different benchmark problems representing different flow characteristics are solved and the results are analysed. It can be shown that in case of a one dimensional problem the best results concerning the accuracy of the approximation can be achieved using the fractional flow approach and the global pressure fractional flow approach, respectively. This applies for advection dominated and diffusion dominated problems as well as for problems combining both processes. Differences concerning the efficiency can be found depending on the nonlinearity introduced by the constitutive relationships used for the relative permeabilities and the capillary pressure. Here, the fully coupled approach shows advantages with increasing nonlinearity. For the considered two dimensional problem the best results can be achieved using the fully coupled approach. The phase pressure fractional flow formulation is expected to combine the possibility to account well for different kinds of transport processes with the advantage of using a phase pressure as physically meaningful quantity. With the numerical schemes applied so far, this can not be approved.

Acknowledgement

We thank the German Research Foundation (DFG) for the funding within the International Research Training Group "Non-Linearities and Upscaling in Porous Media" (NUPUS).

Contents

List of Figures

List of Tables

1 Introduction

Flow and transport processes in porous media are of elementary importance in many fields of research as well as in technical applications. One example of a multiphase porous medium system is the subsurface. Especially in case of a contamination of the ground water, multiphase multicomponent systems have to be considered. To establish optimal remediation strategies the occurring processes have to be well understood. Examples of technical applications dealing with multiphase flow in porous media can be found for example in the automobile industry. One of the latest areas of research in this field is the development of efficient fuel cells.

A good possibility to investigate multiphase flow processes in porous media is the numerical simulation. However, this is still quite difficult. Especially for more complex applications, it is important to find a mathematical as well as a suitable numerical model which describe the appearing processes with sufficient accuracy and efficiency.
There have been two main approaches to model twophase flow in porous media. The first one sets up one balance equation for every phase. The second one combines the two equations of the fluids to yield modified equations which are no longer expressed separately for the phases. Here, the different fluids are accounted for by functions describing the fluid fractions, so-called fractional flow functions.
Investigation and comparison of these formulations has been done for example by *Binning* and *Celia* [2].

The overall aim of this thesis is to compare mathematical and numerical models for two phase flow in porous media. Three alternatives are considered which are

- a standard *fractional flow* formulation with the global pressure and one phase saturation as primary unknowns,
- a modification of the standard *fractional flow* formulation replacing the global pressure by a phase pressure, and
- a *fully coupled* twophase flow formulation where the unknowns are the two phase pressures and the two fluid saturations, respectively. Closure relations, which are also included within the fractional flow formulations, have to be used to reduce the number of unknowns of the *fully coupled* formulation.

For the time discretisation, a standard IMPES (IMplicit Pressure - Explicit Saturation) scheme is used for both *fractional flow* formulations while a fully implicit scheme is employed for the *fully coupled* model.
In space, the saturation equation of the *fractional flow* formulation is discretized by higher order finite volumes with slope limiter and the pressure equation by a usual finite volume method. A finite element-finite volume box scheme is applied for the space discretisation of the *fully coupled* twophase flow formulation.
The emphasis of the study is to test the resulting numerical schemes by means of different benchmark problems. These are:

- the *Buckley-Leverett* problem (1D, advection dominated),
- the *McWhorter problem* (1D, diffusion dominated),
- the *five-spot waterflood* problem (2D, advection dominated), and
- an *advection-diffusion* problem (1D, combining advection and diffusion).

The different mathematical models and numerical schemes are at first described and compared theoretically. Afterwards the numerical experiments are discussed and analysed. Qualitative as well as quantitative differences in the results using the different models are evaluated where the formulations are directly compared with each other and the solution behaviour of the different formulations and models is analysed concerning the influence of different constitutive relationships.

Finally, depending on the dominating processes, a superior scheme is tried to be determined which can be used for more complex applications.

DuMu^x

The numerical experiments are carried out using the software framework **DuMu^x** (**Du**ne for **Mu**lti-{physics, phase, component, scale} Flow in Porous Media). It is based on **DUNE** (**D**istributed and **U**nified **N**umerics **E**nvironment) which is a modular toolbox for solving partial differential equations with grid based methods (see [8]). The underlying idea of DUNE is to create slim interfaces allowing an efficient use of legacy and/or new libraries. Modern C++ programming techniques enable very different implementations of the same concept (i.e. grids, solvers, etc.) using a common interface at a very low overhead [8].

DuMu^x expands DUNE by the additional module dune-mux. For the numerical calculations done in this study, the basic components of DuMu^x which have already been available are used and expanded. As DuMu^x is in the stage of development the performed numerical experiments can also be interpreted as a benchmarking of this simulation tool.

2 Basic Concepts

In nature as well as in technical applications, a multitude of materials can be considered as porous media which consist of a matrix of solid material like soil material in the subsurface (e.g. sand, clay, rock) and void spaces in between which are also called pores. In most cases, it is impossible to describe the detailed geometry of the pore structure. Therefore, a continuum approach in which the microscale properties are averaged over a representative elementary volume (REV) is used in most porous media flow models. Through this averaging process a set of new macroscale parameters like the saturation and the porosity is generated. This chapter consists of some definitions concerning multiphase flow, the porous media approach, and the relationship between multiphase fluid behaviour on the microscale and the macroscale parameters (for more details on the following definitions and concepts it is referred to [6]).

2.1 Definitions

2.1.1 Phases - Wetting and Non-Wetting Fluids

If two or more fluids fill a volume (e.g. the pore volume) and are immiscible and separated by a sharp interface, each fluid is called a phase of the multiphase system. For flow in porous media, formally, the solid matrix can also be considered as a phase. If the solubility between the phases is not negligible a fluid system has to be considered as multiphase - multicomponent system.

Different fluid phases can be divided into wetting and non-wetting phases. Here the important property is the contact angle θ between fluid-fluid interface and solid surface (Fig. 2.1). If the contact angle lies between 0° and 90°, a fluid is called wetting phase. If the contact angle lies between 90° and 180°, a fluid is called non-wetting fluid (Fig. 2.1). In this study water and oil are used as fluids in the calculations, where water is the wetting fluid and oil is the non-wetting fluid.

2.1.2 Porosity

A porous medium consists of a solid matrix and the pores. The ratio of the pore space within the REV and the total volume of the REV is defined as porosity ϕ:

$$\phi = \frac{\text{volume of pore space within the REV}}{\text{total volume of the REV}}. \tag{2.1}$$

To account for the effect that usually not all pores are connected, which can lead to dead-end pores, an effective porosity ϕ_{eff} can be defined:

$$\phi_{eff} = \frac{\text{volume of the pore space available for the flow within the REV}}{\text{total volume of the REV}}. \tag{2.2}$$

In this case only the part of the pore volume is considered which is usable for the flow. Thus, the effective porosity is always equal to or smaller as the porosity defined in Equation (2.1).

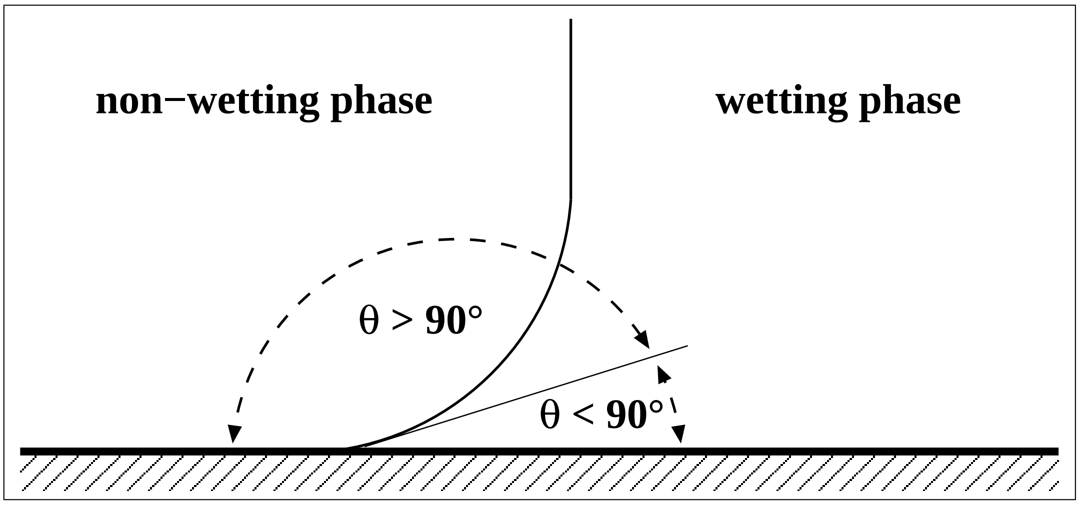

Figure 2.1: Contact angle between a wetting and a non-wetting fluid.

If the solid matrix is assumed to be steady the porosity is constant and independent of temperature, pressure or other variables.

2.1.3 Permeability

When considering flow through porous media, the interaction between a fluid and the solid matrix is essential. In a macroscopic approach these interactions are covered by one parameter, the hydraulic conductivity $\mathbf{K}_f$, which accounts for the influence of fluid viscosity and adhesion at the surface of the solid matrix. The hydraulic conductivity can be defined as

$$\mathbf{K}_f = \mathbf{K}\frac{\rho_f g}{\mu} \qquad \left[\frac{m}{s}\right], \tag{2.3}$$

where ρ_f is the fluid density, μ the fluid viscosity, g the gravity and $\mathbf{K}$ the intrinsic permeability. $\mathbf{K}$ is a tensor characterising the porous medium and is only a function of the solid matrix. In an anisotropic system in which the coordinate system is transfered to coincide the main flow directions, $\mathbf{K}$ is a diagonal n x n matrix with n as the dimension of the considered flow system:

$$\mathbf{K} = \begin{pmatrix} K_{xx} & 0 \\ 0 & K_{yy} \end{pmatrix} \qquad \text{(2-D)}. \tag{2.4}$$

If the porous medium is isotropic the permeability is equal in all directions ($K_{xx} = K_{yy}$).
For a two- or more fluid system the hydraulic conductivity is expanded by the relative permeability $k_{r\alpha}$ of phase α (sec. 2.2.2), which is a dimensionless number assumed to depend on the multiphase fluid and porous medium system:

$$\mathbf{K}_f = k_{r\alpha}\,\mathbf{K}\,\frac{\rho_{f\alpha} g}{\mu_\alpha} \qquad \left[\frac{m}{s}\right], \tag{2.5}$$

where

$$0 \leq \sum_{\alpha=1}^{n_\alpha} k_{r\alpha}(\mathbf{X}_\alpha) \leq 1. \tag{2.6}$$

Here, the vector $\mathbf{X}_\alpha$ represents the parameters $k_{r\alpha}$ is depending on. The product of the relative and the intrinsic permeability $k_{r\alpha}\,\mathbf{K}$ in Equation (2.5) is often called total permeability $\mathbf{K}_{tot}$ or effective permeability $\mathbf{K}_{eff}$.

2.1.4 Saturation

In multiphase flow of immiscible fluids in porous media the pore space is divided and filled by the different phases. In the macroscopic approach this is expressed by the saturation of each phase α. It is defined as the ratio of the volume of phase α within the REV and the volume of the pore space within the REV:

$$S_\alpha = \frac{\text{volume of phase } \alpha \text{ within the REV}}{\text{volume of the pore space within the REV}}. \tag{2.7}$$

Here the pore space of the REV is assumed to be completely filled by the fluid phases α. Thus, the sum of the phase saturations must be equal to one:

$$\sum_\alpha S_\alpha = 1. \tag{2.8}$$

If no phase transition occurs, the saturations change due to displacement of one phase through another phase. Two processes can be distinguished: imbibition and drainage. Usually, the character of the drainage of a porous medium is different to the character of the imbibition. This effect is called hysteresis. Hysteresis occurs due to three main effects. These are are boundary angle hysteresis, ink bottle effect, and residual saturation (details, see [6]). For a wetting phase, a residual saturation occurs if parts of the displaced wetting phase are held back in the finer pore channels during the drainage process which can only be further removed by phase transition. Additionally, fingering may lead to entrapment of certain amounts of displaced fluid. On the other side, a residual saturation for the non-wetting phase may occur if bubbles of the displaced non-wetting phase are trapped by surrounding wetting phase during the imbibition process. Therefore, a residual saturation may depend on the pore geometry, the heterogeneity and the displacement process, but also on the number of drainage and imbibition cycles. If the saturation of a phase S_α is smaller than its residual saturation, the relative permeability (sec. 2.2.2) of phase α is equal to zero which means that no darcy flux can take place. This implies that a darcy flux can only occur, if the saturation of a phase α lies between the residual saturation and one ($S_{\alpha r} \leq S_\alpha \leq 1$). The relative permeability is then a function of the saturation. With the residual saturation an effective saturation for a two phase system can be defined in the following way:

$$S_e = \frac{S_w - S_{wr}}{1 - S_{wr}} \qquad S_{wr} \leq S_w \leq 1. \tag{2.9}$$

Alternatively, in many models the following definition is used:

$$S_e = \frac{S_w - S_{wr}}{1 - S_{wr} - S_{nr}} \qquad S_{wr} \leq S_w \leq 1 - S_{nr}. \tag{2.10}$$

Which definition is used, depends on the capillary pressure and the relative permeability curve, respectively (see Section 2.2.1 and 2.2.2).

2.2 Constitutive Relationships

2.2.1 Capillarity

Due to interfacial tension, forces occur at the interface of two phases. This effect is caused by interactions of the fluids on molecular scale. Therefore, the interface between a wetting and a non-wetting phase is curved and the equilibrium at the interface leads to a pressure difference between the phases called capillary pressure $\mathrm{p_c}$:

$$p_c = p_n - p_w, \tag{2.11}$$

where p_n is the non-wetting phase and p_w the wetting phase pressure. On the microscale, the capillary pressure can be formulated as Laplace equation, depending on the radius of the pore space and the interfacial tension of the different fluid combinations as

$$p_c = \sigma_{12}\left(\frac{1}{r_x} + \frac{1}{r_y}\right) = \frac{4\sigma_{12} cos\,\alpha}{d}, \tag{2.12}$$

with σ representing the interfacial tension, r_x and r_y the main curvature radii, α the boundary angle and d the pore diameter. Equation 2.12 shows that the capillary pressure is higher for smaller diameters corresponding to smaller pores. For porous media saturated with the wetting phase, this implies that the wetting phase retreats to smaller pores during a drainage process. In the case of imbibition the wetting phase penetrates into larger pores, as the capillary pressure decreases with increasing pore diameter (details, see [6]).

In a macroscopic consideration of multiphase systems in porous, media an increase of the non-wetting phase saturation leads to a decrease of the wetting phase saturation, and, according to the microscopic consideration, to the retreat of the wetting fluid to smaller pores. Thus, the macroscopic capillary pressure can be related to the saturation as

$$p_c = p_c(S_w), \tag{2.13}$$

the so-called capillary pressure-saturation relation. The simplest way to define a capillary pressure-saturation function is a linear approach (Fig. 2.2):

$$p_c(S_e(S_w)) = p_{c_{max}}(1 - S_e(S_w)). \tag{2.14}$$

The most common p_c-S_w-relations for a twophase system are those of *Brooks and Corey* and *van Genuchten* (details, see [6]).

In the *Brooks-Corey* model,

$$p_c(S_e(S_w)) = p_d S_e(S_w)^{-\frac{1}{\lambda}} \qquad p_c \leq p_d, \tag{2.15}$$

the capillary pressure is a function of the effective Saturation S_e (sec. 2.1.4). The entry pressure p_d represents the minimum pressure needed for a non-wetting fluid to enter a medium initially saturated by a wetting fluid. The parameter λ is called pore-size distribution index and usually lies between 0.2 and 3.0. A very small λ-parameter describes a single size material, while a very large parameter indicates a highly non-uniform material.

The parameters of the *Brooks-Corey* relation are determined by calibration to experimental data. The effective saturation definition (sec. 2.1.4) which is used in this parameter fitting is also the one to choose for later application of the respective capillary pressure or relative permeability (sec. 2.2.2) function.

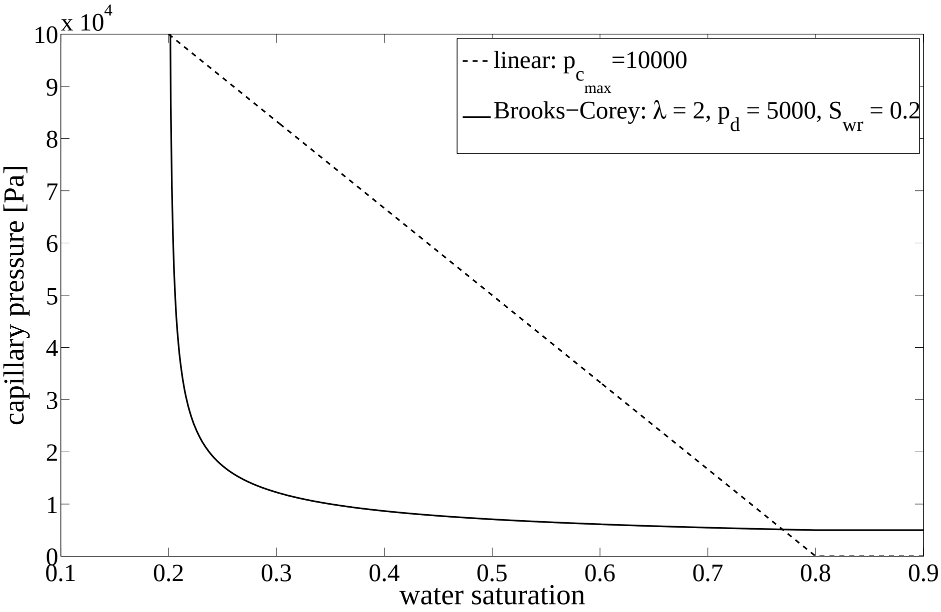

Figure 2.2: Linear p_c-S_w-relations and relation after *Brooks-Corey.*

2.2.2 Relative Permeability

Flow in porous media is strongly influenced by the interaction between the fluid phase and the solid phase. This is taken into account by the concept of a hydraulic conductivity including the intrinsic permeability (sec. 2.1.3). If more than one fluid phase fill the pore space, the presence of one phase also disturbs the flow behaviour of another phase. Therefore, the relative permeability $k_{r\alpha}$ which can be considered as a scaling factor is included into the definition of the hydraulic conductivity (Eq. 2.5).

Considering a two fluid phase system, the space available for one of the fluids depends on the amount of the second fluid within the system. The wetting phase for example has to flow around those parts of the porous media that are filled with non-wetting fluid or has to displace the non-wetting fluid to find new flow paths. In a macroscopic view, this means that the cross-sectional area available for the flow of a phase is depending on its saturation. If the disturbance of the flow of one phase is only due to the restriction of available pore volume caused by the presence of the other fluid, a linear correlation for the relative permeability can be applied (Fig. 2.3):

$$k_{rw}(S_e(S_w)) = S_e(S_w) \tag{2.16}$$

$$k_{rn}(S_e(S_w)) = 1 - S_e(S_w). \tag{2.17}$$

This formulation also implies that the relative permeability becomes zero if the residual saturation, representing the amount of immobile fluid, is reached.

In reality one phase usually not only influences the flow of another phase just by the restriction in available volume, but also by additional interactions between the fluids. If capillary effects occur, the wetting phase, for example, fills the smaller pores if the saturation is small. This means that in case of an increasing saturation of the wetting phase, the relative permeability k_{rw} has to increase slowly if the saturations are still small and it has to increase fast if the

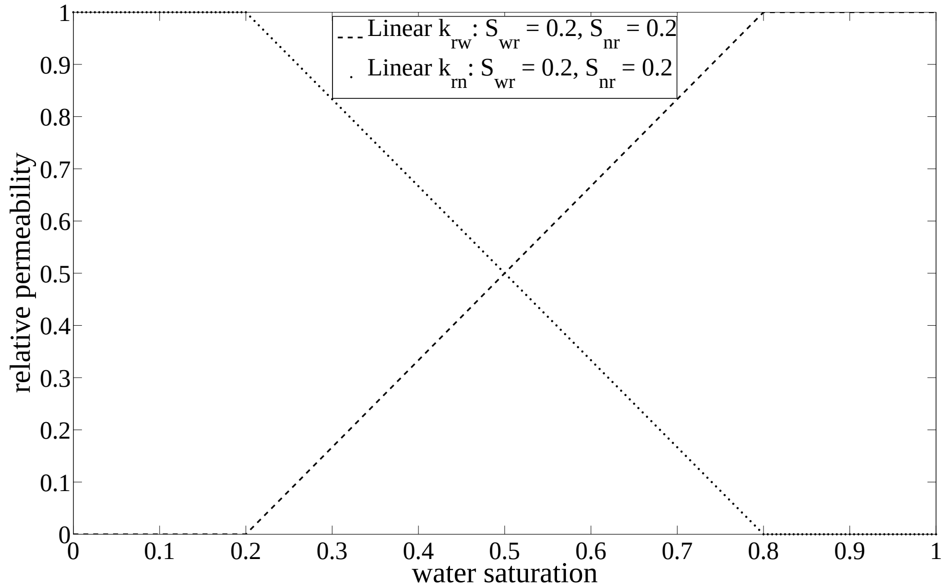

Figure 2.3: Linear k_r-S_w-relation.

saturations become larger. Then the wetting phase begins to fill the larger pores. For the non-wetting phase the opposite situation is the case. Increasing the saturation, the larger pores are filled at first causing a faster rise of k_{rn}. At higher saturations the smaller pores become filled which slows down the increase of the relative permeability. Therefore, correlations for the relative permeabilities can be defined using the known capillary pressure-saturation relationships (details, see [6]). Besides capillary pressure effects also other effects might occure. For two phase flow the *Brooks-Corey* model can be defined as

$$k_{rw}(S_e(S_w)) = S_e(S_w)^{\frac{2+3\lambda}{\lambda}} \tag{2.18}$$

$$k_{rn}(S_e(S_w)) = (1 - S_e(S_w))^2 \left[1 - S_e(S_w)^{\frac{2+\lambda}{\lambda}}\right], \tag{2.19}$$

where λ is the empirical constant from the *Brooks-Corey* $p_c(S)$-relationship (Eq. 2.15).
As can be seen in Figure 2.4 the relative permeabilities after *Brooks-Corey* do not add up to one as for the linear relationship (Fig. 2.3). This is caused by the effects described before and means that one phase is slowed down stronger by the other phase as it would be only due to the restricted volume available for the flow.

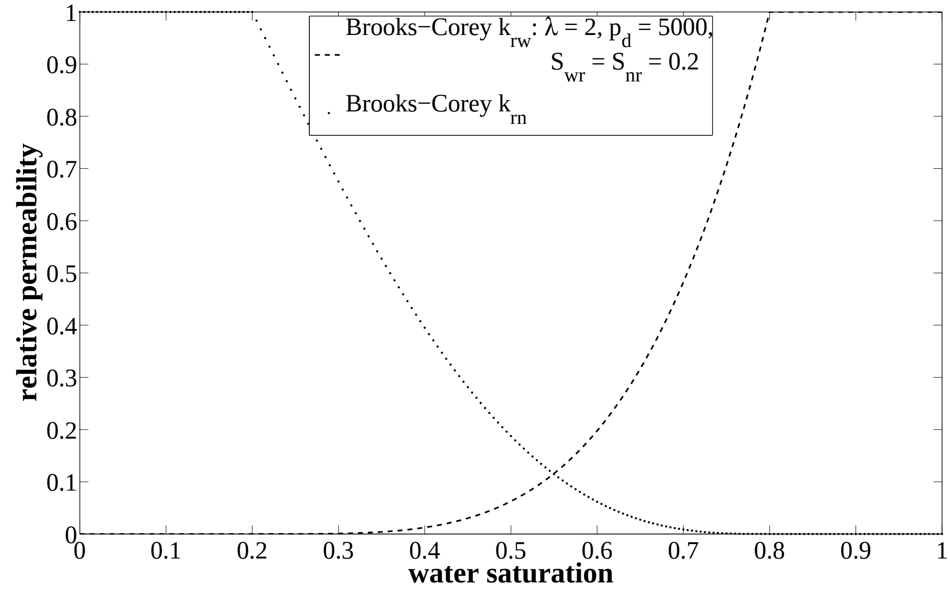

Figure 2.4: k_r-S_w-relation after *Brooks-Corey.*

3 Mathematical Modelling and Discretisation

3.1 Fully Coupled Formulation

Considering flow through porous media, *Darcy*'s law which was originally obtained experimentally for single phase flow can be used as momentum equation in an macroscopic approach. For multiphase systems a generalised *Darcy* law

$$\mathbf{v}_\alpha = -\frac{k_{r_\alpha}}{\mu_\alpha}\mathbf{K}(\nabla p_\alpha - \rho_\alpha \mathbf{g}) \tag{3.1}$$

can be formulated for each phase (details, see [6], [10]), where k_{r_α} is the relative permeability, μ_α the dynamic fluid viscosity, p_α the pressure and ρ_α the density of phase α, and $\mathbf{g}$ is the gravity vector, acting in vertical direction. It further appears that the conductivity of a phase $\mathbf{K}_\alpha$ is the fluid independent intrinsic permeability $\mathbf{K}$ scaled with the relative permeability of the phase k_{r_α} which depends on the saturation of the present phases (Ch. 2.2.2). The mobility of a phase can then be defined as $\lambda_\alpha = \frac{k_{r_\alpha}}{\mu_\alpha}$.
Inserting the generalised *Darcy* law (Eq. 3.1) into the mass balance equation for phase α of a multiphase system, namely,

$$\frac{\partial(\phi\rho_\alpha S_\alpha)}{\partial t} + \nabla\cdot(\rho_\alpha \mathbf{v}_\alpha) - \rho_\alpha q_\alpha = 0 \tag{3.2}$$

leads to the general form of the multiphase flow equation

$$\frac{\partial(\phi\rho_\alpha S_\alpha)}{\partial t} - \nabla\cdot(\rho_\alpha\lambda_\alpha\mathbf{K}(\nabla p_\alpha - \rho_\alpha\mathbf{g})) - \rho_\alpha q_\alpha = 0, \tag{3.3}$$

with the porosity ϕ, the saturation of phase alpha S_α and the source/sink term q_α. The supplementary constraints to close the system of equations are

$$\sum_{\alpha=1}^{n_{phase}} S_\alpha = 1 \tag{3.4}$$

and

$$p_{c\psi\alpha} = p_\psi - p_\alpha, \qquad \alpha \neq \psi, \tag{3.5}$$

where $p_{c\psi\alpha}$ is the capillary pressure between phase ψ and phase α depending on the saturations (Ch. 2.2.1).
Combination of Equations (3.3), (3.4) and (3.5) for a two phase system then yields the *fully coupled* twophase flow formulation. For a pressure-saturation formulation using the wetting phase pressure p_w and the non-wetting saturation S_n as primary variables, the following system of equations is obtained:

$$L_w(p_w, S_n) := -\frac{\partial(\phi\rho_w S_n)}{\partial t} - \nabla\cdot(\rho_w\lambda_w\mathbf{K}(\nabla p_w - \rho_w\mathbf{g})) - \rho_w q_w = 0, \tag{3.6}$$

$$L_n(p_w, S_n) := \frac{\partial(\phi\rho_n S_n)}{\partial t} - \nabla\cdot(\rho_n\lambda_n\mathbf{K}(\nabla p_w + \nabla p_c - \rho_n\mathbf{g})) - \rho_n q_n = 0. \tag{3.7}$$

Similarly, a p_n-S_w formulation can be derived:

$$L_w(p_n, S_w) := \frac{\partial(\phi\rho_w S_w)}{\partial t} - \nabla\cdot(\rho_w\lambda_w\mathbf{K}(\nabla p_n - \nabla p_c - \rho_w\mathbf{g})) - \rho_w q_w = 0, \tag{3.8}$$

$$L_n(p_n, S_w) := -\frac{\partial(\phi\rho_n S_w)}{\partial t} - \nabla\cdot(\rho_n\lambda_n\mathbf{K}(\nabla p_n - \rho_n\mathbf{g})) - \rho_n q_n = 0. \tag{3.9}$$

The single equations of these systems of equations (Eq. (3.6), (3.7) and (3.8), (3.9)) are strongly coupled and parabolic. Furthermore, the behaviour of the equations is highly nonlinear because of the nonlinear relationship between capillary pressure and saturation on the one hand and relative permeability and saturation on the other hand (Ch. 2.2.1 and 2.2.2). Capillary effects are explicitly included in the system of equations. Therefore, it can also be applied if sub-domains of small pressure gradients occur. Because of the strong coupling of the equations, a fully coupled formulation should be solved simultaneously. Corresponding numerical schemes are discussed later in Sections 3.3 and 3.4.

3.2 Fractional Flow Formulation

The *fractional flow* formulation of a multiphase system decouples the system of equations of a *fully coupled* system (Eq. (3.6), (3.7) or (3.8), (3.9)) into one pressure equation and one saturation equation. This weakly coupled equations can then be solved separately, in such a way that the results of the pressure equation are used to solve the transport equation for the saturation.

3.2.1 Pressure Equation

The pressure equation can be derived by addition of the phase mass balance equations of a multiphase system. Division of equation (3.2) through ρ_α and addition for all phases α leads to the equation:

$$\sum_\alpha S_\alpha \frac{\partial\phi}{\partial t} + \sum_\alpha \left[\frac{1}{\rho_\alpha}\left(\phi S_\alpha \frac{\partial\rho_\alpha}{\partial t} + \rho_\alpha\phi\frac{\partial S_\alpha}{\partial t} + \nabla\cdot(\mathbf{v}_\alpha\rho_\alpha) - \rho_\alpha q_\alpha\right)\right] = 0. \tag{3.10}$$

Inserting Equation (3.4) into Equation (3.10) and rewriting the term $\nabla(\mathbf{v}_\alpha\rho_\alpha)$ yields the general pressure equation:

$$\frac{\partial\phi}{\partial t} + \sum_\alpha \nabla\cdot\mathbf{v}_\alpha + \sum_\alpha \left[\frac{1}{\rho_\alpha}\left(\phi S_\alpha\frac{\partial\rho_\alpha}{\partial t} + \mathbf{v}_\alpha\nabla\rho_\alpha\right)\right] - \sum_\alpha q_\alpha = 0. \tag{3.11}$$

A detailed derivation of the pressure equation can be found in Appendix A. Furthermore, a total velocity v_t is introduced, where

$$\mathbf{v}_t = \sum_\alpha \mathbf{v}_\alpha \tag{3.12}$$

and

$$\nabla\cdot\mathbf{v}_t = \nabla\cdot\sum_\alpha\mathbf{v}_\alpha = \sum_\alpha\nabla\cdot\mathbf{v}_\alpha. \tag{3.13}$$

Now, the generalised *Darcy* law (Eq. 3.1) can be inserted into Equation (3.12) resulting in

$$\mathbf{v}_t = -\mathbf{K} \sum_\alpha (\lambda_\alpha \nabla p_\alpha - \lambda_\alpha \rho_\alpha \mathbf{g}). \tag{3.14}$$

If a total mobility $\lambda_t = \sum_\alpha \lambda_\alpha$ and the fractional flow function $f_\alpha = \frac{\lambda_\alpha}{\lambda_t}$ is introduced, a relation for the total velocity $\mathbf{v_t}$ with a form similar to the form of the *Darcy* law can be formulated as

$$\mathbf{v}_t = -\lambda_t \mathbf{K} \left(\sum_\alpha f_\alpha \nabla p_\alpha - \sum_\alpha f_\alpha \rho_\alpha \mathbf{g} \right). \tag{3.15}$$

Global Pressure Fractional Flow Formulation

Defining a global pressure $\bar{p}$, such that $\nabla \bar{p} = \sum_\alpha f_\alpha \nabla p_\alpha$, Equation (3.15) can be rewritten as a function of $\bar{p}$:

$$\mathbf{v}_t = -\lambda_t \mathbf{K} \left(\nabla \bar{p} - \sum_\alpha f_\alpha \rho_\alpha \mathbf{g} \right). \tag{3.16}$$

The pressure equation of the *global pressure fractional flow* formulation can then be formulated by inserting Equations (3.13) and (3.16) into Equation (3.11). For a twophase system of one wetting phase and one non-wetting phase, in which both phases are assumed to be incompressible and the porosity ϕ to be constant, this leads to:

$$\nabla \cdot \mathbf{v}_t - \sum_\alpha q_\alpha = -\nabla \cdot \left[\lambda_t \mathbf{K} \left(\nabla \bar{p} - \sum_\alpha f_\alpha \rho_\alpha \mathbf{g} \right) \right] - \sum_\alpha q_\alpha = 0, \qquad \alpha = n, w. \tag{3.17}$$

To point out one consequence of applying this approach compared to the alternative approach described later the corresponding boundary conditions are looked at. Accordingly, for a domain Ω with boundary $\Gamma = \Gamma_D \cup \Gamma_N$, where Γ_D denotes a *Dirichlet* and Γ_N a *Neumann* boundary, the boundary conditions are

$$\begin{aligned} \bar{p} &= p_D \quad \text{on} \quad \Gamma_D \qquad \text{and} \\ \mathbf{v}_t \cdot \mathbf{n} &= v_N \quad \text{on} \quad \Gamma_N. \end{aligned} \tag{3.18}$$

Considering the global pressure, the definition of the capillary pressure between two phases (Ch. 2.2.1) yields $\bar{p} = p_w = p_n$, if the capillary pressure between the phases is neglected like for the *Buckley-Leverett* problem (Ch. 4.1) or for the *five-spot waterflood* problem (Ch. 4.2).

Phase Pressure Fractional Flow Formulation

Compared to the global pressure formulation described above in which a global pressure $\bar{p}$ is used, the pressure equation can also be derived using a phase pressure p_α which is a physically more meaningful parameter in a multiphase system. Investigation of a *phase pressure fractional flow* formulation has been done for example by *Hoteit* and *Firoozabadi* [7]. Inserting Equation (3.5) into Equation (3.15) and considering a two phase system of one wetting phase and one non-wetting phase, Equation (3.15) can be rewritten in terms of the wetting phase pressure:

$$\mathbf{v}_t = -\lambda_t \mathbf{K} \left(\nabla p_w + f_n \nabla p_c - (f_w \rho_w + f_n \rho_n) \mathbf{g} \right). \tag{3.19}$$

Substituting $\mathbf{v}_t$ in the general pressure equation (Eq. 3.11) by Equation (3.19) and assuming both fluids to be incompressible and the porosity to be constant leads to:

$$\nabla \cdot \mathbf{v}_t - \sum_\alpha q_\alpha = -\nabla \cdot \left[\lambda_t \mathbf{K} \left(\nabla p_w + f_n \nabla p_c - \sum_\alpha f_\alpha \rho_\alpha \mathbf{g}\right)\right] - \sum_\alpha q_\alpha = 0, \qquad \alpha = n, w. \tag{3.20}$$

The boundary conditions can be formulated in analogy to the global pressure formulation but using the phase pressure on the *Dirichlet* boundary:

$$\begin{aligned} p_w &= p_D \quad \text{on} \quad \Gamma_D \qquad \text{and} \\ \mathbf{v}_t \cdot \mathbf{n} &= v_N \quad \text{on} \quad \Gamma_N. \end{aligned} \tag{3.21}$$

Similarly, a pressure equation for the non-wetting phase pressure can be formulated:

$$\nabla \cdot \mathbf{v}_t - \sum_\alpha q_\alpha = -\nabla \cdot \left[\lambda_t \mathbf{K} \left(\nabla p_n - f_w \nabla p_c - \sum_\alpha f_\alpha \rho_\alpha \mathbf{g}\right)\right] - \sum_\alpha q_\alpha = 0, \qquad \alpha = n, w. \tag{3.22}$$

Once p_w and p_n are known, the corresponding phase velocities can be calculated using the generalised *Darcy* law (Eq. 3.1). Alternatively, a modified phase velocity $\mathbf{v}_{\alpha_{mod}}$ can be introduced and calculated as

$$\mathbf{v}_{\alpha_{mod}} = -\lambda_t \mathbf{K}(\nabla p_\alpha - \rho_\alpha g) = \frac{\mathbf{v}_\alpha}{f_\alpha}. \tag{3.23}$$

This modified phase velocity including the total mobility λ_t shows a similar form as the total velocity (Eq. 3.16) which can give an advantage in the numerical application (see Section 3.4).

3.2.2 Saturation Equation

As mentioned above, the solution of the pressure equation yielding the velocity is required before solving the equation for the saturation. Obviously, for the phase pressure formulation of the pressure equation the saturation can then be calculated directly from the general balance equation (Eq. 3.2). For the wetting phase of a twophase system with one wetting phase and one non-wetting phase in which both phases are assumed to be incompressible and the porosity ϕ to be constant this equation simplifies to

$$\phi \frac{\partial S_w}{\partial t} + \nabla \cdot (\mathbf{v}_w) - q_w = 0 \tag{3.24}$$

or alternatively to

$$\phi \frac{\partial S_w}{\partial t} + \nabla \cdot (f_w \mathbf{v}_{w_{mod}}) - q_w = 0. \tag{3.25}$$

Formally, Equations (3.24) and (3.25) are equal, but because of numerical reasons it can be an advantage to use Equation (3.25) with the modified phase velocity $\mathbf{v}_{w_{mod}}$ instead of Equation (3.24) with the phase velocity $\mathbf{v}_w$ (see Section 3.4). For the global pressure formulation of the pressure equation yielding the total velocity $\mathbf{v}_t$ but not the phase velocity a special transport equation for saturation has to be derived. Certainly, this saturation equation can also be applied to the alternative approach of the pressure equation.

The saturation equation of the *global pressure fractional flow* formulation like the pressure equation can be derived from the general multiphase mass balance equation (Eq. 3.2). Considering a two-phase system, *Darcy*'s law for a wetting and a non-wetting phase can be formulated by using Equation (3.1) combined with Equation (3.5) as

$$\mathbf{v}_w = -\lambda_w \mathbf{K}(\nabla p_w - \rho_w \mathbf{g}) \tag{3.26}$$

and

$$\mathbf{v}_n = -\lambda_n \mathbf{K}(\nabla p_w + \nabla p_c - \rho_w \mathbf{g}). \tag{3.27}$$

If Equation (3.27) is solved for $\mathbf{K}\nabla p_w$ and inserted into Equation (3.26), this yields the *fractional flow* equation for $\mathbf{v}_w$:

$$\mathbf{v}_w = \frac{\lambda_w}{\lambda_n}\mathbf{v}_n + \lambda_w \mathbf{K}[\nabla p_c + (\rho_w - \rho_n)\mathbf{g}]. \tag{3.28}$$

Equation (3.12) yields $\mathbf{v}_n = \mathbf{v}_t - \mathbf{v}_w$, and with Equation (3.28) this leads to the *fractional flow* equation:

$$\mathbf{v}_w = \frac{\lambda_w}{\lambda_w + \lambda_n}\mathbf{v}_t + \frac{\lambda_w \lambda_n}{\lambda_w + \lambda_n}\mathbf{K}[\nabla p_c + (\rho_w - \rho_n)\mathbf{g}], \tag{3.29}$$

which can be further inserted into the wetting phase mass balance equation

$$\frac{\partial(\phi \rho_n S_w)}{\partial t} + \nabla \cdot (\rho_w \mathbf{v_w}) - \rho_w q_w = 0. \tag{3.30}$$

With the *fractional flow* function

$$f_w = \frac{\lambda_w}{\lambda_w + \lambda_n}, \qquad \text{and} \qquad \bar{\lambda} = \frac{\lambda_w \lambda_n}{\lambda_w + \lambda_n}$$

the resulting equation is

$$\frac{\partial(\phi \rho_w S_w)}{\partial t} + \nabla \cdot [\rho_w (f_w \mathbf{v}_t + \bar{\lambda}\mathbf{K}(\nabla p_c + (\rho_w - \rho_n)\mathbf{g}))] - \rho_w q_w = 0. \tag{3.31}$$

Some terms of Equation (3.31) can be reformulated in dependence on the saturation (details, see [6]). Applying these reformulations and assuming incompressible fluids for both phases and a constant porosity, the saturation equation of a two-phase system can finally be formulated as

$$\begin{aligned} L(S_w) := \nabla \cdot &\left[\bar{\lambda}\mathbf{K}\frac{d\,p_c}{d\,S_w}\nabla S_w\right] \\ &+ \left[\mathbf{v}_t \frac{d\,f_w}{d\,S_w} + (\rho_w \mathbf{g} - \rho_n \mathbf{g})\mathbf{K}\frac{d\,\bar{\lambda}}{d\,S_w}\right]\nabla S_w \\ &+ \phi\frac{\partial S_w}{\partial t} - q_w + f_w q_t = 0, \end{aligned} \tag{3.32}$$

where $q_t = q_w + q_n$.

Considering the two equations of the *global pressure fractional flow* formulation (pressure equation and saturation equation), it becomes clear now that they are only weakly coupled through the presence of the total mobility and the fractional flow functions in the pressure equation which means through the relative permeabilities. This also holds for the *phase pressure fractional flow* formulation. However, in this formulation the coupling is strengthened again due to an additional capillary pressure term in the pressure equation. The strong nonlinearity of the *global pressure fractional flow* formulation occurs due to the use of the global pressure $\bar{p}$ which includes both phase pressures and capillary pressure effects and is therefore directly dependent on the saturation. Additionally, the total mobility and the fractional flow functions are nonlinear dependent on the saturation. Applying the *phase pressure fractional flow* formulation this nonlinearity is weakened as the phase pressure is only indirectly depending on the saturation. Comparing Equations (3.24) and (3.25) to Equations (3.31) and (3.32) shows that for the phase pressure formulation the saturation equation consists only of an accumulation term and an advective term, whereas for the global pressure formulation using a global pressure an additional diffusive term occurs. This shows that in contrast to the *global pressure fractional flow* formulation, the *phase pressure fractional flow* formulation strictly separates diffusive and advective processes where the pressure equation represents the diffusive part and the saturation equation the advective part.

3.3 Numerical Methods and Discretisation of the Fully Coupled Formulation

The *fully coupled* multiphase flow formulation explained in Section 3.1 yields a system of equations with one equation for every phase in which the single equations are highly coupled with each other. In consequence all equations (two for two phase flow) have to be solved simultaneously. Therefore, the system of equations is rewritten in the following form and solved implicitly (details, see [1] or [6]):

$$\frac{\partial}{\partial t}\mathbf{M}(\mathbf{p}_\alpha(t), \mathbf{S}_\alpha(t)) + \mathbf{A}(\mathbf{p}_\alpha(t), \mathbf{S}_\alpha(t)) = \mathbf{R}(t), \tag{3.33}$$

where again α is the index of the phase. $\mathbf{M}$ is called mass matrix and includes the accumulation terms, $\mathbf{A}$ is called coefficient matrix and includes the internal flux terms and $\mathbf{R}$ is the right hand vector which comprises *Neumann* boundary flux terms and source terms.

Furthermore, the fully coupled formulation is non-linear depending on the capillary pressure and relative permeability relationship. For this reason, *Newton-Raphson* iterative solver is used (details, see [6]).

In the problems considered in Chapter 4 of this work, gravity effects are neglected. Therefore, terms containing gravity forces are not taken into account in the following description of the discretisation as they vanish in the application of the problems. Furthermore source and sink terms are not considered.

3.3.1 Space Discretisation

A fully upwind finite-element-finite-volume-box-method (box method) is used to discretise the fully coupled twophase flow equations in space. In this method the model domain is discretized by a finite element mesh at first. Then for each node i of the finite element mesh a control volume (box) B_i with corners at the edge midpoints and on the centres of gravity of the elements surrounding i is chosen (Fig. 3.1), building a secondary finite volume mesh. To establish the box approach, Equation (3.3) (gravity, sources/sinks neglected) is multiplied

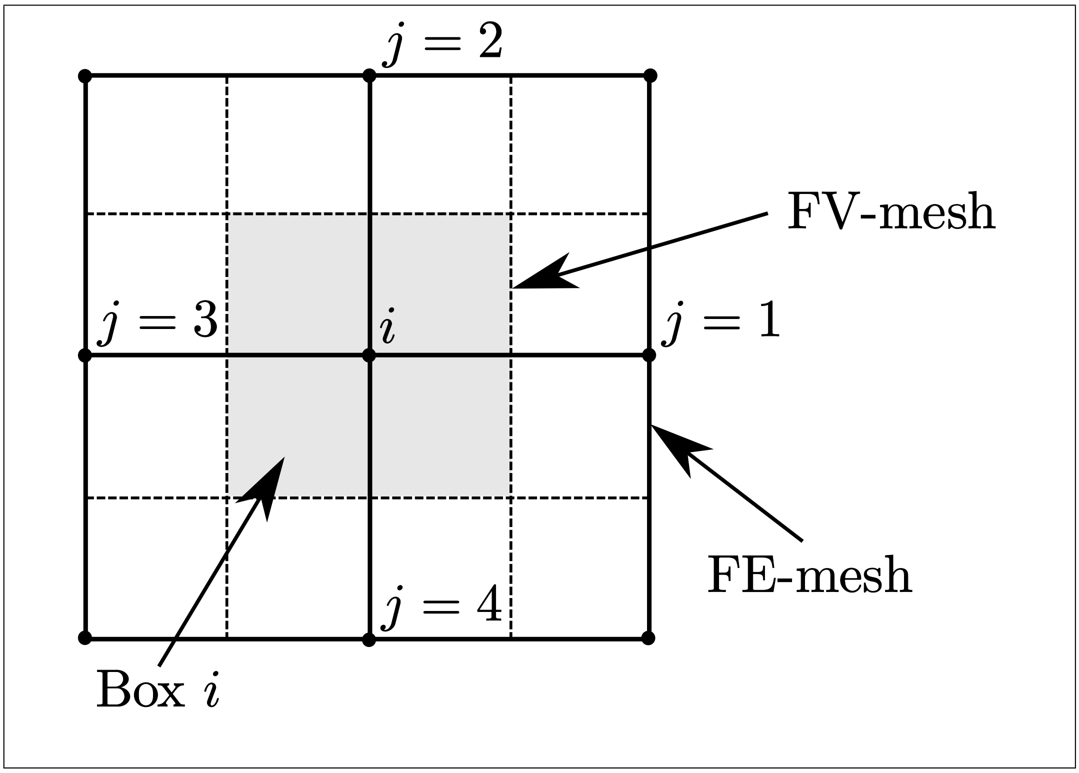

Figure 3.1: Finite Element mesh and Finite Volume mesh of a FE-box-method.

with a weight function W and integrated over the model domain by integration over each finite volume box of the secondary mesh:

$$\int\limits_{FV-Box} W\,\frac{\partial(\phi\rho_\alpha S_\alpha)}{\partial t}\,dB - \int\limits_{FV-Box} W\,\nabla\cdot(\rho_\alpha\lambda_\alpha\mathbf{K}(\nabla p_\alpha))\,dB = 0, \tag{3.34}$$

with $\alpha = w, n$. The unknowns can further be approximated within the model domain as

$$p_\alpha = \sum_i N_i\hat{p}_{\alpha i} \qquad S_\alpha = \sum_i N_i\hat{S}_{\alpha i}, \tag{3.35}$$

where $\hat{p}_{\alpha i}$ and $\hat{S}_{\alpha i}$ are the discrete values at the nodes of the finite element mesh, and N_i is the shape function dedicated to node i. N_i is the usual C^0 finite element polynomial with the value of 1 at node i and 0 at all other nodes. Inserting the finite element approximation for the unknowns and applying the *Green-Gauss* theorem leads to the following equation:

$$\begin{aligned}\frac{\partial(\phi\rho_{\alpha i}\hat{S}_{\alpha i})}{\partial t}\int\limits_{B_i} W_i N_i\,dB + \sum_j(\hat{p}_{\alpha j}-\hat{p}_{\alpha i})\int\limits_{B_i}(\nabla W_i)\rho_{\alpha i}\lambda_\alpha\mathbf{K}\nabla N_j\,dB \\ - \sum_j(\hat{p}_{\alpha j}-\hat{p}_{\alpha i})\oint\limits_{\Gamma_{B_i}} W_i\,\rho_{\alpha ij}\lambda_{\alpha ij}\mathbf{K}\nabla N_j\mathbf{n}\,d\Gamma_B = 0.\end{aligned} \tag{3.36}$$

Here, B denotes the box, Γ_B the boundary of the box and j the neighbour nodes of node i. $\lambda_{\alpha ij}$ is the mobility and $\rho_{\alpha ij}$ the density at interface between box i and j. Each box represents a subdomain of the whole region of interest. Therefore, the weight functions W_i are now chosen according to the subdomain collocation method as:

$$W_i(\mathbf{x}) = \begin{cases} 1 & \text{if } \mathbf{x} \in B_i \\ 0 & \text{otherwise} \end{cases} \tag{3.37}$$

This method forces the average of the residual over each subdomain to be equal to zero which means in a physical kind of view that local mass conservation is enforced. This can also be seen applying this choice of the weight functions to Equation (3.36) which gives

$$\frac{\partial(\phi \rho_{\alpha i} \hat{S}_{\alpha i})}{\partial t} \int\limits_{B_i} N_i \, dB - \sum_j (\hat{p}_{\alpha j} - \hat{p}_{\alpha i}) \oint\limits_{\Gamma_{B_i}} \rho_{\alpha ij} \lambda_{\alpha ij} \mathbf{K} \nabla N_j \mathbf{n} \, d\Gamma_B = 0. \tag{3.38}$$

As the derivatives of the weight functions are always zero now, the volume integral on the right hand side of Equation (3.36) vanishes. Comparable to an usual finite volume method, the fluxes over the interfaces of the boxes are directly balanced. With

$$\int\limits_{B_i} N_i \, dB = V_i = \text{volume of box } i$$

and the stiffness matrix

$$\gamma_{\alpha ij} = \oint\limits_{\Gamma_{B_i} \notin \Gamma_{N,\alpha}} \mathbf{K} \nabla N_j \mathbf{n} \, d\Gamma_B,$$

where $\Gamma_{N,\alpha}$ denotes a *Neumann* boundary dedicated to phase α, together with the supplementary Equations (3.4) and (3.5) a *p-S* formulation is finally discretized in space as:

$$(-1)^{\delta_{\alpha w}} \frac{\partial(\phi \rho_{\alpha i} \hat{S}_{\alpha i})}{\partial t} V_i - \left[\sum_j (\hat{p}_{\alpha j} - \hat{p}_{\alpha i}) - \delta_{\alpha n} \sum_j (\hat{p}_{cj} - \hat{p}_{ci}) \right] \rho_{\alpha ij} \lambda_{\alpha ij} \gamma_{\alpha ij} - m_{\alpha i} = 0. \tag{3.39}$$

Here, $m_{\alpha i}$ is the term including the *Neumann* boundary conditions and $\delta_{\alpha k}$ is the Kronecker delta. Since a fully upwind scheme is used, the mobility at the box interface $\lambda_{\alpha ij}$ is determined in the following way:

$$\lambda_{\alpha ij} = \begin{cases} \lambda_{\alpha i} & \text{if} \quad (\hat{p}_{\alpha j} - \hat{p}_{\alpha i}) - \delta_{\alpha n}(\hat{p}_{cj} - \hat{p}_{ci}) \geq 0 \\ \lambda_{\alpha j} & \text{if} \quad (\hat{p}_{\alpha j} - \hat{p}_{\alpha i}) - \delta_{\alpha n}(\hat{p}_{cj} - \hat{p}_{ci}) \leq 0. \end{cases} \tag{3.40}$$

3.3.2 Time Discretisation

The time discretisation of the *fully coupled* multiphase flow formulation is done applying the implicit *Euler* method. For an unknown u a general form of this method can be formulated as:

$$u^{k+1} = u^k + \Delta t \, f(u^{k+1}), \tag{3.41}$$

where k is the index of the time step. Using Equation (3.41) together with Equation (3.33) leads to:

$$\mathbf{S}_\alpha^{k+1} = \mathbf{S}_\alpha^k + (\mathbf{M}(\mathbf{p}_\alpha^{k+1}))^{-1} (\mathbf{A}(\mathbf{p}_\alpha^{k+1}, \mathbf{S}_\alpha^{k+1}) - \mathbf{R}^{k+1}). \tag{3.42}$$

Following this general form of a time discretisation of a twophase flow system in porous media, Equation (3.39) can finally be written in a completely discretized form as:

$$\hat{S}_{\alpha i}^{k+1} = \hat{S}_{\alpha i}^{k} - (-1)^{\delta_{\alpha w}} \frac{\Delta t}{\phi V_i} \left[\sum_j (\hat{p}_{\alpha j}^{k+1} - \hat{p}_{\alpha i}^{k+1}) - \delta_{\alpha n} \sum_j (\hat{p}_{cj}^{k+1} - \hat{p}_{ci}^{k+1}) \right] \lambda_{\alpha ij}^{k+1} \gamma_{\alpha ij}, \tag{3.43}$$

where V_i and $\gamma_{\alpha ij}$ are time independent as long as the finite element mesh and the form of the shape functions do not change with time. This is the case if no adaptive methods are used. The porosity ϕ is assumed to be independent of pressure and time. Furthermore, the fluids are assumed to be incompressible which implies that the density ρ is only a function of the temperature. If the temperature is assumed to be constant over time and space as it is done here, ρ is also not depending on time and the position within the domain (for more details on the described discretisation techniques it is referred to [1] and [6]).

3.4 Numerical Methods and Discretisation of the Fractional Flow Formulation

As derived before in Section 3.2, the *fractional flow* formulation decouples the system of equations of a multiphase flow formulation into a pressure equation and a saturation equation. Numerically, this is usually done by using the IMPES scheme (IMplicit Pressure - Explicit Saturation). Therefore, the implicitly formulated pressure equation is solved first. From the resulting pressure field the velocity field can be calculated and can be further used to get an explicit solution of the saturation equation. As the equations are still weakly coupled due to the presence of the mobility which is a function of the saturation (Ch. 2.2.2) in the pressure equation, it can be necessary to repeat this solution sequence until a sufficient quality of the results is achieved. The mobility in the pressure equation is then always calculated using the latest result of the saturation equation. How many iterations are needed depends on the problem to be solved and on the aspired accuracy.
Like before in Section 3.3, terms containing gravity forces as well as source and sink terms are not further considered during the following discretisation sections, since they do not appear in the problem formulations considered in Chapter 4 of this work.

3.4.1 Space Discretisation

Pressure Equation

For the space discretisation of the pressure equation, a cell centred finite volume method is applied. To account for the elliptic character of the equation, central differences are used as differencing scheme. The finite volume formulation for the *global pressure fractional flow* formulation is then obtained by integration of Equation (3.17) over each element of the discretized domain (Fig. 3.2):

$$\int\limits_{FV-element} \nabla \cdot (\lambda_t \mathbf{K} \nabla \bar{p}) \; dV = 0. \tag{3.44}$$

Application of *Gauss*' divergence theorem leads to:

$$\oint\limits_{\Gamma_e} (\lambda_t \mathbf{K} \nabla \bar{p}) \, \mathbf{n} \, d\Gamma = 0, \tag{3.45}$$

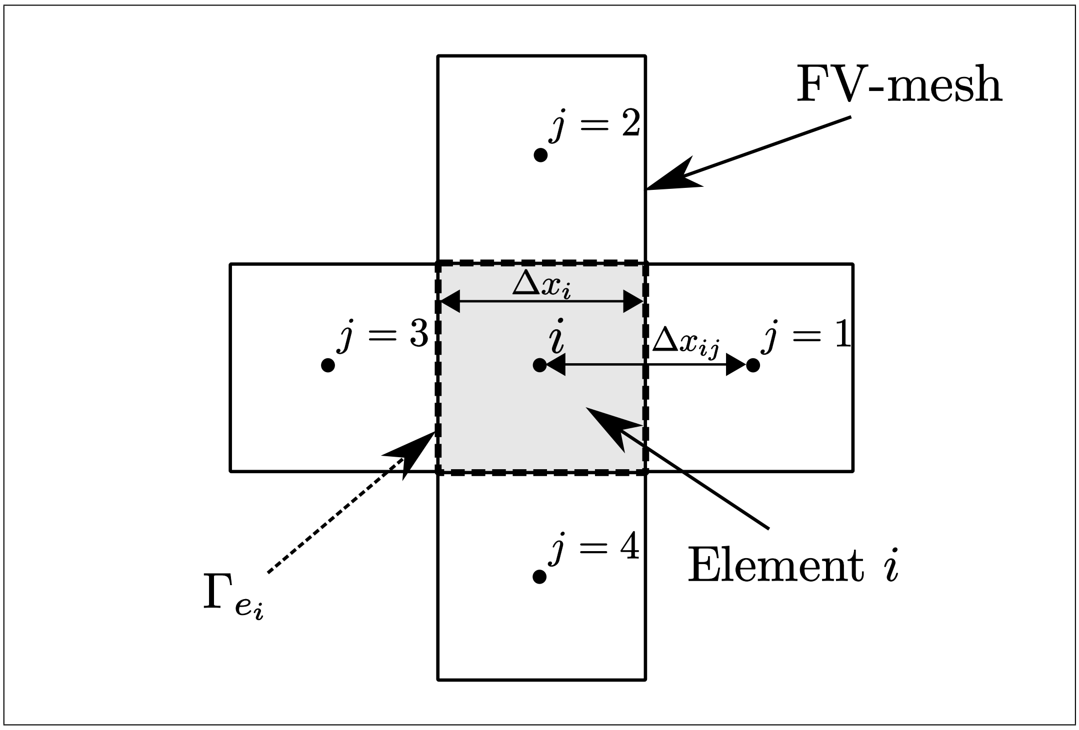

Figure 3.2: Finite Volume mesh.

where Γ_e is the boundary of one finite volume element. This integral can also be read as the sum of the fluxes over the faces of one element and Equation (3.45) can therefore be rewritten as:

$$\sum_{faces\ of\ i}\left(\lambda_{tij}\mathbf{K}\,\frac{\bar{p}_j-\bar{p}_i}{\Delta x_{ij}}A_{ij}\right)=0, \tag{3.46}$$

where i is the index of element i, j is the index of a neighbour element j, Δx_{ij} is the distance between the centre of element i and the centre of element j, and A_{ij} is the area of the interface between element i and j (Fig. 3.2). The total mobility λ_{tij} at the interface between element i and j is determined in the following way:

$$\lambda_{tij}=0.5\,(\lambda_{ti}+\lambda_{tj}). \tag{3.47}$$

This arithmetic averaging is correct as long as an equidistant mesh is used. Otherwise λ_{ti} and λ_{tj} can be weighted differently by a weighting factor ϵ:

$$\lambda_{tij}=\epsilon\,\lambda_{ti}+(1-\epsilon)\lambda_{tj}, \tag{3.48}$$

where $\epsilon=\frac{0.5\Delta x_i}{\Delta x_{ij}}$ with the element width Δx_i (Fig. 3.2). As the saturation is assumed to be known when the pressure equation is solved, the mobility at the elements which depends on the saturation is known, too.

The finite volume formulation for the *phase pressure fractional flow* formulation is obtained in the same way as described before for the *global pressure fractional flow* formulation. Therefore, Equation (3.20) and (3.22), respectively, is integrated over each element of the discretized domain (Fig. 3.2):

$$\int\limits_{FV-element} \nabla \cdot \left[\lambda_t \mathbf{K} \left(\nabla p_\alpha + (-1)^{\delta_{\alpha n}} f_{\beta \neq \alpha} \nabla p_c\right)\right] \, dV = 0. \tag{3.49}$$

Here $\delta_{\alpha n}$ is the Kronecker delta and α, $\beta = w, n$. In Equation (3.49) as well as in Equation (3.44) a pressure term of the same form $\nabla \cdot [\lambda_t \mathbf{K} (\nabla p)]$ can be found . In Equation (3.49) an additional term

$$\nabla \cdot [\lambda_t \mathbf{K} (f_{\beta \neq \alpha} \nabla p_c)] = \nabla \cdot (\lambda_{\beta \neq \alpha} \mathbf{K} \nabla p_c) \tag{3.50}$$

including capillary pressure appears which has to be further considered. As demonstrated in Equation (3.50) the capillary pressure term can be rewritten, resulting also in the form of Equation (3.44). Thus, the discretized pressure equation of the *phase pressure fractional flow* formulation can be directly written down following the formulation derived for the *global pressure fractional flow* formulation (Eq. 3.46):

$$\sum_{faces\,of\,i} \left(\lambda_{tij} \mathbf{K} \frac{p_{wj} - p_{wi}}{\Delta x_{ij}} A_{ij}\right) + (-1)^{\delta_{\alpha n}} \sum_{faces\,of\,i} \left(\lambda_{(\beta \neq \alpha) ij} \mathbf{K} \frac{p_{cj} - p_{ci}}{\Delta x_{ij}} A_{ij}\right) = 0. \tag{3.51}$$

In the macroscopic context the capillary pressure is only a function of the saturation which is assumed to be known when the pressure equation is solved. Thus, for the phase pressure formulation the capillary pressure is also assumed to be known. The phase mobility $\lambda_{(\beta \neq \alpha) ij}$ at the interface between element i and j is calculated similarly to the total mobility λ_{tij} (Eq. 3.47 and 3.48).

Saturation Equation

The saturation equation is discretized in space by application of a higher order cell centred finite volume method. In this method, the unknown is not assumed to be constant within one finite volume element but to show a functional behaviour. In the method applied here, a linear distribution of the saturation within one finite volume element is assumed. Therefore on each discretisation cell a corresponding slope is introduced (see [4])

$$\tilde{p}_i = \frac{u_{i+1} - u_{i-1}}{\Delta x_i + 0.5 \Delta x_{i-1} + 0.5 \Delta x_{i+1}}, \tag{3.52}$$

where u_i is the unknown at node i which in case of the saturation equation is the saturation S_i (Fig. 3.3). In case of a two dimensional domain, two slopes corresponding to node i have to be determined. The indices $i+1$ and $i-1$ then denote the neighbour nodes in the direction of the respective slope and Δx the corresponding element width. However, the two dimensional grid should be rectangular and structured.

Further the slopes are limited in order for the scheme to remain stable and to avoid over- and undershooting:

$$p_i = \alpha_i \tilde{p}_i. \tag{3.53}$$

The formula used for the limitation factor α_i can vary, depending on what is needed to achieve stability (details, see [4]). In case of a two dimensional domain two slopes corresponding to node i have to be calculated. Equation 3.52

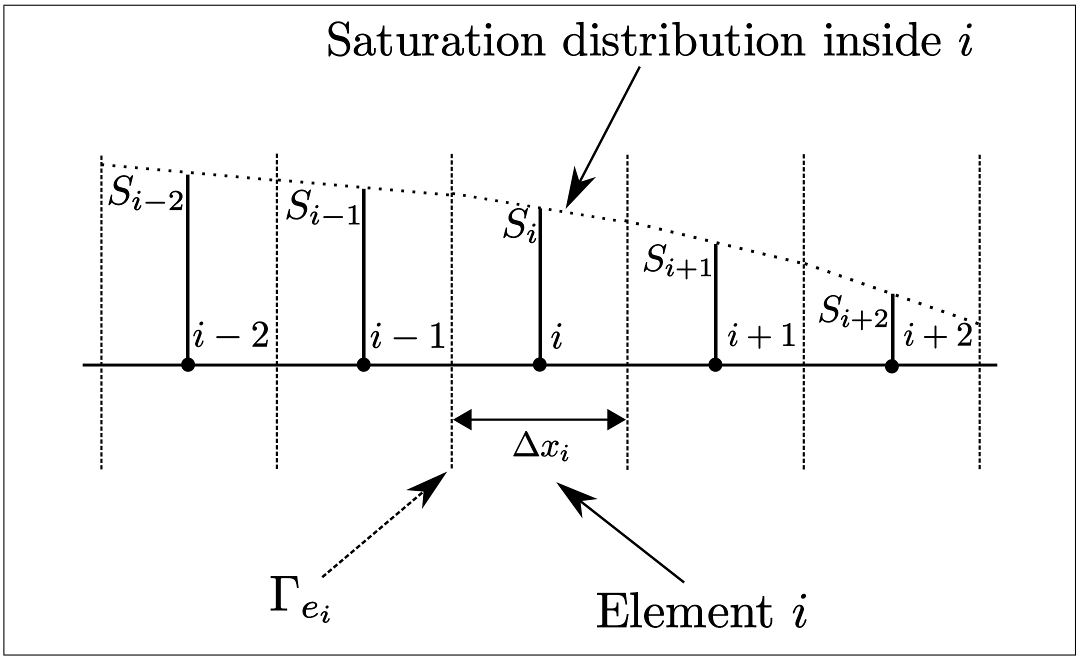

Figure 3.3: Schematic illustration of the slopes inside each finite volume cell.

To obtain the finite volume formulation of the saturation equation of the *global pressure fractional flow* formulation, Equation (3.31) is integrated over each element of the discretized domain

$$\int\limits_{FV-element} \frac{\partial(\phi\rho_w S_w)}{\partial t}\, dV + \int\limits_{FV-element} \nabla \cdot \left[\rho_w(f_w \mathbf{v}_t + \bar{\lambda}\mathbf{K}\nabla p_c)\right] dV = 0. \tag{3.54}$$

With *Gauss*' divergence theorem Equation (3.54) can be rewritten as

$$\frac{\partial(\phi\rho_w S_w)}{\partial t} V_e + \oint\limits_{\Gamma_e} \rho_w(f_w \mathbf{v}_t + \bar{\lambda}\mathbf{K}\nabla p_c)\, d\Gamma = 0, \tag{3.55}$$

where V_e is the element volume and Γ_e the element boundary. In a usual finite volume discretisation, the unknown is assumed to be constant within one element. Therefore, the first term in Equation (3.54) can be rewritten into the first term in Equation (3.55). In a higher order scheme as described before, the saturation is not constant but assumed to show a linear distribution over the element. Anyhow, the change of mass over time of a volume element remains the same than for a constant distribution because the saturation value at the centre of an element is equal to an arithmetic average of the linear concentration distribution. This is demonstrated in Figure 3.4 for an one dimensional element. For two different time steps k and $k+1$ area A and B which represent the change of mass from time step k to time step $k+1$ have the same size because $a_k = b_k$ and $a_{k+1} = b_{k+1}$. Therefore, the first term in Equation (3.54) can be rewritten into the first term in Equation (3.55) although the saturation varies within the element.

The capillary pressure term $\bar{\lambda}\nabla p_c$ in Equation (3.55) can also be written as $\bar{\lambda}\frac{dp_c}{dS_w}\nabla S_w$ according to Equation (3.32). Reformulating the boundary integral in the second term of Equation

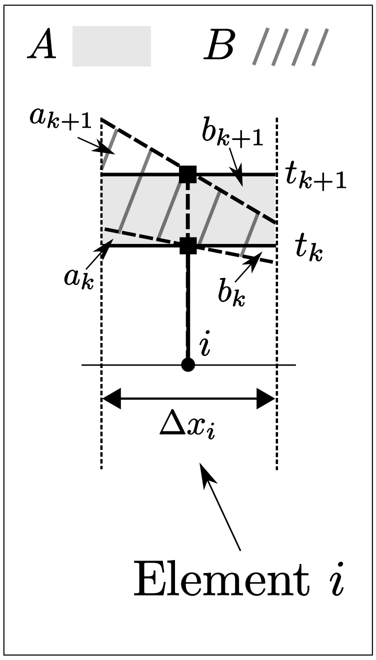

Figure 3.4: Change of mass of one phase over time for a cell centred finite volume approach with constant distribution of the saturation and with linear distribution of the saturation.

(3.55) as the sum of the fluxes through the faces of an element the saturation equation can be discretized in space as

$$\frac{\partial(\phi\rho_{wi}S_{wi})}{\partial t}V_i + \sum_{faces\,of\,i}\left[\rho_{wij}\left(f_{wij}\mathbf{v}_{tij} + \bar{\lambda}_{ij}\mathbf{K}(\frac{d\,p_c}{d\,S_w})_{ij}\,(\nabla S_w)_{ij}\right)A_{ij}\right] = 0. \tag{3.56}$$

As before, i denotes the value at the centre of element i and ij the value at the interface of element i and a neighbour element j. A_{ij} is the area of the interface between element i and j. The saturations at the interface S_{ij} are calculated using the slopes defined in Equation (3.52):

$$S_{(wij)_i} = S_{wi} + 0.5\,\Delta x_i\,p_i, \tag{3.57}$$

$$S_{(wij)_j} = S_{wj} - 0.5\,\Delta x_j\,p_j. \tag{3.58}$$

The fractional flow function at the interface f_{wij} is then determined using an upwind scheme

$$f_{wij} = \begin{cases} f_w(S_{(wij)_i}) & \text{if} \quad \nabla S_w = \frac{S_{wj}-S_{wi}}{\Delta x_{ij}} < 0 \\ f_w(S_{(wij)_j}) & \text{if} \quad \nabla S_w > 0, \end{cases} \tag{3.59}$$

to account for the advective character of the term $f_{wij}\mathbf{v}_{tij}$.
The mobility $\bar{\lambda}_{ij}$ and the capillary pressure derivative $(\frac{d\,p_c}{d\,S_w})_{ij}$ at the interface are obtained as an arithmetic average corresponding to a central differencing scheme as:

$$\bar{\lambda}_{ij} = 0.5\left[\bar{\lambda}(S_{(wij)_i}) + \bar{\lambda}(S_{(wij)_j})\right], \tag{3.60}$$

$$\left(\frac{d\,p_c}{d\,S_w}\right)_{ij} = 0.5\left[\left(\frac{d\,p_c}{d\,S_w}\right)\left(S_{(wij)_i}\right) + \left(\frac{d\,p_c}{d\,S_w}\right)\left(S_{(wij)_j}\right)\right]. \tag{3.61}$$

This assures that the diffusive character of the cappilary pressure term is expressed.

For one-dimensional application, this higher order method provides a possibility to reduce the numerical diffusion introduced by a first order upwind scheme because more nodes are included in the determination of the interface values (four nodes at one interface). Application to two dimensions as it is also done here for the solution of the *five-spot* problem (Sec. 4.2) can even increase the numerical diffusion caused by the upwind method.
As pointed out by *Helmig* [6] one explanation for cross diffusion is that upwind methods use a value which is computed along the element edge. This implies that also information can only be transported parallel to the element edges. The consequence is that if the streamlines are not parallel to the grid there are not all nodes taken into account to determine the interface values that would have to. Therefore, information is lost. An approach to solve that problem is described by *Helmig* [6].
For the higher order finite volume method this effect is even stronger developed as more nodes representing a wrong upwind direction are taken into account if the streamlines are not parallel to the element edge. The problem of cross-diffusion is discussed in more detail in Section 4.2.

For the *phase pressure fractional flow* formulation the finite volume discretisation is formulated by integration of Equation (3.2) and application of *Gauss*' divergence theorem

$$\int\limits_{FV-element} \frac{\partial(\phi\rho_\alpha S_\alpha)}{\partial t}\, dV_e + \oint\limits_{\Gamma_e} \nabla(\rho_\alpha f_\alpha \mathbf{v}_{\alpha_{mod}})\, d\Gamma_e = 0. \tag{3.62}$$

According to Equation (3.25) the modified phase velocity $v_{\alpha_{mod}}$ is used here. The advantage of this formulations points out comparing Equations (3.62) and (3.55). Formally the only difference is the capillary pressure term in Equation (3.55). Therefore, Equation (3.62) can be written in discretized form analogically to Equation (3.56):

$$\frac{\partial(\phi\rho_{\alpha i} S_{\alpha i})}{\partial t} V_i + \sum_{faces\, of\, i} \rho_{\alpha ij} f_{\alpha ij} \mathbf{v}_{\alpha_{mod} ij} A_{ij} = 0. \tag{3.63}$$

This similarity also means that an implementation of the *global pressure fractional flow* formulation can be switched easily into an implementation of a *phase pressure fractional flow* formulation. Only one capillary pressure term has to be added in the implementation of the pressure equation (Eq. 3.51) and one capillary pressure term has to be set to zero in the saturation equation (Eq. 3.56).

3.4.2 Time Discretisation

Pressure Equation

The time dependence of the pressure equation exists due to the dependence on the mobility and in case of the *phase pressure fractional flow* formulation also due to the dependence on the capillary pressure on the saturation. Therefore, the following expressions are obtained for the fully discretized pressure equation of the *global pressure fractional flow* formulation

$$\sum_{faces\, of\, i} \left(\lambda_{tij}^{k+1} \mathbf{K} \frac{\bar{p}_j^{k+1} - \bar{p}_i^{k+1}}{\delta_{x_{ij}}} A_{ij} \right) = 0 \tag{3.64}$$

and for the *phase pressure fractional flow* formulation

$$\begin{aligned}\sum_{faces\,of\,i}&\left(\lambda_{tij}^{k+1}\mathbf{K}\,\frac{p_{wj}^{k+1}-p_{wi}^{k+1}}{\delta_{x_{ij}}}A_{ij}\right)\\&+(-1)^{\delta_{\alpha n}}\sum_{faces\,of\,i}\left(\lambda_{(\beta\neq\alpha)ij}^{k+1}\mathbf{K}\,\frac{p_{cj}^{k+1}-p_{ci}^{k+1}}{\delta_{x_{ij}}}A_{ij}\right)=0,\end{aligned} \tag{3.65}$$

where $k+1$ denotes the dependence on the saturation of the latest time step.

Saturation Equation

The time discretisation of the saturation equation is done applying an explicit Euler method. For an unknown u a general form of this method can be formulated as:

$$u^{k+1}=u^k+\Delta t\,f(u^k), \tag{3.66}$$

where k is the index of the time step. Using Equation (3.66) together with Equation (3.56) leads to

$$S_{wi}^{k+1}=S_{wi}^k+\frac{\Delta t}{\phi}\sum_{faces\,of\,i}\left[f_{wij}^k\mathbf{v}_{tij}^k+\bar{\lambda}_{ij}^k\mathbf{K}(\frac{d\,p_c}{d\,S_w})_{ij}^k\,(\nabla S_w)_{ij}^k\right]A_{ij}=0 \tag{3.67}$$

for the *global pressure fractional flow* formulation and

$$S_{\alpha i}^{k+1}=S_{\alpha i}^k+\frac{\Delta t}{\phi}\sum_{faces\,of\,i}\left[f_{\alpha ij}^k\mathbf{v}_{\alpha ij}^k\right]=0 \tag{3.68}$$

for the *phase pressure fractional flow* formulation.
Again the porosity ϕ is assumed to be independent of pressure and time. Furthermore, the density ρ is only a function of the temperature if the fluids are assumed to be incompressible. If the temperature is assumed to be constant over time and space what it is done here, ρ is also constant and cancels out in Equations (3.67) and (3.68).

3.5 Summary and comparison of the formulations

In this chapter, different formulations describing twophase flow in porous media are derived: a formulation named *fully coupled* formulation and a *fractional flow* formulation.
The *fully coupled* formulation models the motion of each phase by formulating one equation for each phase. These equations are strongly coupled through the constitutive and closure relationships that are needed. Furthermore, the behaviour of the equations is highly nonlinear because of the nonlinear relationship between capillary pressure and saturation on the one hand and relative permeability and saturation on the other hand. Both equations are of similar form and show a parabolic character.
The *fractional flow* formulation models the motion of one total fluid driven by a total pressure with a total velocity. The individual phases are then described as fractions of the total fluid and accounted for by the fractional flow functions. Two alternatives of the *fractional flow* formulation are introduced. A *global pressure fractional flow* formulation defining a global pressure and a *phase pressure fractional flow* formulation.

The two equations of the *global pressure fractional flow* formulation (pressure equation and saturation equation) are only weakly coupled through the presence of the total mobility and the fractional flow functions in the pressure equation, which means through the relative permeabilities. The global pressure $\bar{p}$ includes both phase pressures and capillary pressure effects and is therefore directly depending on the saturation. Additionally, the mobility terms and therefore, the fractional flow functions in both equations are nonlinear dependent on the saturation. Together this leads to a strong nonlinearity of this formulation. Formally, the pressure equation is elliptic whereas the saturation equation is parabolic, including advective as well as diffusive terms.

In the *phase pressure fractional flow* formulation, the pressure equation is formulated in terms of a phase pressure which leads to an additional capillary pressure term. Therefore, the coupling between pressure equation and saturation equation is strengthened again compared to the *global pressure fractional flow* formulation. In return, the nonlinearity is weakened as the phase pressure is only indirectly dependent on the saturation. In contrast to the *global pressure fractional flow* formulation, the *phase pressure fractional flow* formulation strictly separates diffusive and advective processes where the formally elliptic pressure equation represents the diffusive part and the hyperbolic saturation equation the advective part.

Numerically, the equations of the *fully coupled* formulation have to be solved simultaneously due to the strong coupling. The *phase pressure fractional flow* formulation can be solved decoupled, most common using an IMPES scheme (IMplicit Pressure - Explicit Saturation). The decoupled explicit solution is less expensive than an implicit scheme. However, an explicit scheme is more restricted in time step size. It may depend on the problem which feature is more advantageous.

An advantage of the *fully coupled* formulation is that the equations have a relative simple form and that they have an equal form. An disadvantage is that it can not be accounted for different flow characters by an corresponding discretisation scheme as it can not be distinguished between diffusive and advective terms.

The advantage of the *fractional flow* formulation is that the equations show a well known form, where the pressure equation is an elliptic equation and the saturation equation is similar to a classical transport equation. It can be easily distinguished between diffusive and advective terms and corresponding differencing schemes can be used. However in presence of capillary effects, the saturation equation is still parabolic which means that still one discretisation method has to be used to account for both kinds of processes.

Problems occur for the *global pressure fractional flow* formulation due to the derivative of the capillary pressure $\frac{dp_c}{dS_w}$ in the saturation equation. Depending on the capillary pressure-saturation relation this derivative can become very large or also tend to zero which causes numerical problems.

Finally, the *phase pressure fractional flow* formulation shows the strictest separation of the different processes. All diffusive processes are included in the pressure equation, the advective processes in the saturation equation. Thus, these processes can be accounted for in a most effective way. Compared to the *global pressure fractional flow* formulation another important advantage is the use of a phase pressure which is a real physical property. This makes it easier to define *Dirichlet* boundary conditions for pressure, and provides a better comparability to the *fully coupled* formulation. Furthermore, it might give an advantage for the consideration of heterogeneous porous media if the pressure equation is formulated in terms of a phase pressure (see [7]).

4 Comparative Study of Mathematical Models and Numerical Schemes on Selected Examples

To compare the different kinds of formulations described in the previous chapter, some simple problems are set up and solved. The term formulation includes the mathematical model as well as the numerical method. Thus, referring to Chapter 3 the term *fully coupled* formulation implies the box method as corresponding numerical scheme and the term *fractional flow* formulation the finite volume and higher order finite volume method, respectively.
To account for advection dominated flow the *Buckley-Leverett* problem is chosen as a one dimensional example (Sec. 4.1). In analogy, the *Five-spot Waterflood* problem is chosen for two dimensional consideration (Sec. 4.2). Diffusion dominated flow is investigated by solving the *McWhorter* problem (Sec. 4.3). In addition to their simple form one further advantage of *Buckley-Leverett* and *McWhorter* problem is the existence of analytical solutions. Finally, a problem combining advection and diffusion is considered (Sec. 4.4). The comparison of the formulations is done with regard to accuracy and efficiency. Therefore, also different constitutive relationships are used.

4.1 Buckley-Leverett Problem

The *Buckley-Leverett* problem describes the instationary displacement of oil by water in an one-dimensional, horizontal system (Fig. 4.1). An analytical solution of the problem was developed by *Buckley* and *Leverett* [3]. The assumptions of the *Buckley-Leverett* problem are as follows:

- Capillary pressure effects are neglected.
- Gravity effects are neglected.
- There exist no sources or sinks.
- The fluids are incompressible and immiscible.
- The fluid viscosities are equal.
- The porous medium is homogeneous.

The *fully coupled* formulation is used as p_w-S_n formulation. With the above assumptions Equations (3.6) and (3.7) are simplified to

$$L_w(p_w, S_n) := -\phi \frac{\partial S_n}{\partial t} - \nabla \cdot (\lambda_w \mathbf{K} \nabla p_w) = 0, \tag{4.1}$$

$$L_n(p_w, S_n) := \phi \frac{\partial S_n}{\partial t} - \nabla \cdot (\lambda_n \mathbf{K} \nabla p_w) = 0. \tag{4.2}$$

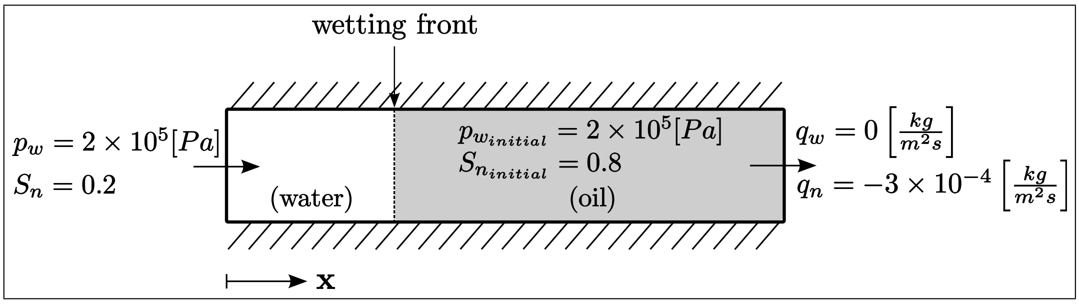

Figure 4.1: *Buckley-Leverett* problem with initial and boundary conditions.

Without capillary pressure, $\bar{p} = p_w = p_n$ and the differences between the two fractional flow formulations described in Section 3.2 vanish. Thus, under the above assumptions the fractional flow *Buckley-Leverett* equations are

$$-\nabla \cdot (\lambda_t \mathbf{K} \nabla \bar{p}) = 0, \tag{4.3}$$

$$\phi \frac{\partial S_w}{\partial t} + \nabla \cdot (f_w \mathbf{v}_t) = 0. \tag{4.4}$$

4.1.1 Analytical solution

The *Buckley-Leverett* equation (Eq. 4.4) shows the property of a quasilinear hyperbolic differential equation. One important feature of the hyperbolic character is that discontinuous solutions called "shocks" are allowed. To ensure an unique solution, additional conditions have to be fulfilled. These are the *Rankine-Hugoniot jump condition* and the *Entropy condition* (details, see [6]). To obtain an analytical solution, Equation (4.4) can be rewritten according to Equation (3.32) as

$$\phi \frac{\partial S_w}{\partial t} + \mathbf{v}_t \frac{df_w}{dS_w} \nabla S_w = 0. \tag{4.5}$$

The saturation at the wetting front is constant. Thus, one can write

$$dS_w(x,t) = \frac{\partial S_w}{\partial x} dx + \frac{\partial S_w}{\partial t} dt = 0. \tag{4.6}$$

Substituting Equation (4.6) into Equation (4.5) gives

$$\frac{dx}{dt} = \frac{\mathbf{v}_t}{\phi} \frac{df_w}{dS_w} \tag{4.7}$$

which can be integrated in time to obtain an expression for the front position x_f:

$$x_f = \frac{\mathbf{v}_t \, t}{\phi} \frac{df_w}{dS_w}, \tag{4.8}$$

where t is the point in time at which the front is considered. If the relative permeability saturation relationships k_r are nonlinear, the resulting profile of the saturation front may look similar to Figure 4.2. Based on the conditions mentioned before, the analytical solution can be found applying the equal area rule. The position of the saturation discontinuity is then determined by balancing the areas A and B (Fig. 4.3)(details, see [6]).

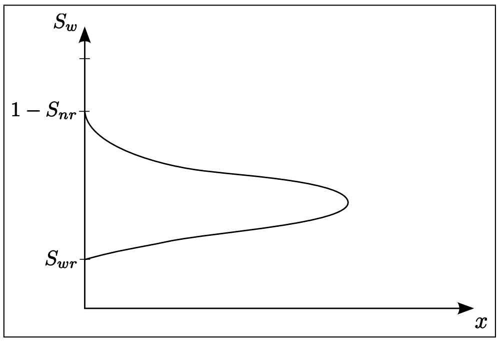

Figure 4.2: Saturation profile without saturation jump.

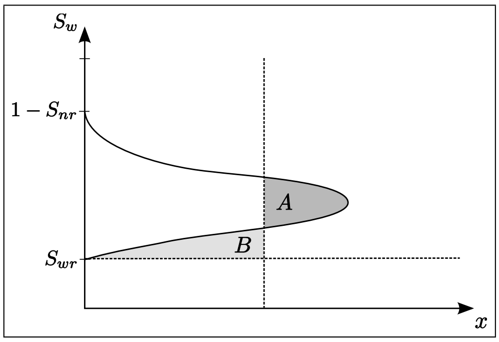

Figure 4.3: Analytical solution with the equal area rule.

geometry	**length** [**m**]
	300

	number of cells	**Δx** [**m**]	**Δt** [s]			
			fully coupled f.		**fractional flow f.**	
			linear	*Brooks-Corey*	linear	*Brooks-Corey*
discreti-sation	15	20	8×10^6	2.67×10^6	8×10^6	2.67×10^6 (∅)
	30	10	4×10^6 4.32×10^5 2.16×10^5 1.08×10^5	1.33×10^6 4.32×10^5 $= 5\,d$ 2.16×10^5 $= 2.5\,d$ 1.08×10^5 $= 1.25\,d$	4×10^6	1.33×10^6 (∅)
	60	5	2×10^6	6.67×10^5	2×10^6	6.67×10^5 (∅)
	120	2.5	1×10^6	3.33×10^5	1×10^6	3.33×10^5 (∅)

Table 4.1: Geometry and discretisation.

4.1.2 Calculations

The numerical simulations were carried out using one dimensional elements. The considered domain has a length of 300 m. Different grids are used, the coarsest one consisting of 15 elements. Finer grids are constructed by halvening all elements (Tab. 4.1). The time step size which is given in Table 4.1 is determined in the following way: First, a simulation is done applying the *fractional flow* formulation. Here, an automatic time step adaption is implemented using a *Courant-Friedrichs-Lewy* criterion (details, see [6]) for the explicit *Euler* time steps. The average time step of this simulation is then used as constant time step in the simulation using the *fully coupled* formulation.

The initial and boundary conditions are given in Table 4.2, where *Dirichlet* boundary conditions are set on the left side of the domain ($x = 0$ m) and *Neumann* boundary conditions on the right side of the domain ($x = 300$ m)(Fig. 4.1). Initially, the domain is oil saturated. A linear, as well as a *Brooks-Corey* relationship are selected to analyse the influence of the relative permeability-saturation relation on the solution. The corresponding parameters as well as other porous medium and fluid properties are shown in Table 4.3.

In order to compare the results of the numerical experiments using the different formulations

	parameter	**value**
boundary conditions	$\mathbf{x = 0\,m}$	
	water pressure $p_w = \bar{p}$	$2 \times 10^5\ [Pa]$
	oil saturation S_n	$0.2\ [-]$
	$\mathbf{x = 300\,m}$	
	flow rate of water q_w	$0\ [kg/(m^2 s)]$
	flow rate of oil q_n	$-3 \times 10^{-4}\ [kg/(m^2 s)]$
initial conditions	water pressure $p_w = \bar{p}$	$2 \times 10^5\ [Pa]$
	oil saturation S_n	$0.8\ [-]$

Table 4.2: Initial and boundary conditions.

	parameter	**value**
fluid properties	water density ρ_w	$1000\ [kg/m^3]$
	oil density ρ_n	$1000\ [kg/m^3]$
	dyn. viscosity water μ_w	$0.001\ [kg/(ms)]$
	dyn. viscosity oil μ_n	$0.001\ [kg/(ms)]$
solid matrix properties and constitutive relationships	intrinsic permeability $\mathbf{K}$	$10^{-7}\ [m^2]$
	porosity Φ	$0.2\ [-]$
	pore size distr. index λ	$2.00\ [-]$
	res. saturation water S_{wr}	$0.2\ [-]$
	res. saturation oil S_{nr}	$0.2\ [-]$
	rel. permeability $k_r(S_w)$	linear/Brooks-Corey

Table 4.3: Fluid and porous medium properties.

and to estimate the accuracy of the approximation, an error with respect to the analytical solution is calculated. The analytical solution itself is calculated simultaneously during the numerical simulation and on the corresponding simulation grid. A weighted averaged error is then calculated for each time step as

$$E^k = \sqrt{\sum_i \frac{\Delta x_i}{L} \left(S^k_{w_{\mathrm{an},i}} - S^k_{w_{\mathrm{num},i}} \right)^2}, \tag{4.9}$$

where i indicates the cells and the vertexes respectively depending on the discretisation and k the time step. L is the domain length, Δx_i the element length and the box length respectively, $S^k_{w_{\mathrm{an},i}}$ the saturation of the analytical solution and $S^k_{w_{\mathrm{num},i}}$ the saturation of the numerical solution. For equidistant meshes $\Delta x_i = \Delta x_{i+1} = \Delta x$ holds. Thus, Equation (4.9) can be reformulated into the form

$$E^k = \sqrt{\frac{\Delta x}{L} \sum_i \left(S^k_{w_{\mathrm{an},i}} - S^k_{w_{\mathrm{num},i}} \right)^2}, \tag{4.10}$$

which is equivalent to a quadratic average of the difference between analytical and numerical solution.

Following, the results of the different calculations are discussed. Therefore, the saturation distributions of the infiltrating water phase are shown after a period of 500 days.
Figures 4.4a and 4.4b compare the numerical results calculated on different grids using a linear relative permeability-saturation relation to the analytical solution. It can be seen that for both formulations the numerical solution converges to the analytical solution when increasing the number of elements. It can also be observed that the *fully coupled* formulation causes much stronger numerical diffusion due to the fully upwinding. Compared to the *fractional flow* formulation, this leads to a stronger smearing of the saturation front. Using the *fractional flow* formulation the results are almost equal to the exact solution for the finest grid and are also much more accurate for the coarser grids than using the *fully coupled* formulation.
This can also be observed comparing the results using a *Brooks-Corey* relative permeability-saturation relation. Using the *fully coupled* formulation on the finest grid, the smearing of the saturation front is still relatively strong (Fig. 4.5a). In contrast, with the *fractional flow* formulation the saturation front of the numerical calculation using the finest grid shows a shape almost equal to the analytical solution (Fig. 4.5b). It has to be noted that the saturation at the left boundary of the domain is equal for both formulations. The differences which can be observed arise from the visualisation of the data, where the cell centred data resulting from the calculations with the *fractional flow* formulation are converted into point data.
Comparing the different approaches for the relative permeability-saturation relation, it can be observed that applying the *fully coupled* formulation significantly smaller elements would be needed with the linear approach to get an approximation of a quality equal to the approximation using the *Brooks-Corey* approach. The *fractional flow* formulation shows a comparable, good convergence against the analytical solution with increasing element numbers for both the linear as well as the non-linear approach.
Figures 4.6a and 4.6b show the averaged weighted error described by Equation (4.10) for the linear relative permeability-saturation relationship. The error using a *Brooks-Corey* approach

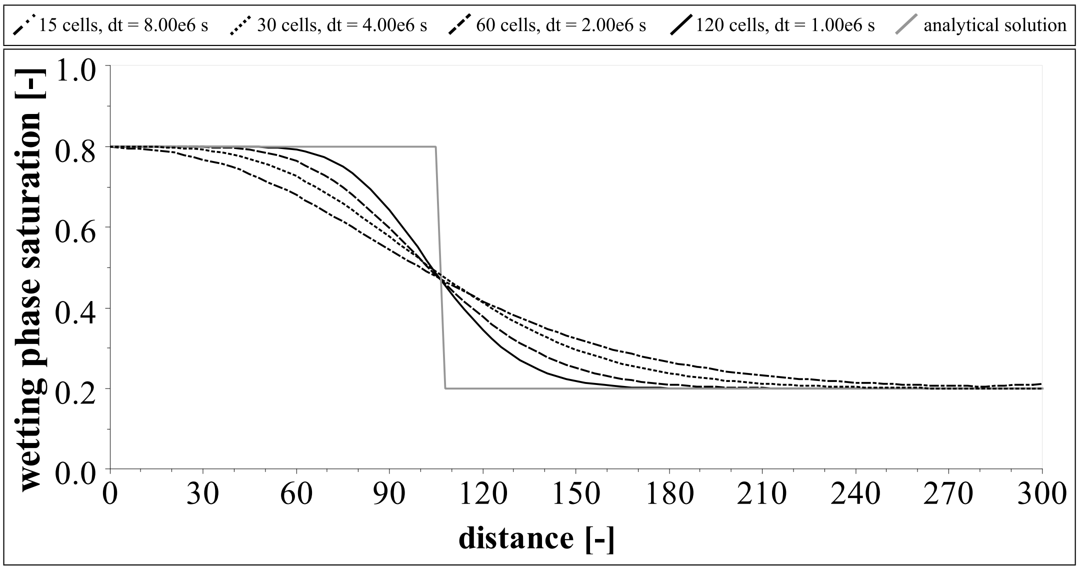

(a) *fully coupled* formulation

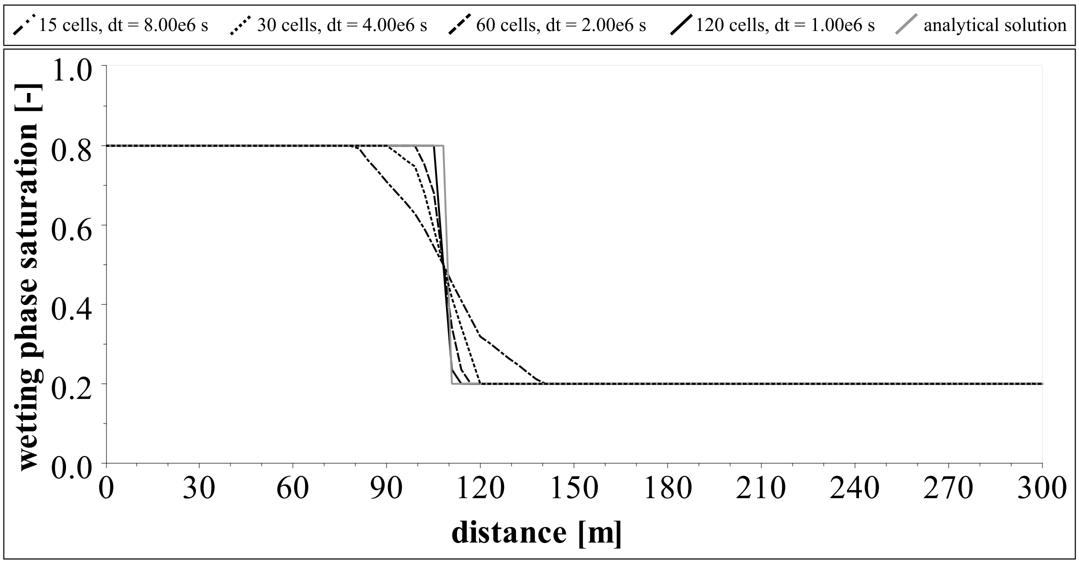

(b) *fractional flow* formulation

Figure 4.4: Saturation profiles of the Buckley-Leverett problem at $t = 500\,d$ for different number of cells (linear).

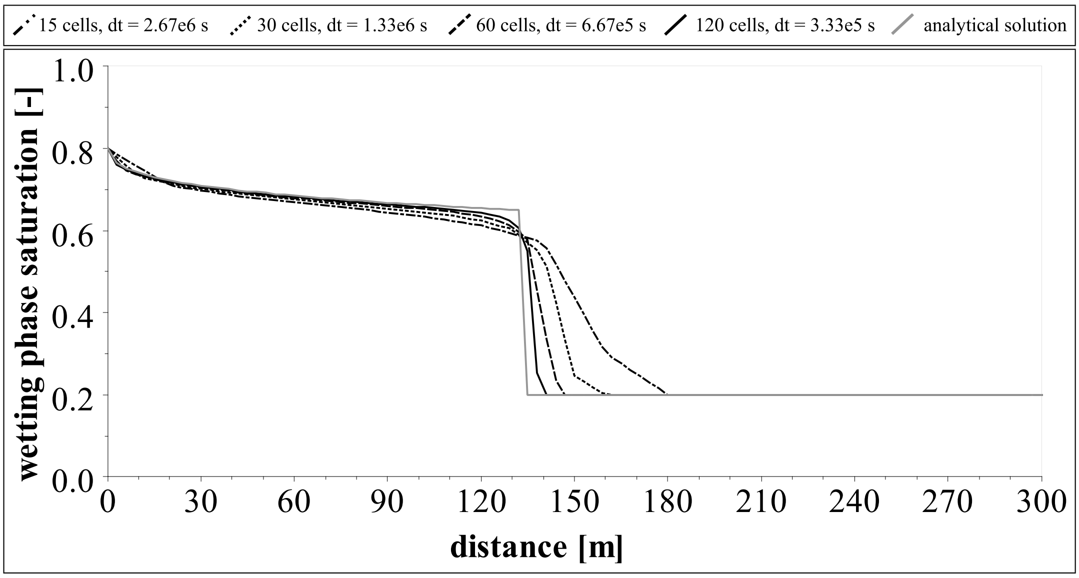

(a) *fully coupled* formulation

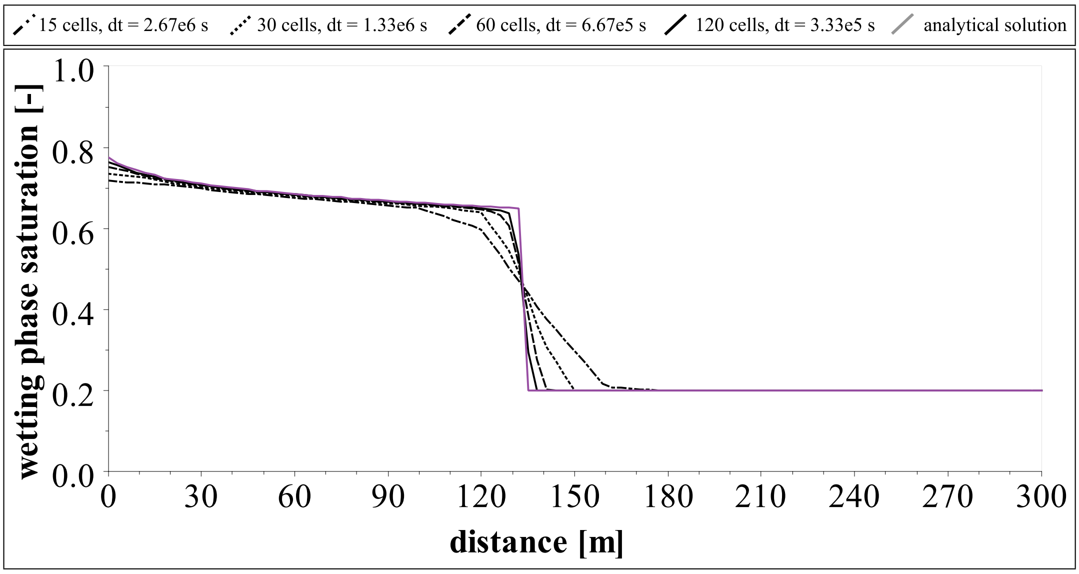

(b) *fractional flow* formulation

Figure 4.5: Saturation profiles of the Buckley-Leverett problem at $t = 500\,d$ for different number of cells (*Brooks-Corey*).

is shown in Figures 4.7a and 4.7b. Consideration of the error confirms what was observed above for the saturation distributions. The level of the error is decreasing with increasing number of elements for both relative permeability-saturation functions and for both twophase flow formulations. Furthermore, using the *fully coupled* formulation the error calculated for the linear approach is greater than the error calculated for the nonlinear *Brooks-Corey* approach. The error oscillations which occur are dependent on the grid and become smaller with increasing element number. They show that the front is not moving continuously. It jumps from one element into another from one time step to the next one. The error oscillations are generated because the front of the analytical and the numerical solution do not move at the same time step.

To achieve better comparability, the averaged weighted error is additionally averaged over time. The results are shown in Figure 4.8. Both error curves using the *fractional flow* formulation lie below the corresponding curve of the *fully coupled* formulation. Thus, it can be noted that the *fractional flow* formulation approximates the *Buckley-Leverett* problem more accurately than the *fully coupled* formulation. Furthermore, considering the curves of the *fully coupled* formulation it can be observed, that the curve of the linear relative permeability-saturation function lies above the curve of the *Brooks-Corey* relation which implies that with *Brooks-Corey* a better approximation relative to the corresponding analytical solution can be achieved. The smallest error is achieved using the *fractional flow* formulation with a linear relative permeability-saturation relationship. This coincides with the analysis of the saturation distributions.

As described above, the time steps applying the *fractional flow* formulation are determined using a *Courant-Friedrichs-Lewy* criterion to guarantee a stable solution. The time steps do not have to be constant but are adapted during the calculation if this is necessary. For the *fully coupled* formulation constant time steps are chosen. Therefore, the impact of the time step size has to be looked at. As can be seen in Table 4.1, calculations have been done using a grid consisting of 30 elements for four different time step sizes. The resulting saturation profiles are shown in Figures 4.9 and 4.11. As can be observed, the solution for both relative permeability-saturation functions converge to a solution with decreasing time steps. However, only between the largest and the next smaller time step a noticeable difference can be detected. Further bisecting of the time step does no longer change the solution. Thus, the solutions can be assumed to be converged for the finer time steps. The same can be observed analysing the error distribution (Fig. 4.10 and 4.12) which also shows convergence after the second largest time step. This also implies that the error oscillations can not be further reduced by decreasing the time step below this level. Thus, from that moment they are only related to the grid as pointed out above.

Besides the accuracy, the efficiency is a second aspect to be discussed. Therefore, the execution time is measured and shown in Table 4.4. The table shows that linearity and nonlinearity, respectively, have a strong influence concerning the computing speed. While for the linear case the *fractional flow* formulation is faster for all grids, for the nonlinear case using a *Brooks-Corey* relative permeability-saturation function the *fully coupled* formulation becomes faster if the element number increases.

To achieve additional comparability, Table 4.5 shows some execution time ratios. The first two ratios (FC-BC/FC-linear, FF-BC/FF-linear) relate the execution time of the nonlinear case to that of the linear case for the two twophase flow formulations. For both formulations the ratio is greater than one. That means that the calculation of the linear case is faster although the

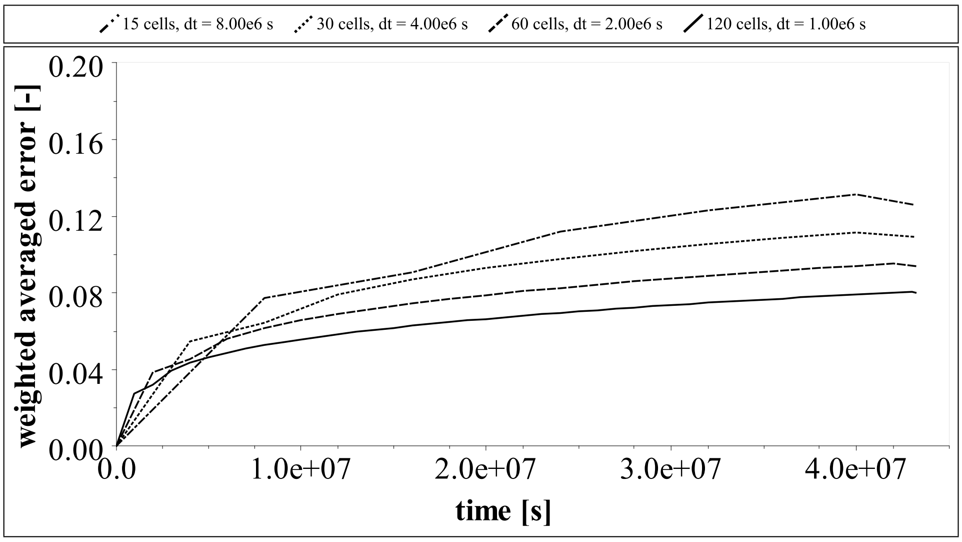

(a) *fully coupled* formulation

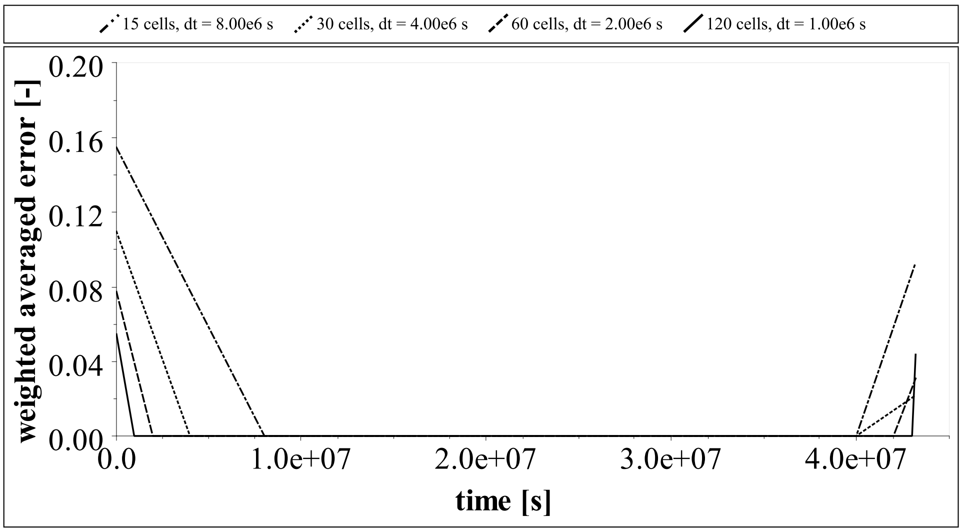

(b) *fractional flow* formulation

Figure 4.6: Weighted averaged error over time for different number of cells (linear).

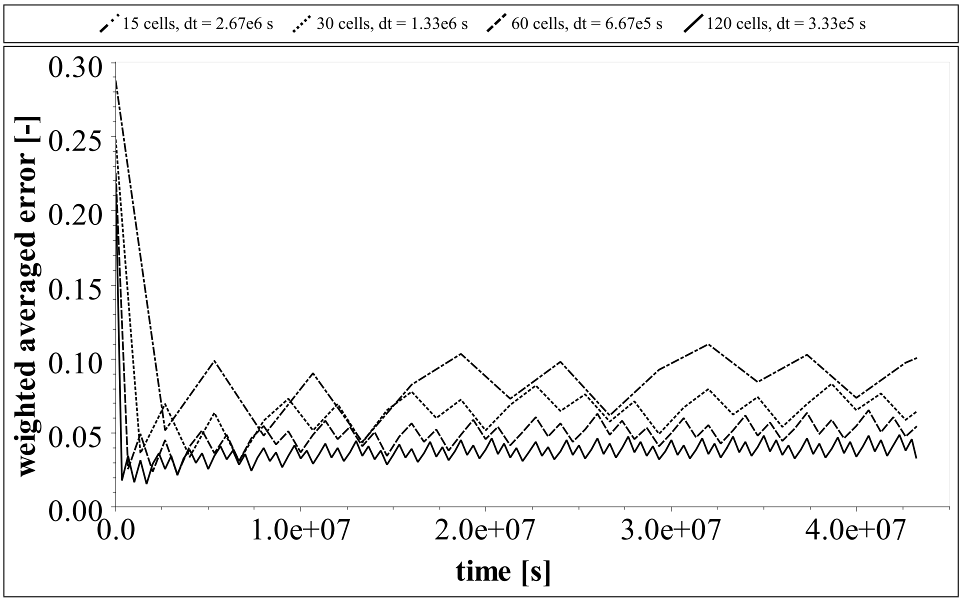

(a) *fully coupled* formulation

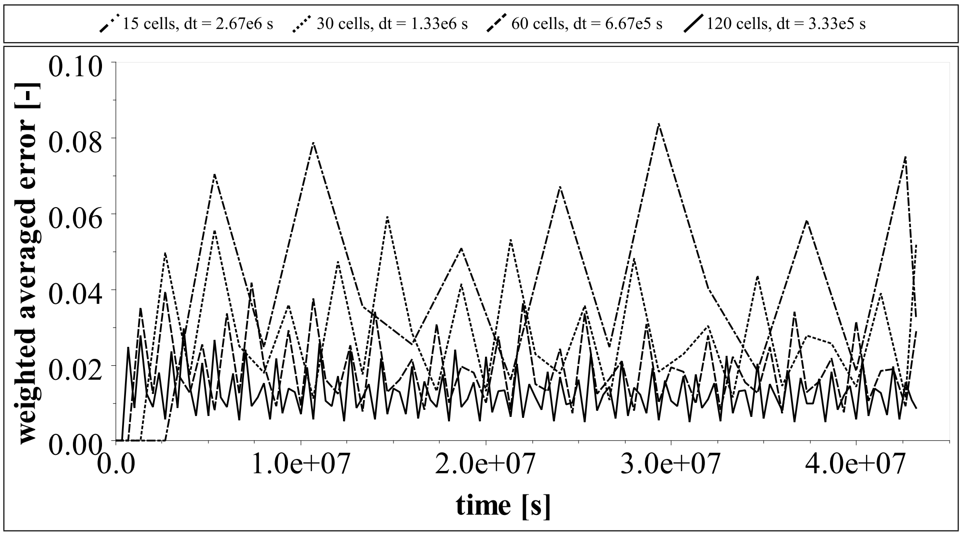

(b) *fractional flow* formulation

Figure 4.7: Weighted averaged error over time for different number of cells (*Brooks-Corey*).

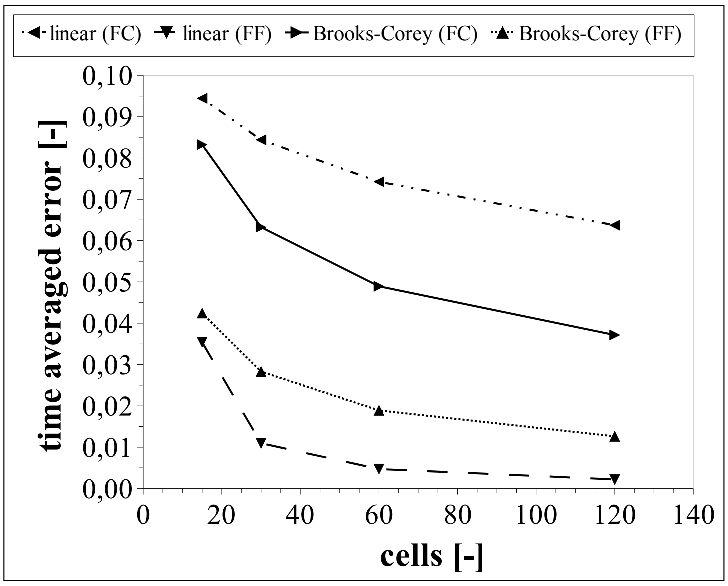

Figure 4.8: Time averaged error of the different formulations over number of cells (*fully coupled* (FC), *fractional flow* (FF)).

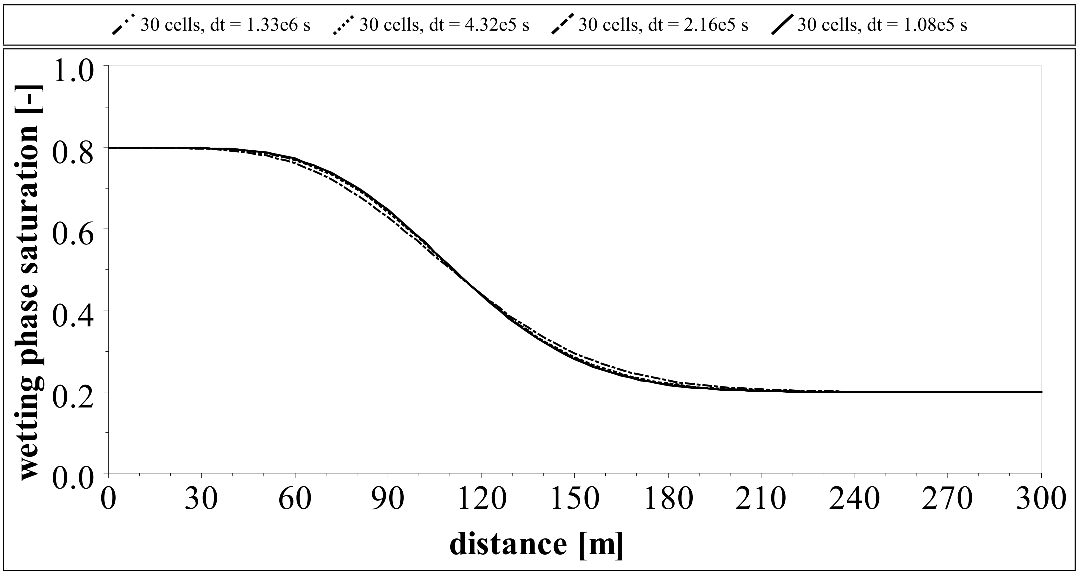

Figure 4.9: Saturation profiles of the Buckley-Leverett problem at $t = 500\,d$ for different time steps (*fully coupled* formulation, linear).

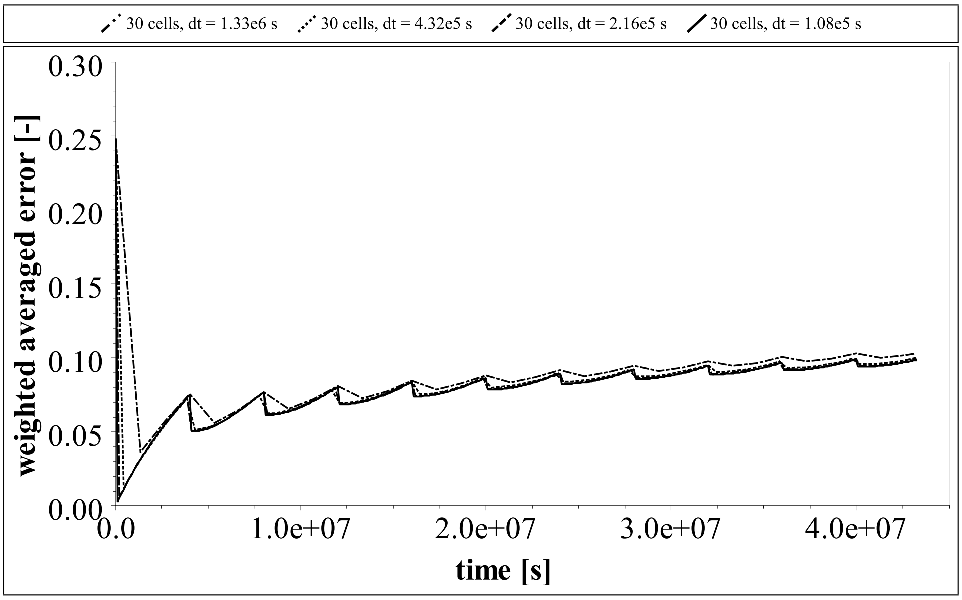

Figure 4.10: Weighted averaged error over time for different time steps (*fully coupled* formulation, linear).

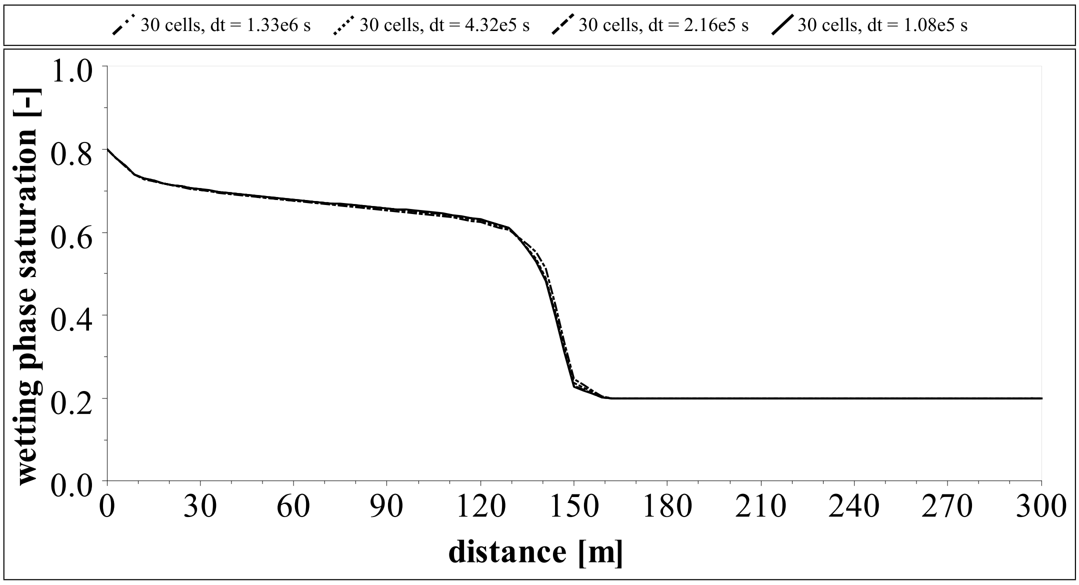

Figure 4.11: Saturation profiles of the Buckley-Leverett problem at $t = 500\,d$ for different time steps (*fully coupled* formulation, *Brooks-Corey*).

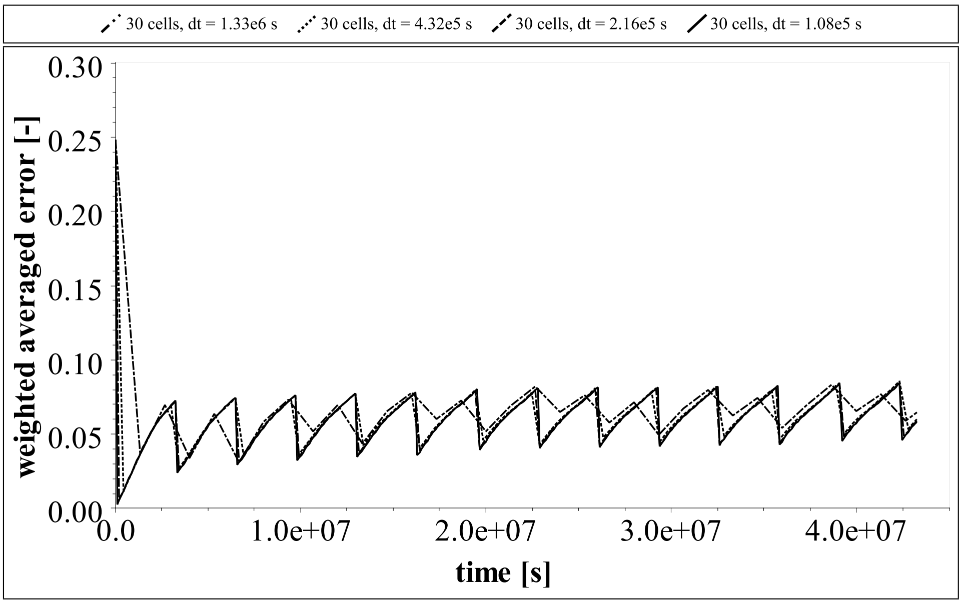

Figure 4.12: Weighted averaged error over time for different time steps (*fully coupled* formulation, *Brooks-Corey*).

differences in speed become smaller for increasing element numbers. However, the decrease of the ratios and thus the equalisation of the execution times also slows down with increasing element numbers. The third and fourth ratio (FF-linear/FC-linear, FF-BC/FC-BC) relate the execution times of the different twophase flow formulations to each other. For the linear case, the ratio is always smaller than one which shows that the *fractional flow* formulation is always faster than the *fully coupled* formulation. The ratio of the nonlinear case is increasing with increasing element numbers. For the first grid, it is smaller than one and the *fractional flow* formulation is faster than the *fully coupled* formulation. For the second and the following grids, the ratio is greater than one and therefore, the *fully coupled* formulation is faster. The increase of the ratio slows down with increasing element number and seems to converge for further refinement of the grid.
The difference between the formulations is that the *fully coupled* formulation is solved implicitly using *Newton-Raphson* iterations to linearise the nonlinear problem during the calculation of a time step whereas the *fractional flow* formulation accounts for the nonlinearity by iterating between the two equations to be solved (pressure and saturation, Eq. 4.3 and 4.4) until the solution for the time step is converged. Here, the faster convergence behaviour of the Newton-Raphson iteration method causes the advantage in speed of the *fully coupled* formulation.

Combining accuracy and efficiency, the *fractional flow* formulation is the better choice to solve the one dimensional quasilinear hyperbolic *Buckley-Leverett* problem. It is slightly disadvantaged concerning the execution time for the nonlinear case with larger number of elements. However, it shows a considerably better approximation of the analytical solution. Concerning the *fully coupled* formulation, it has to be mentioned that even larger time steps might be applicable due to the implicit scheme which would be an advantage. However, a lower accuracy can be expected for this case. In the analysis of the *McWhorter* problem in

	cells	**15**	**30**	**60**	**120**
***fully coupled* f.**	**linear**	0.016	0.052	0.188	0.644
	Brooks-Corey	0.084	0.172	0.388	1.124
***fractional flow* f.**	**linear**	0.004	0.036	0.104	0.316
	Brooks-Corey	0.080	0.184	0.476	1.412

Table 4.4: Execution time [s].

	cells	**15**	**30**	**60**	**120**
execution time ratio	**FC-BC/FC-linear**	5.25	3.31	2.06	1.75
	FF-BC/FF-linear	20.00	5.11	4.58	4.47
	FF-linear/FC-linear	0.250	0.692	0.553	0.491
	FF-BC/FC-BC	0.732	1.070	1.227	1.256

Table 4.5: Some execution time ratios (fully coupled (FC), fractional flow (FF), *Brooks-Corey* (BC)).

Section 4.3 this advantage and disadvantage, respectively, is discussed.

4.2 Five-Spot Waterflood Problem

In analogy to the *Buckley-Leverett* problem, the *five-spot waterflood* problem is selected, describing the displacement of a non-wetting fluid by a wetting fluid in a two dimensional horizontal system. The assumptions of the *Buckley-Leverett* problem also hold for the *five-spot* problem:

- Capillary pressure effects are neglected.
- Gravity effects are neglected.
- There exist no sources or sinks.
- The fluids are incompressible and immiscible.
- The fluid viscosities are equal.
- The porous medium is homogeneous.

The resulting equations are the same as those derived for the *Buckley-Leverett* problem (Eq. 4.1 and 4.2, 4.3 and 4.4). Two different cases are formulated:

- Case 1: gradient diagonal to the grid (Fig. 4.13a).
- Case 2: gradient parallel to the grid (Fig. 4.13b).

These different cases can be used in order to quantify the numerically caused diffusion error, especially concerning numerical cross diffusion.

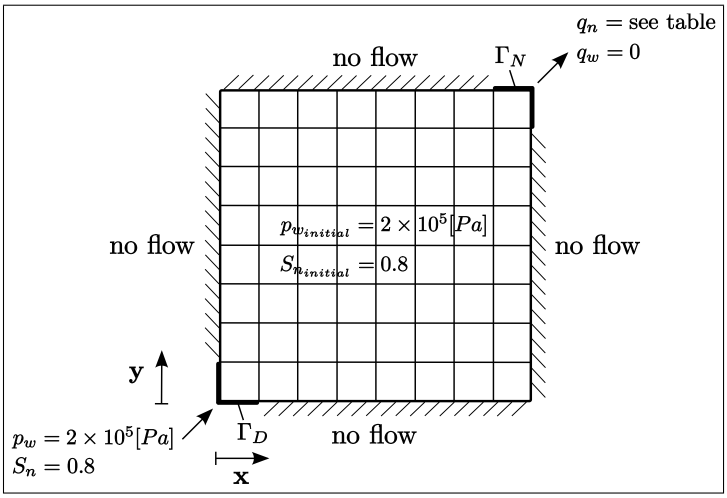

(a) case 1

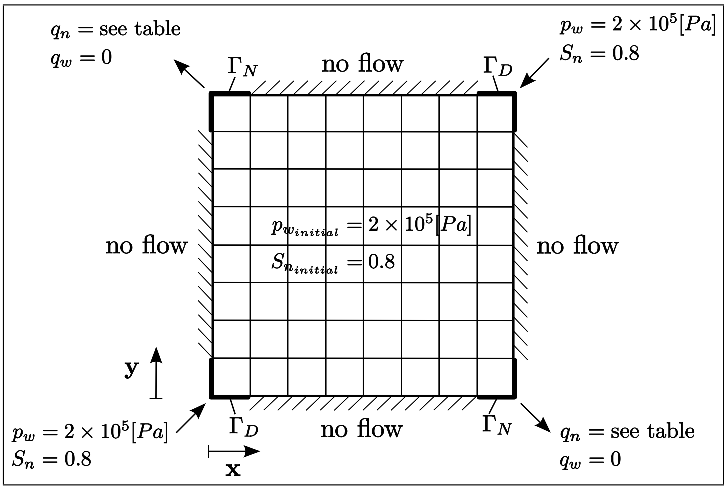

(b) case 2

Figure 4.13: *Five-spot* problem with initial and boundary conditions.

4.2.1 Calculations

The numerical simulations are carried out using a two dimensional equidistant grid of rectangular elements. The considered quadratic domain has a length and a width of 300 m. Different grids are used, the coarsest one consisting of 15 × 15 elements. Finer grids are constructed by bisecting all elements in each direction (Tab. 4.6). As described for the *Buckley-Leverett* problem the time step size which is given in Table 4.6 is determined as follows: First, a simulation is done applying the *fractional flow* formulation. Here, an automatic time step adaption is implemented using a *Courant-Friedrichs-Lewy* criterion (details, see [6]) for the explicit *Euler* time steps. The average time step of this simulation is then used as constant time step in the simulation using the *fully coupled* formulation.

The initial and boundary conditions for the two cases are given in Tables 4.7 and 4.8. For case 1, *Dirichlet* boundary conditions are set on the lower left corner of the domain and *Neumann* boundary conditions on the upper right corner of the domain (Fig. 4.13a). For case 2, *Dirichlet*

geometry	**length × width** [**m**]			
	300 × 300			
discretisation	**number of cells**	$\mathbf{\Delta x} = \mathbf{\Delta y}$ [**m**]	$\mathbf{\Delta t}$ [**s**]	
			fully coupled f.	**fractional flow f.**
	15 × 15	20	6×10^5	6×10^5 $(\varnothing)$
	30 × 30	10	1.5×10^5	1.5×10^5 $(\varnothing)$
	60× 60	5	3.75×10^4	3.75×10^4 $(\varnothing)$

Table 4.6: Geometry and discretisation.

boundary conditions are set on the lower left and on the upper right corner of the domain and *Neumann* boundary conditions on the lower right and on the upper left corner of the domain (Fig. 4.13b). No flow boundary conditions are used on the remaining boundaries (Fig. 4.13a and 4.13b). Initially, the domain is oil saturated. A linear as well as a *Brooks-Corey* relationship are selected to analyse the influence of the relative permeability-saturation relation on the solution. The corresponding parameters as well as other porous medium and fluid properties are shown in Table 4.9.

	parameter	**value**
boundary conditions case 1: 15 × 15 elements	**0 m ≤ x ≤ 20 m** und **0 m ≤ y ≤ 20 m**	
	water pressure $p_w = \bar{p}$	2×10^5 $[Pa]$
	oil saturation S_n	0.2 $[-]$
	280 m ≤ x ≤ 300 m und **280 m ≤ y ≤ 300 m**	
	flow rate of water q_w	0 $[kg/(m^2 s)]$
	flow rate of oil q_n	-1×10^{-3} $[kg/(m^2 s)]$
boundary conditions case 1: 30 × 30 elements	**0 m ≤ x ≤ 10 m** und **0 m ≤ y ≤ 10 m**	
	water pressure $p_w = \bar{p}$	2×10^5 $[Pa]$
	oil saturation S_n	0.2 $[-]$
	290 m ≤ x ≤ 300 m und **290 m ≤ y ≤ 300 m**	
	flow rate of water q_w	0 $[kg/(m^2 s)]$
	flow rate of oil q_n	-2×10^{-3} $[kg/(m^2 s)]$
boundary conditions case 1: 60 × 60 elements	**0 m ≤ x ≤ 5 m** und **0 m ≤ y ≤ 5 m**	
	water pressure $p_w = \bar{p}$	2×10^5 $[Pa]$
	oil saturation S_n	0.2 $[-]$
	295 m ≤ x ≤ 300 m und **295 m ≤ y ≤ 300 m**	
	flow rate of water q_w	0 $[kg/(m^2 s)]$
	flow rate of oil q_n	-4×10^{-3} $[kg/(m^2 s)]$
initial conditions	water pressure $p_w = \bar{p}$	2×10^5 $[Pa]$
	oil saturation S_n	0.8 $[-]$

Table 4.7: Initial and boundary conditions (case 1).

	Parameter	**Value**
boundary conditions case 2: 15×15 elements	$\mathbf{0\,m \le x \le 20\,m}$ und $\mathbf{0\,m \le y \le 20\,m}$, $\mathbf{280\,m \le x \le 300\,m}$ und $\mathbf{280\,m \le y \le 300\,m}$	
	water pressure $p_w = \bar{p}$	$2 \times 10^5\ [Pa]$
	oil saturation S_n	$0.2\ [-]$
	$\mathbf{280\,m \le x \le 300\,m}$ und $\mathbf{0\,m \le y \le 20\,m}$, $\mathbf{0\,m \le x \le 20\,m}$ und $\mathbf{280\,m \le y \le 300\,m}$	
	flow rate of water q_w	$0\ [kg/(m^2 s)]$
	flow rate of oil q_n	$-1 \times 10^{-3}\ [kg/(m^2 s)]$
boundary conditions case 2: 30×30 elements	$\mathbf{0\,m \le x \le 10\,m}$ und $\mathbf{0\,m \le y \le 10\,m}$, $\mathbf{290\,m \le x \le 300\,m}$ und $\mathbf{290\,m \le y \le 300\,m}$	
	water pressure $p_w = \bar{p}$	$2 \times 10^5\ [Pa]$
	oil saturation S_n	$0.2\ [-]$
	$\mathbf{290\,m \le x \le 300\,m}$ und $\mathbf{0\,m \le y \le 10\,m}$, $\mathbf{0\,m \le x \le 10\,m}$ und $\mathbf{290\,m \le y \le 300\,m}$	
	flow rate of water q_w	$0\ [kg/(m^2 s)]$
	flow rate of oil q_n	$-2 \times 10^{-3}\ [kg/(m^2 s)]$
boundary conditions case 2: 60×60 elements	$\mathbf{0\,m \le x \le 5\,m}$ und $\mathbf{0\,m \le y \le 5\,m}$, $\mathbf{295\,m \le x \le 300\,m}$ und $\mathbf{295\,m \le y \le 300\,m}$	
	water pressure $p_w = \bar{p}$	$2 \times 10^5\ [Pa]$
	oil saturation S_n	$0.2\ [-]$
	$\mathbf{295\,m \le x \le 300\,m}$ und $\mathbf{0\,m \le y \le 5\,m}$, $\mathbf{0\,m \le x \le 5\,m}$ und $\mathbf{295\,m \le y \le 300\,m}$	
	flow rate of water q_w	$0\ [kg/(m^2 s)]$
	flow rate of oil q_n	$-4 \times 10^{-3}\ [kg/(m^2 s)]$
initial conditions	water pressure $p_w = \bar{p}$	$2 \times 10^5\ [Pa]$
	oil saturation S_n	$0.8\ [-]$

Table 4.8: Initial and boundary conditions (case 2).

	parameter	**value**
fluid properties	water density ρ_w	1000 $[kg/m^3]$
	oil density ρ_n	1000 $[kg/m^3]$
	dyn. viscosity water μ_w	0.001 $[kg/(ms)]$
	dyn. viscosity oil μ_n	0.001 $[kg/(ms)]$
solid matrix properties and constitutive relationships	intrinsic permeability $\mathbf{K}$	10^{-7} $[m^2]$
	porosity Φ	0.2 $[-]$
	pore size distr. index λ	2.00 $[-]$
	res. saturation water S_{wr}	0.2 $[-]$
	res. saturation oil S_{nr}	0.2 $[-]$
	rel. permeability $k_r(S_w)$	linear/Brooks-Corey

Table 4.9: Fluid and porous medium properties.

Figures 4.14a to 4.15d show the contour lines of the saturation distribution of the diagonal case (case 1) and the parallel case (case 2) for a linear relative permeability-saturation relation after a period of 500 days. For the coarse as well as for the fine grid, it can be observed that the front approximation of the *fully coupled* formulation does not significantly differ from the approximation of the *fractional flow* formulation. The coarse grid shows no radial-symmetric front propagation. In fact, the saturation front becomes straightened because it is moving faster parallel to the boundaries. This can be seen more clearly in Figures 4.16a to 4.17b in which the saturation profiles along the diagonal of the domain and parallel to the lower boundary are plotted. As expected, numerical diffusion is decreasing resulting in the sharpening of the front if the grid is refined, corresponding to the results of Section 4.1. The differences according to the amount between the front velocity along the boundaries and along the diagonal of the domain also decrease if the elements are refined. Comparing the two cases, good agreement can be observed in Figures 4.14a to 4.15d. However, Figures 4.16a to 4.17b show that the differences between the diagonal and the parallel saturation profiles described before are a little more distinct for the parallel case (case 2).

The nonlinear case using a *Buckley-Leverett*-relative permeability-saturation function is shown in Figures 4.18a to 4.19d. Here, the *fractional flow* formulation results in a smoother saturation front than the *fully coupled* formulation. However, the contour lines only show an interpolation of the data calculated for the vertexes (*fully coupled*) and the cell centres (*fractional flow*), respectively. So the comparison between the vertex and cell based data strongly depends on how the interpolation is done in the visualisation tool. The interpolation of the cell centred data (*fractional flow*), done to achieve comparability to the vertex centred data, might smooth out unregularities. In accordance to the linear case, the radial symmetry of the distribution is improved for both formulations if the grid is refined. This means that according to their absolute value, the diagonal front velocity and the velocity parallel to the grid converge to each other.

Again, Figures 4.20a to 4.21b compare the saturation profiles along the diagonal of the domain to the profiles parallel to the boundaries. As mentioned before in Section 4.1 the saturation at the boundary of the domain is equal for both formulations. The differences which can be observed arise from the visualisation of the data, where the cell centred data resulting from

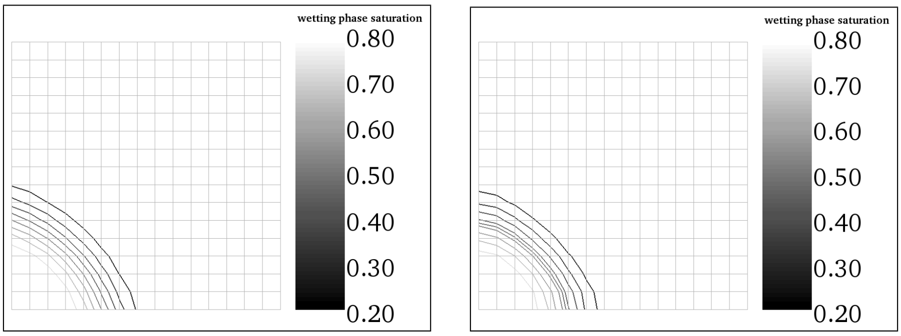

(a) case 1: *fully coupled* formulation (b) case 1: *fractional flow* formulation

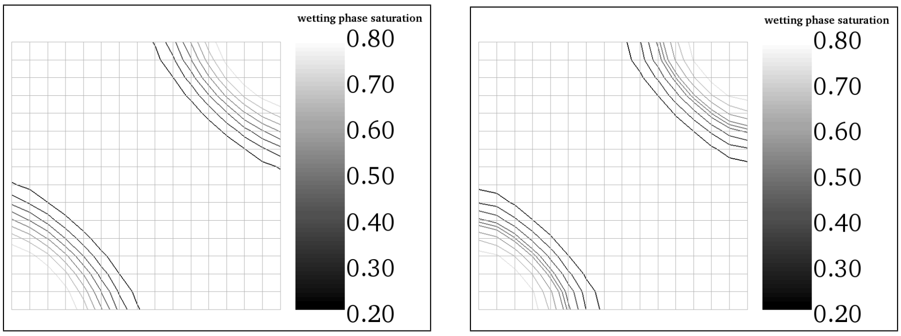

(c) case 2: *fully coupled* formulation (d) case 2: *fractional flow* formulation

Figure 4.14: 15 × 15 elements, $t = 500\,d$, linear.

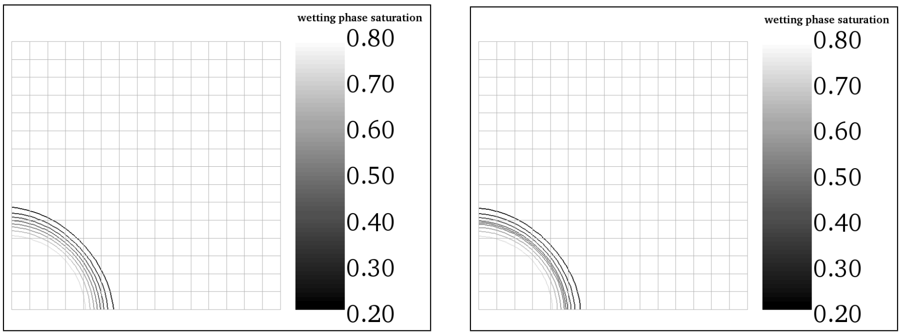

(a) case 1: *fully coupled* formulation (b) case 1: *fractional flow* formulation

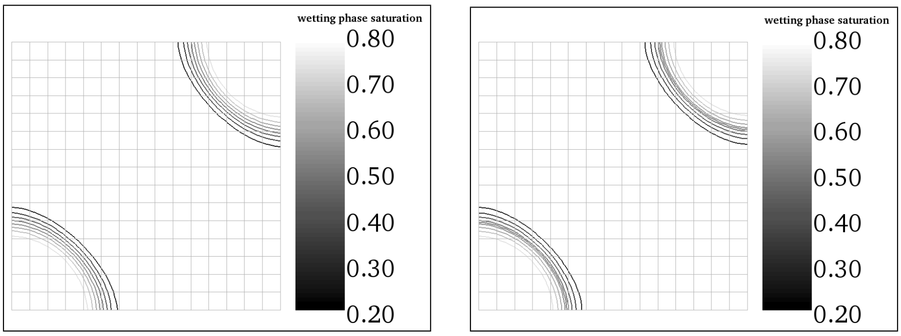

(c) case 2: *fully coupled* formulation (d) case 2: *fractional flow* formulation

Figure 4.15: 60 × 60 elements, $t = 500\,d$, linear.

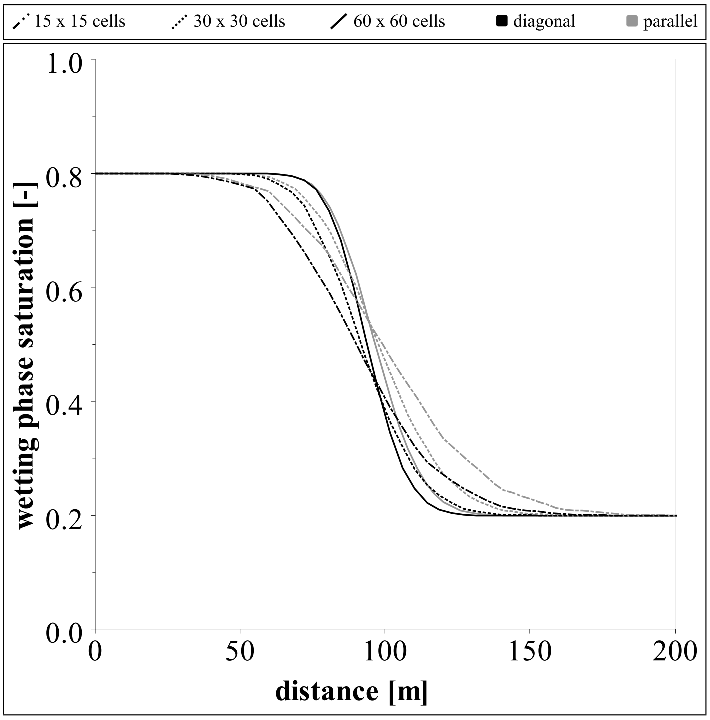

(a) case 1

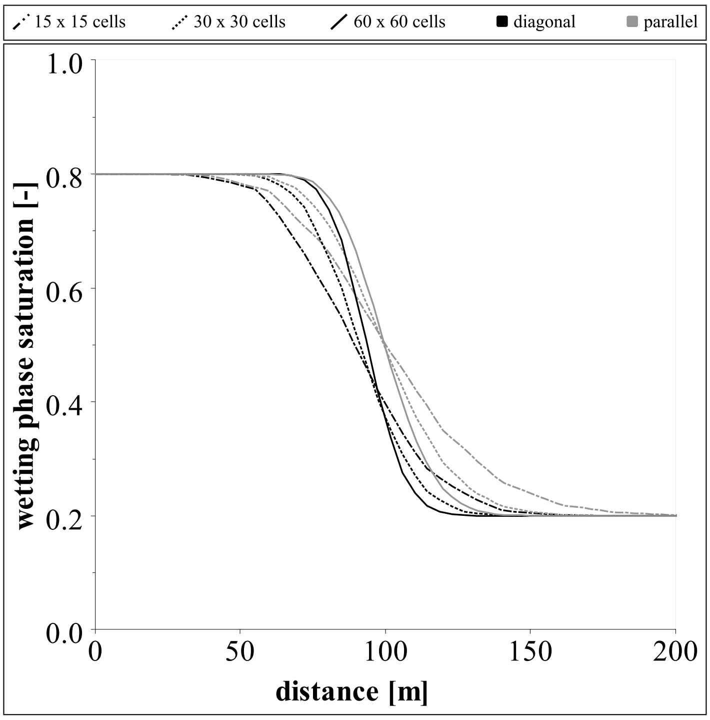

(b) case 2

Figure 4.16: Saturation profiles along the diagonal of the domain and parallel to the lower boundary (*fully coupled* formulation, linear).

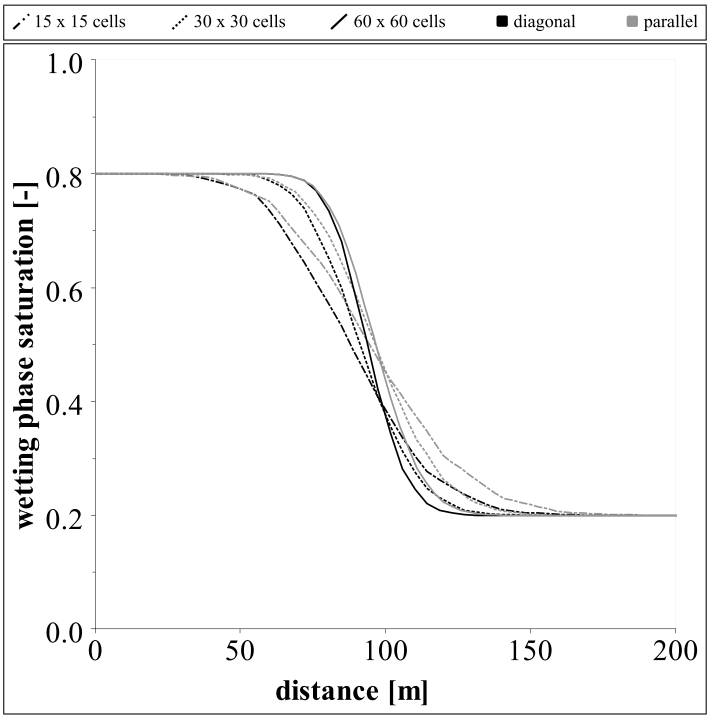

(a) case 1

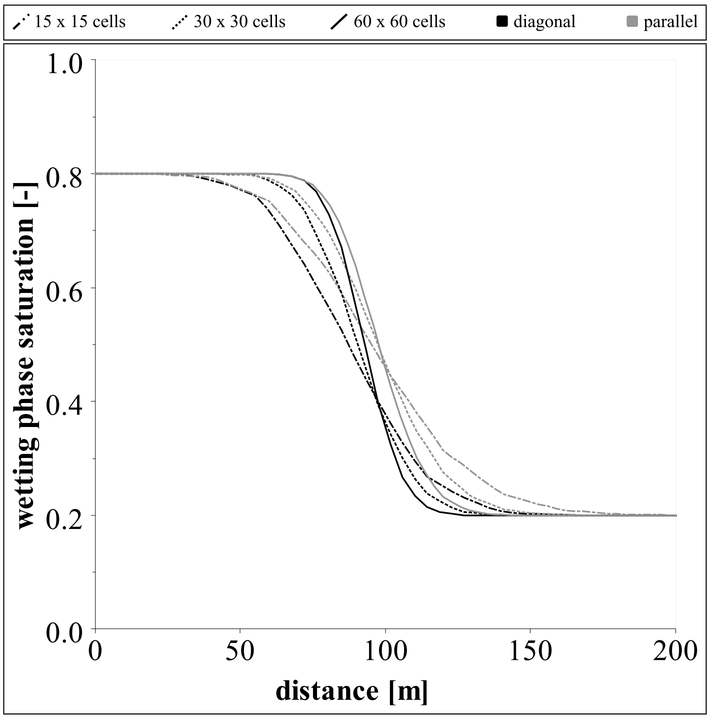

(b) case 2

Figure 4.17: Saturation profiles along the diagonal of the domain and parallel to the lower boundary (*fractional flow* formulation, linear).

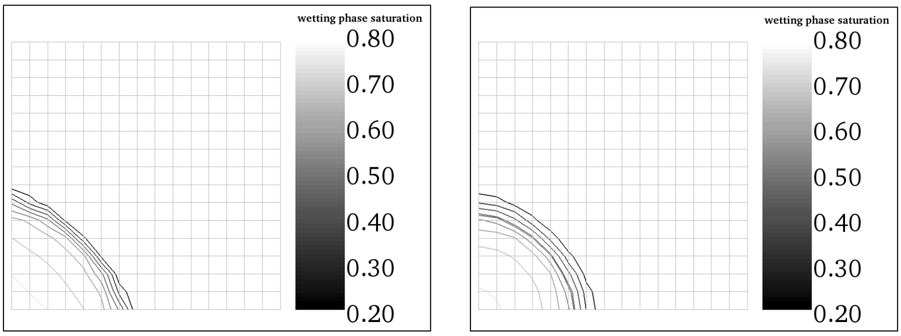

(a) case 1: *fully coupled* formulation (b) case 1: *fractional flow* formulation

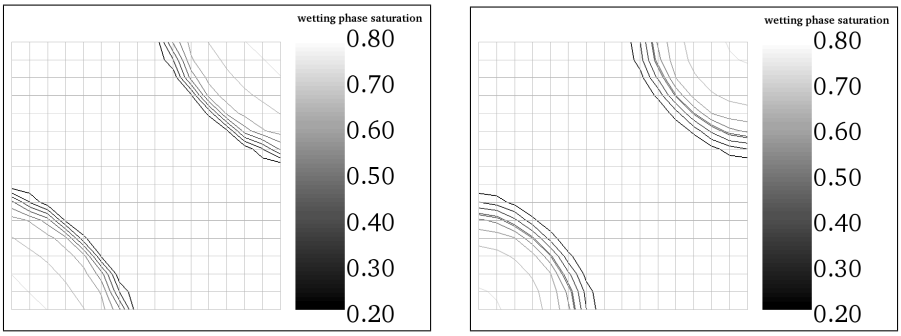

(c) case 2: *fully coupled* formulation (d) case 2: *fractional flow* formulation

Figure 4.18: 15 × 15 elements, $t = 500\,d$, *Brooks-Corey*.

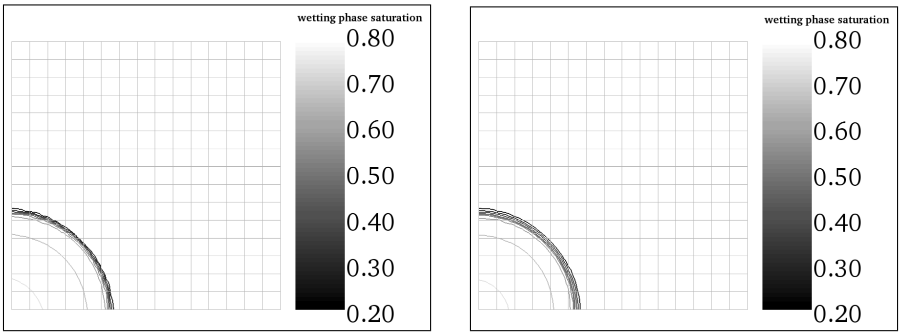

(a) case 1: *fully coupled* formulation (b) case 1: *fractional flow* formulation

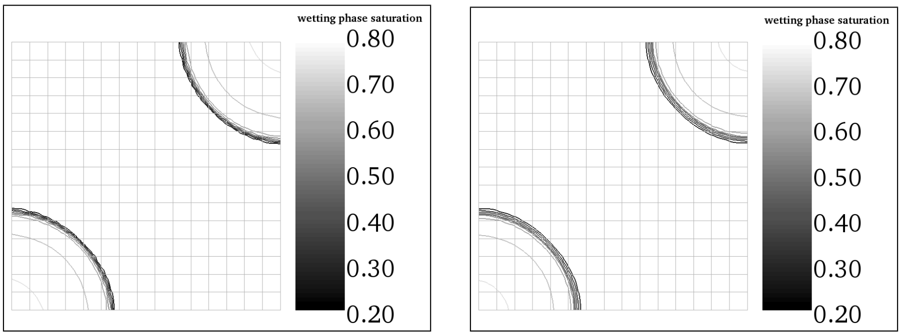

(c) case 2: *fully coupled* formulation (d) case 2: *fractional flow* formulation

Figure 4.19: 60 × 60 elements, $t = 500\,d$, *Brooks-Corey*.

the calculations with the *fractional flow* formulation are converted into point data. Similar to the linear case, the front is sharpening and thus, numerical diffusion is decreasing if the grid is refined. Contrary to the results of the one dimensional *Buckley-Leverett* problem (Ch. 4.1), it can be observed that the *fully coupled* formulation shows less smearing of the saturation front than the *fractional flow* formulation. According to their absolute values, differences of the diagonal front velocity and the velocity parallel to the boundaries are decreasing with increasing refinement level. For the nonlinear case, these differences are smaller than for the linear case (Fig. 4.16a to 4.17b). The diagonal saturation profile of case 1 using the finest grid is almost the same than the parallel one for both *fractional flow* and *fully coupled* formulation.

Figures 4.22a and 4.22b show a comparison of the saturation profiles along the diagonal of the domain for the different formulations and the different cases, and for two different grids. For the coarse grid, a small difference between the two formulations can be observed where the front of the *fully coupled* formulation is little faster than the front of the *fractional flow* formulation. The profiles of the two cases are almost equal for both formulations. The fine grid (Fig. 4.22b) shows pretty much the same profiles for both formulations and both cases.
The corresponding profiles using a nonlinear relative permeability-saturation relation are shown in Figures 4.23a and 4.23b. As described before, it can be observed that the *fully coupled* formulation shows less smearing of the saturation front and therefore less numerical diffusion. The profiles of the different cases show good agreement for both formulations on both grids.

The application of the *five-spot* problem to a diagonal grid (case 1) and a parallel grid (case 2) is done in order to quantify the effect of numerical diffusion and thus, the mesh dependency of different numerical methods. Especially, an influence of numerical cross diffusion can be analysed. As pointed out by *Helmig* [6], usual first order upwind methods do in general not account for diagonal effects in a sufficient way and cause cross diffusion. As mentioned in Section 3.4.1, if diagonal effects occur, higher order finite volumes schemes can even increase the numerical diffusion due to the upwinding depending on how the slope is calculated.

One measure for numerical cross diffusion is the kind of front propagation of the diagonal case (case 1) which should be radial symmetric without the cross diffusion. As pointed out before, this is not the case for the coarse grid independent on the used formulation or the used relative permeability-saturation relation. For the fine grid, the propagation is almost radial symmetric. This means that the numerical cross diffusion is dependent on the number and thus, on the size of the elements.
Unlike expected referring to the results of Section 4.1, the *fully coupled* formulation shows less smearing of the saturation front compared to the *fractional flow* formulation, especially for the nonlinear case. Additionally, the differences between the diagonal front velocity and the velocity parallel to the boundaries are a bit larger for the *fractional flow* formulation. From this, it follows that the fully upwind box method (Sec. 3.3) accounts in a better way for the diagonal gradient than the finite volume method (Sec. 3.4). One reason could be the cross diffusion introduced by the upwind scheme together with the higher order finite volume method as explained before. Another reason might be that the finite volume method corresponds to a five-spot scheme concerning the unknown (the saturation) (Fig. 3.2) whereas the box method corresponds to a nine-spot scheme (Fig. 3.1).

A second way to analyse the effect of cross diffusion is the kind of front propagation of the

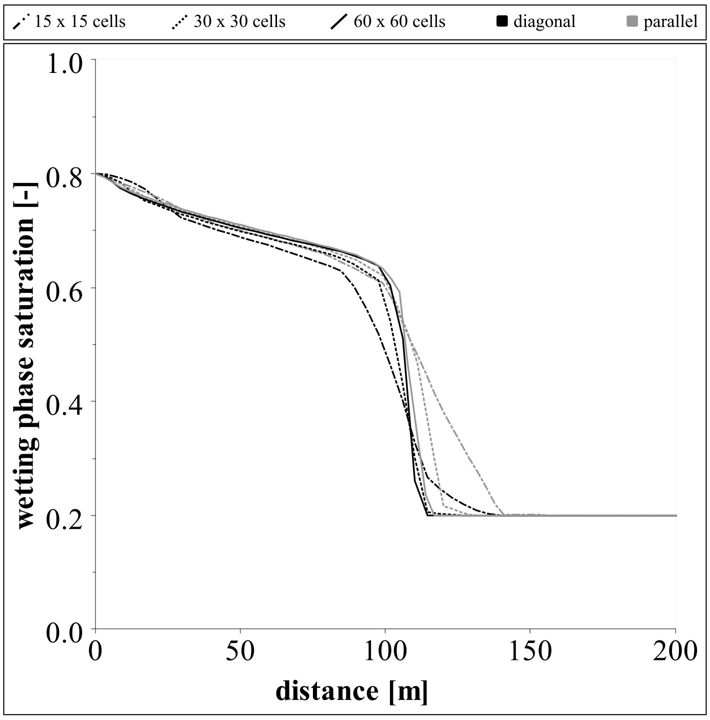

(a) case 1

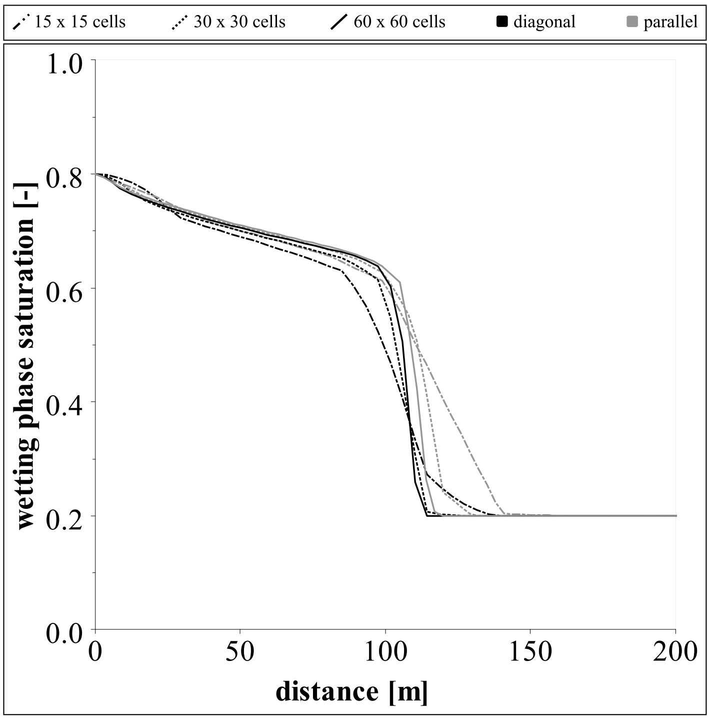

(b) case 2

Figure 4.20: Saturation profiles along the diagonal of the domain and parallel to the lower boundary (*fully coupled* formulation, *Brooks-Corey*).

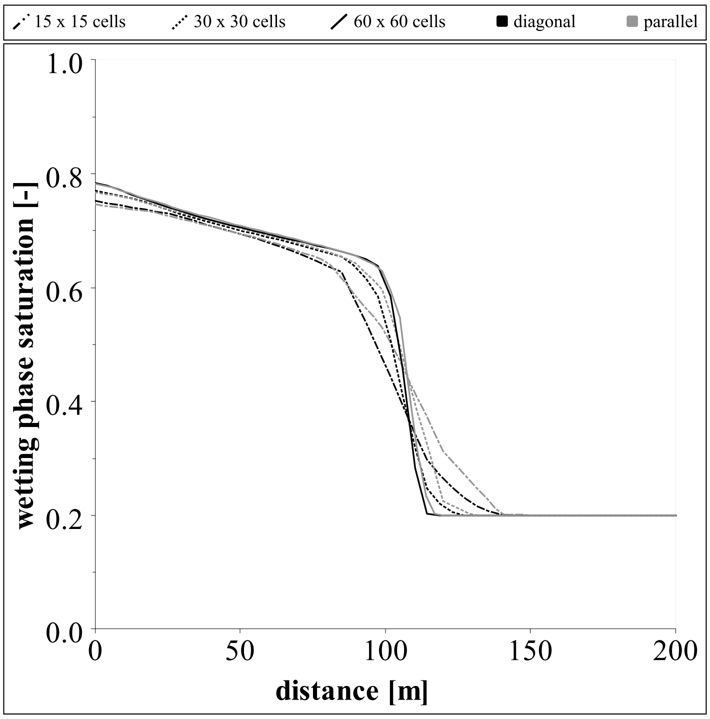

(a) case 1: *fractional flow* formulation

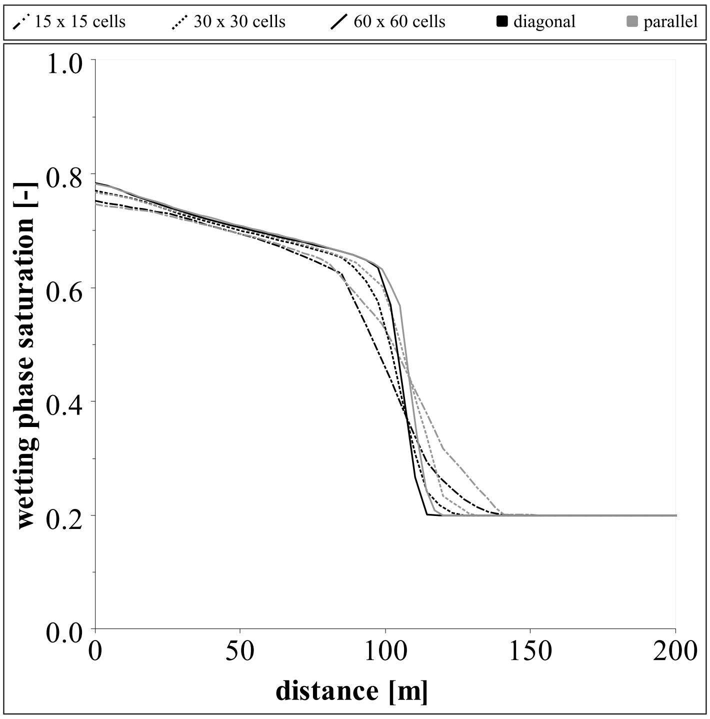

(b) case 2: *fractional flow* formulation

Figure 4.21: Saturation profiles along the diagonal of the domain and parallel to the lower boundary (*fractional flow* formulation, *Brooks-Corey*).

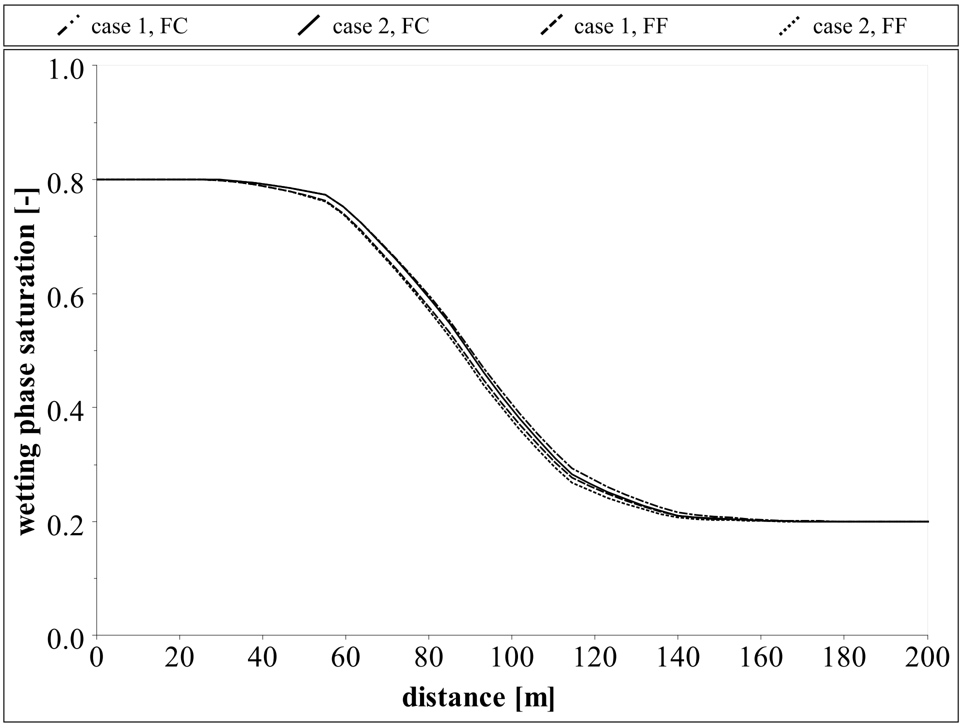

(a) 15 × 15 elements

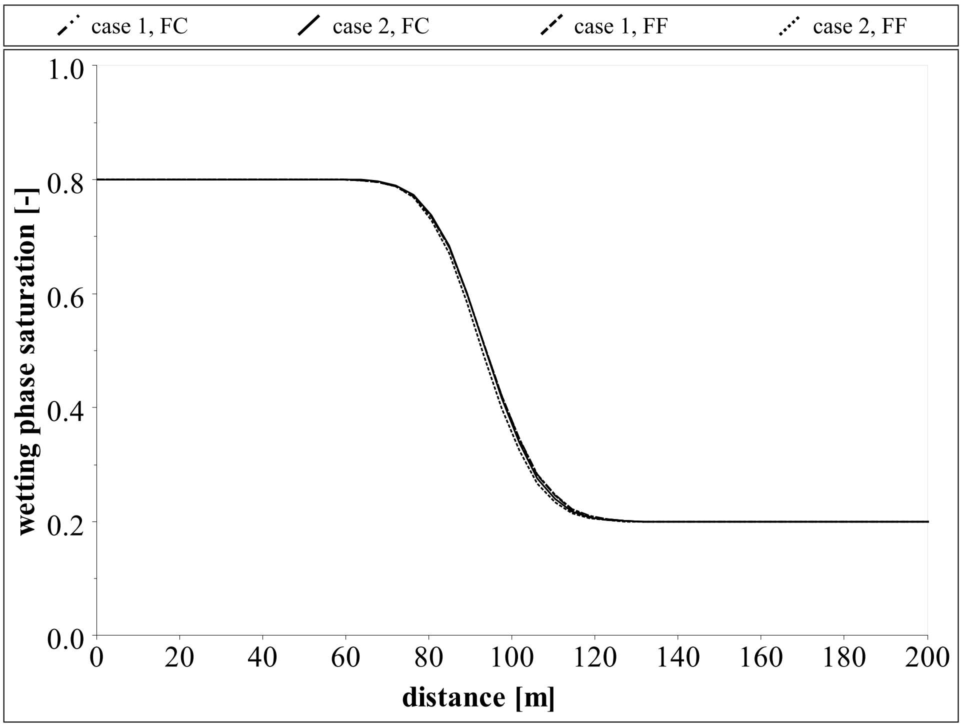

(b) 60 × 60 elements

Figure 4.22: Saturation profiles along the diagonal of the domain(*fully coupled* formulation (FC), *fractional flow* formulation (FF), linear).

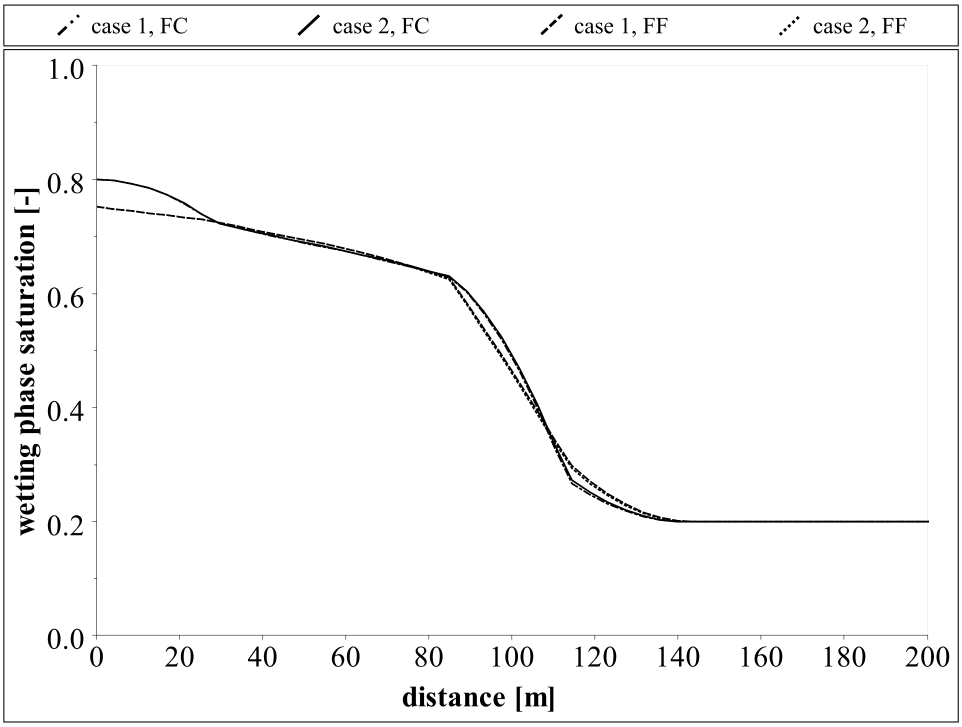

(a) 15 × 15 elements

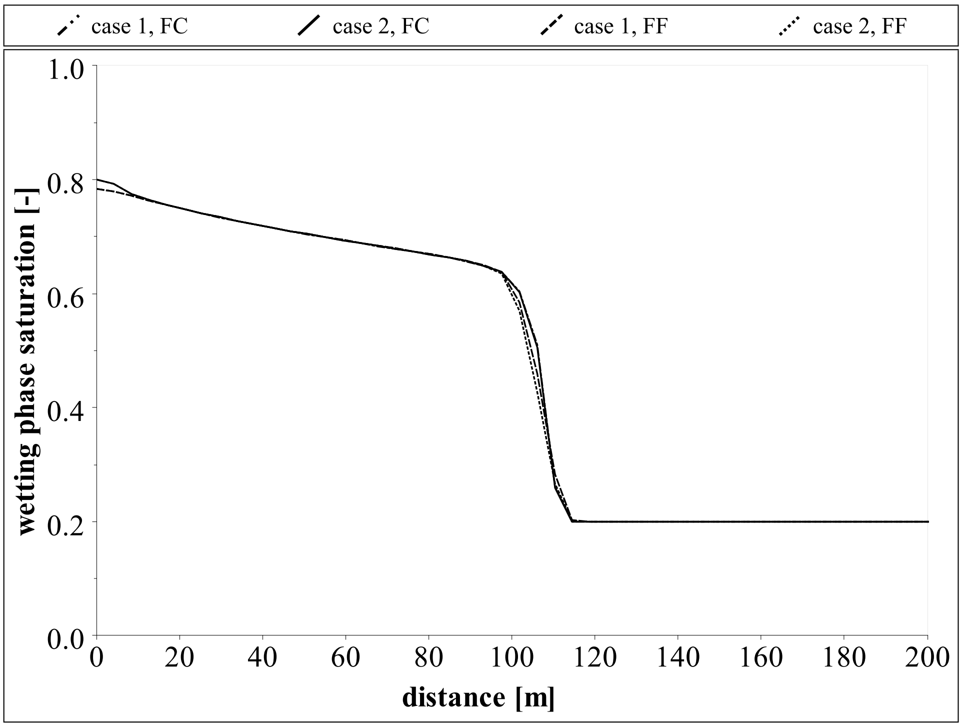

(b) 60 × 60 elements

Figure 4.23: Saturation profiles along the diagonal of the domain (*fully coupled* formulation (FC), *fractional flow* formulation (FF), *Brooks-Corey*).

	cells	**15 × 15**	**30 × 30**	**60 × 60**
***fully coupled* f.**	**linear**	5.304	98.190	2069.133
	Brooks-Corey	5.476	101.422	2174.948
***fractional flow* f.**	**linear**	2.180	33.038	545.498
	Brooks-Corey	15.357	219.294	4064.898

Table 4.10: Execution time $[s]$ (case 1).

parallel case (case 2) which should also be radial symmetric without the cross diffusion at least if the two fronts have not yet moved to far into the domain. The results are comparable to case 1. For the fine grid the propagation is almost radial symmetric whereas this is not the case for the coarse grid, independent on the used formulation or the used relative permeability-saturation relation. This means that also for case 2 the numerical cross diffusion is dependent on the number and thus on the size of the elements.

The comparison of the saturation profiles in the different directions shows that the front is moving faster along the boundary for both cases. For case 2, the differences between these front velocities according to their absolute values are even more distinct than for case 1. This can especially be observed for the linear relative permeability-saturation relation. Comparing the different formulations concerning the smearing of the front, the same effect as discussed for case 1 can be observed.

Finally, a comparison of the diagonal case (case 1) and the parallel case (case 2) can be done. If a method is totally independent on the direction of the gradient, the same results should be provided for both cases. As observed before, in general, good agreement can be achieved for the two cases, independent of the formulation. However, as pointed out for case 2, the differences between the front velocities in diagonal and parallel direction according to their absolute value are more distinct than for case 1.

Both used methods (*fully coupled* formulation - box method, *fractional flow* formulation - finite volumes/higher order finite volumes) are mesh dependent concerning the direction of the occurring gradients. The effect of this mesh dependency can be reduced by a refinement of the grid. The *fully coupled* formulation shows less numerical diffusion especially in diagonal direction. Most likely, as mentioned before, the reason for this is that more nodes in diagonal direction are taken into account for the box method. The higher order finite volume method adds additional information but only in grid direction and not diagonal to the grid.

To appraise the efficiency of the different formulations and the corresponding numerical methods, the execution time is measured. The results are shown in Tables 4.10 and 4.11. As can be seen, wide differences appear for the two dimensional case. For a linear relative permeability-saturation function and a grid of 15 × 15 elements, the calculation needs between 2 and 3 seconds whereas for a calculation using a nonlinear relative permeability-saturation relation and a grid of 60 × 60 elements, around 4100 seconds ($\cong 1.14\,h$) are needed.

To achieve a better comparability, some execution time ratios are calculated and shown in Tables 4.12 and 4.13. As the two cases of the *five-spot* problem behave similarly concerning the execution time, it is not further differentiated between these cases.

The first two ratios (FC-BC/FC-linear, FF-BC/FF-linear) relate the execution time of the nonlinear case to the execution time of the linear case. For both twophase flow formulations,

	cells	**15 × 15**	**30 × 30**	**60 × 60**
***fully coupled* f.**	**linear**	5.344	102.702	2116.432
	Brooks-Corey	5.612	105.595	2218.699
***fractional flow* f.**	**linear**	2.436	32.245	552.334
	Brooks-Corey	14.645	223.718	4125.658

Table 4.11: Execution time [s] (case 2).

the ratios are greater than one. Thus, the calculations are faster using a linear relative permeability-saturation relation. However, a wide difference can be observed between the two twophase formulations. The ratio of the *fully coupled* formulation (FC-BC/FC-linear) ranges around one which means that there are no notable differences concerning the execution time between the linear and the nonlinear case. For the *fractional flow* formulation the calculations using a linear relative permeability-saturation function are 6 to 7.5 times faster than the calculations using a nonlinear relation.
The third and fourth ratio (FF-linear/FC-linear, FF-BC/FC-BC) relate the execution times of the different twophase flow formulations to each other. For the linear case, the ratio is always smaller than one. This shows that the *fractional flow* formulation is always faster than the *fully coupled* formulation in this case. Further, the ratio (FF-linear/FC-linear) is decreasing with increasing element number which means that the execution time using the *fully coupled* formulation is increasing stronger with increasing element number than the time using the *fractional flow* formulation. The ratio of the nonlinear case (FF-BC/FC-BC) is also decreasing with increasing element numbers. As can be seen, however, it is also greater than one. Therefore, the *fully coupled* formulation is faster than the *fractional flow* formulation for the nonlinear relative permeability-saturation relation. This is consistent with the results of the *Buckley-Leverett* problem. The implicit solution method implemented for the *fully coupled* formulation using Newton-Raphson iterations to linearise the nonlinear problem shows a faster convergence behaviour than the IMPES scheme applied for the *fractional flow* formulation if nonlinear constitutive relationships are used. However, with increasing element number the time needed for each iteration does stronger affect the execution time. Therefore, the advantage arising of a smaller number of iteration steps is damped.

Combining the results of the discussions carried out concerning the accuracy and the efficiency, it has to be differentiated depending on the relative permeability-saturation function which is used.
For calculations applying a linear relative permeability-saturation relation, the *fractional flow* formulation is the one to choose. The two formulations show comparable results concerning the accuracy, but the *fractional flow* formulation is considerably less expansive concerning computational time.
In case of a nonlinear relative permeability-saturation function, the *fully coupled* formulation shows advantages concerning both accuracy and efficiency. It introduces less numerical diffusion than the *fractional flow* formulation. Additionally, it is more efficient in the linearisation of the nonlinear problem and thus less expansive concerning computational time.
As introduced, the terms *fully coupled* formulation and *fractional flow* formulation imply the mathematical model as well as the according numerical method.

	cells	**15 × 15**	**30 × 30**	**60 × 60**
execution time ratio	**FC-BC/FC-linear**	1.032	1.033	1.051
	FF-BC/FF-linear	7.044	6.462	7.452
	FF-linear/FC-linear	0.411	0.346	0.264
	FF-BC/FC-BC	2.804	2.162	1.869

Table 4.12: Some execution time ratios for case 1 (fully coupled (FC), fractional flow (FF), *Brooks-Corey* (BC)).

	cells	**15 × 15**	**30 × 30**	**60 × 60**
execution time ratio	**FC-BC/FC-linear**	1.050	1.028	1.048
	FF-BC/FF-linear	6.012	6.938	7.469
	FF-linear/FC-linear	0.456	0.314	0.261
	FF-BC/FC-BC	2.609	2.119	1.859

Table 4.13: Some execution time ratios for case 2 (fully coupled (FC), fractional flow (FF), *Brooks-Corey* (BC)).

4.3 McWhorter Problem

Like the *Buckley-Leverett* problem, the *McWhorter* problem describes the instationary, one-dimensional displacement of oil by water in a horizontal system(Fig. 4.24). Contrary to the *Buckley-Leverett* problem, capillary pressure effects are taken into account. The configuration of the *McWhorter* problem illustrated in Figure 4.24 leads to a countercurrent displacement where the flow is purely driven by capillary forces. This allows for the examination of a diffusion dominated flow system described by parabolic differential equations. The assumptions made for the *McWhorter* problem are:

- Gravity effects are neglected.
- There exist no sources or sinks.
- The fluids are incompressible and immiscible.
- The fluid viscosities are equal.
- The porous medium is homogeneous.

With these assumptions, the *fully coupled* p_n-S_w formulation (Eq. 3.8) yields:

$$L_w(p_n, S_w) := \phi \frac{\partial S_w}{\partial t} - \nabla \cdot (\lambda_w \mathbf{K}(\nabla p_n - \nabla p_c)) = 0, \tag{4.11}$$

$$L_n(p_n, S_w) := -\phi \frac{\partial S_w}{\partial t} - \nabla \cdot (\lambda_n \mathbf{K} \nabla p_n) = 0. \tag{4.12}$$

Further, the equations of the *global pressure fractional flow* formulation can be simplified as

$$-\nabla \cdot (\lambda_t \mathbf{K} \nabla \bar{p}) = 0, \tag{4.13}$$

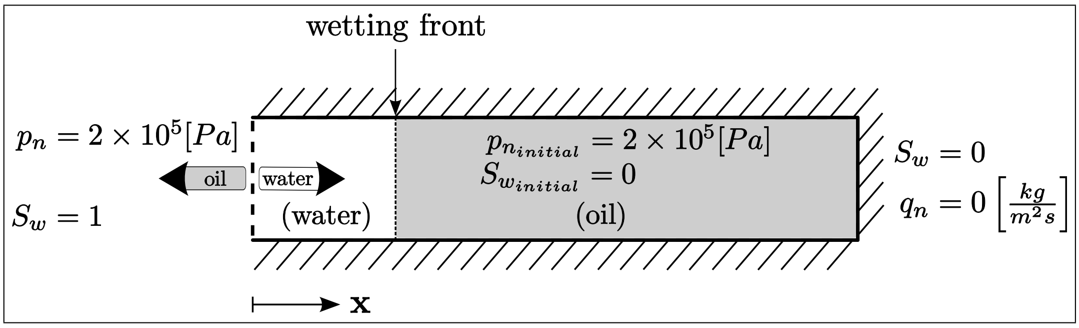

Figure 4.24: *Buckley-Leverett* problem with initial and boundary conditions.

and

$$\phi \frac{\partial S_w}{\partial t} + \nabla \cdot \left(f_w \mathbf{v}_t + \bar{\lambda} \nabla p_c \right) = 0. \tag{4.14}$$

According to Equation (3.32), Equation (4.14) can also be formulated as

$$\phi \frac{\partial S_w}{\partial t} + \mathbf{v}_t \frac{d\,f_w}{d\,S_w} \nabla S_w + \nabla \cdot \left(\bar{\lambda} \frac{d\,p_c}{d\,S_w} \nabla S_w \right) = 0. \tag{4.15}$$

Finally, applying the above assumptions to the *phase pressure fractional flow* formulation, the pressure equation in terms of the non-wetting phase pressure p_n (Eq. 3.22) can be rewritten as

$$\nabla \cdot \left[\lambda_t \mathbf{K} \left(\nabla p_n - f_w \nabla p_c \right) \right] = 0, \tag{4.16}$$

with the corresponding saturation equation

$$-\phi \frac{\partial S_w}{\partial t} + \nabla \cdot \left(f_n \mathbf{v}_{n_{mod}} \right) = 0. \tag{4.17}$$

4.3.1 Analytical solution

A quasi-analytical solution for the computation of the *McWhorter* problem using the concept of a fractional flow formulation has been derived by *McWhorter* and *Sunada* [9]. They define a *fractional flow function* which for countercurrent displacement of a non-wetting phase is finally formulated as

$$F(S_w) = 1 - \left(\int_{S_w}^{S_0} \frac{(\beta - S_w)\mathbf{D}}{F} \, d\beta \right) \cdot \left(\int_{S_i}^{S_0} \frac{(S_w - S_i)\mathbf{D}}{F} \, dS_w \right)^{(-1)} \tag{4.18}$$

where $F = F(x,t) = \frac{q_w}{q_0}$, q_w is the volume flux of the wetting phase, $q_0 = q_w(x = 0, t)$, t is the the actual time, S_0 is the wetting phase saturation at $x = 0$ and S_i is the initial wetting phase saturation. $\mathbf{D}$ represents the dispersion tensor $\mathbf{D}(S_w) = \bar{\lambda} \mathbf{K} \frac{dp_c}{dS_w}$ (compare Eq. 4.15). Further, the derivative

$$F'(S_w) = \frac{\partial F(S_w)}{\partial S_w} = \left(\int_{S_w}^{S_0} \frac{\mathbf{D}}{F} \, d\beta \right) \cdot \left(\int_{S_i}^{S_0} \frac{(S_w - S_i)\mathbf{D}}{F} \, dS_w \right)^{(-1)} \tag{4.19}$$

geometry	**length** [**m**]
	2.6

	number of cells	$\mathbf{\Delta x}$ [**m**]	$\mathbf{\Delta t}$ [**s**]	
			fully coupled f.	**classical/global pressure fractional flow f.**
discretisation	26	0.1	22	22 (∅)
			100	-
	52	0.05	4	4 (∅)
			100	-
	104	0.025	1	1 (∅)
			10	-
	208	0.0125	1	-

Table 4.14: Geometry and discretisation.

is formulated. The analytical solution is then expressed by

$$x(S_w, t) = \frac{2A}{\Phi} F'(S_w) t^{\left(-\frac{1}{2}\right)}, \tag{4.20}$$

with the porosity Φ and

$$A^2 = \frac{\Phi}{2} \int\limits_{S_i}^{S_0} \frac{(S_w - S_i)\mathbf{D}}{F} \, dS_w. \tag{4.21}$$

The unknown function $F(S_w)$ can be computed iteratively from the integral equation (Eq. 4.18) where the integrals have to be solved numerically. Thus, the analytical solution is also termed quasi-analytical solution. Iteration schemes are provided by *McWhorter* and *Sunada* [9] and by *Fučík et al.* [5] who also propose a modified method to avoid instabilities of the iterative process. The modified iterative scheme of *Fučík et al.* [5] is used to obtain the analytical solutions shown in the following section.

4.3.2 Calculations

A one dimensional domain with a length of 2.6 m is considered in the numerical simulations. Different grids are used, the coarsest one consisting of 26 elements and the finest one consisting of 104 elements (Tab. 4.14). The time step size is determined as described for the *Buckley-Leverett* problem (Sec. 4.1.2). For the *fully coupled* formulation, an additional, constant time step $\Delta t = 100\ s$ is chosen to test the dependency on the time step (Tab. 4.14).

The initial and boundary conditions are given in Table 4.15. The domain is initially oil saturated. For reasons of numerical stability, a linear saturation distribution is initially assumed close to the left boundary. On the left side of the domain ($x = 0\ m$) *Dirichlet* boundary conditions are set. *Neumann* boundary conditions are defined for the non-wetting phase and *Dirichlet* boundary conditions for the wetting phase on the right side of the domain ($x = 2.6\ m$)(Fig. 4.24). As capillary effects occur, the global pressure $\bar{p}$ and the non-wetting phase pressure p_n are no longer equal. But it can be shown that for $S_w = 1 - S_{nr}$, which is the case at the left boundary, $\bar{p} = p_n - p_c(S_w)$ (see [1]). A *Brooks-Corey* relationship is selected

	parameter	value
boundary conditions	**$\mathbf{x = 0\,m}$**	
	oil pressure p_n	2×10^5 $[Pa]$
	global pressure $\bar{p}$	1.95×10^5 $[Pa]$
	water saturation S_w	1 $[-]$
	$\mathbf{x = 2.6\,m}$	
	water saturation S_w	0 $[-]$
	flow rate of oil q_n	0 $[kg/(m^2 s)]$
initial conditions	water pressure p_n	2×10^5 $[Pa]$
	global pressure $\bar{p}$	1.95×10^5 $[Pa]$
	water saturation S_w	0 $[-]$

Table 4.15: Initial and boundary conditions.

	parameter	value
fluid properties	water density ρ_w	1000 $[kg/m^3]$
	oil density ρ_n	1000 $[kg/m^3]$
	dyn. viscosity water μ_w	0.001 $[kg/(ms)]$
	dyn. viscosity oil μ_n	0.001 $[kg/(ms)]$
solid matrix properties and constitutive relationships	intrinsic permeability $\mathbf{K}$	10^{-10} $[m^2]$
	porosity Φ	0.3 $[-]$
	pore size distr. index λ	2.00 $[-]$
	entry pressure p_d	5000 $[Pa]$
	res. saturation water S_{wr}	0 $[-]$
	res. saturation oil S_{nr}	0 $[-]$
	rel. permeability $k_r(S_w)$	Brooks-Corey

Table 4.16: Fluid and porous medium properties.

as relative permeability-saturation relation. Table 4.16 shows the corresponding parameters as well as other porous medium and fluid properties.
As for the *Buckley-Leverett* problem, an error with respect to the analytical solution is calculated in order to compare the results of the numerical experiments and to estimate the accuracy of the approximation. The analytical solution itself is calculated simultaneously during the numerical simulation and on the corresponding simulation grid. A weighted averaged error is calculated for each time step as defined by Equation (4.10) (Sec. 4.1.2).
The calculations are only carried out for the *fully coupled* and the *global pressure fractional flow* formulation. Applying the present discretisation scheme (Sec. 3.4), the *phase pressure fractional flow* formulation expressed by Equations (4.16) and (4.17) is not able to solve the *McWhorter* problem since the time steps become to small and the number of internal iterations between the two equations too large.

Figures 4.25a and 4.25b compare the results of the simulations using the different formulations

and different grids to the analytical solution. On average, equal time step sizes are used for both kinds of twophase flow formulations. It can be observed that the *fully coupled* formulation shows a stronger dependence on the element size than the *global pressure fractional flow* formulation. The numerical diffusion introduced by the upwinding considerably adds to the modelled physical diffusion which leads to a faster propagation of the wetting phase. If the grid is refined, the approximation using the *fully coupled* formulation converges to the analytical solution (Fig. 4.25a). To show this the grid is refined once more compared to the finest grid used for the *global pressure fractional flow* formulation. However, the *fully coupled* formulation tends to systematically overestimate the speed of the propagation front due to the upwinding.
The *global pressure fractional flow* formulation generates less numerical diffusion. The reason is the central differencing scheme which is implemented here for the diffusive terms (Sec. 3.4.1). This scheme better accounts for the purely diffusive character of the problem than an upwind scheme. As can be seen in Figure 4.25b, the *global pressure fractional flow* formulation shows an approximation almost equal to the exact solution, especially, for the fine grids where the grid is only refined twice for this formulation. Further refinement would lead to very small time steps to fulfil the *Courant* criterion and to ensure numerical stability. As mentioned during the discussion of the *Buckle-Leverett* problem (Sec. 4.1), differences of the saturations at the left boundary of the domain, which can be observed, arise from the visualisation of the data, where the cell centred data resulting from the calculations with the *fractional flow* formulation are converted into point data.

The weighted averaged error of the numerical approximations of the saturation distribution discussed above is shown in Figures 4.26a and 4.26b. The oscillations have already been discussed in Section 4.1. It can be observed that for both formulations the error converges to a quasi constant level. Furthermore, the error decreases if the element size is decreased. This is demonstrated more clearly in Figure 4.3.2 which shows the weighted averaged error averaged over time. It can be observed that the error of both, *fully coupled* formulation as well as *global pressure fractional flow* formulation can be reduced and therefore, the accuracy can be raised if the grid is refined. The *global pressure fractional flow* formulation, however, shows a much smaller error for all compared grids. Even on the finest grid used for the *fully coupled* formulation which is refined once more compared to the finest grid of the *global pressure fractional flow* formulation, the error can hardly be reduced below the error level achieved by using the coarsest grid with the *global pressure fractional flow* formulation. This is consistent with what has been pointed out before concerning the saturation profiles.

Finally, the solution of the *fully coupled* formulation is considered concerning the dependence on the time step size. Figure 4.28 shows the solution of the *McWhorter* problem using one constant time step for all grid types except for the finest grid which is five to ten times larger than the time steps chosen before, depending on the grid refinement level. But as can be observed, the results shown in Figure 4.28 are exactly equal to those shown before in Figure 4.25a. This is especially important for the evaluation of the efficiency.

To analyse the efficiency of the different formulations and the corresponding numerical methods, the execution time is measured and shown in Table 4.17. The *global pressure fractional flow* formulation is faster than the *fully coupled* formulation for all grids if the same averaged time step size is used where the differences are relatively small compared to the execution time. This is shown more clearly in Table 4.18. The ratio GPFF/FC($\Delta t(GPFF)$) is almost

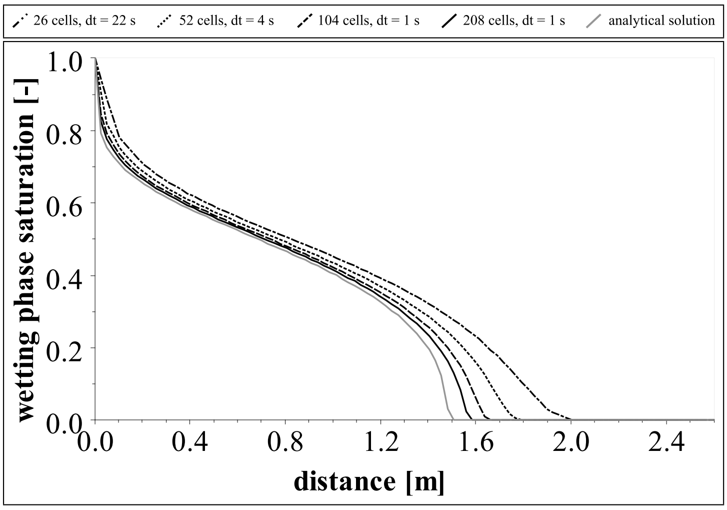

(a) *fully coupled* formulation

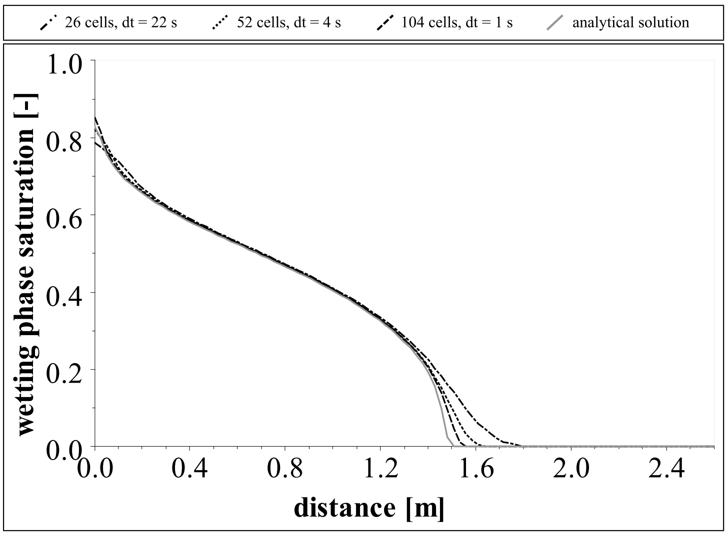

(b) *global pressure fractional flow* formulation

Figure 4.25: Saturation profiles of the *McWhorter* problem at $t = 10000\,s$ for different number of cells.

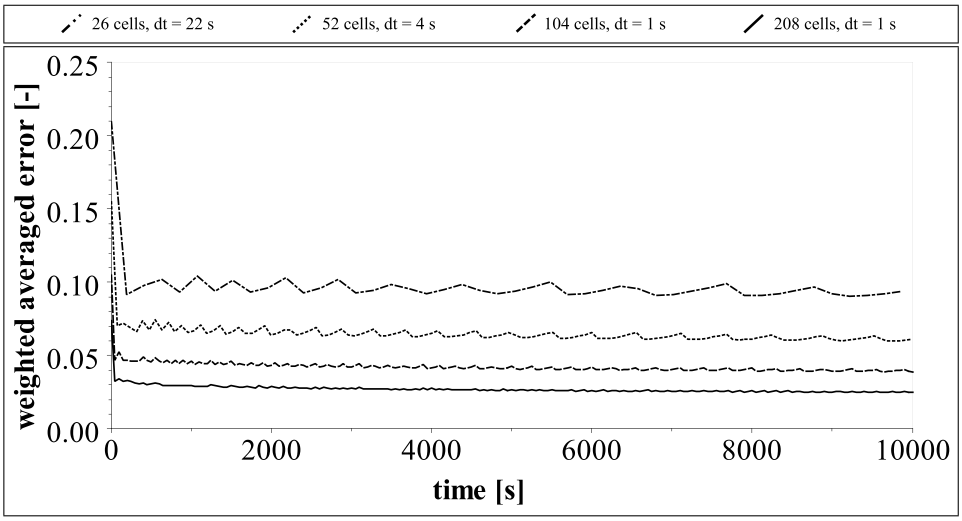

(a) *fully coupled* formulation

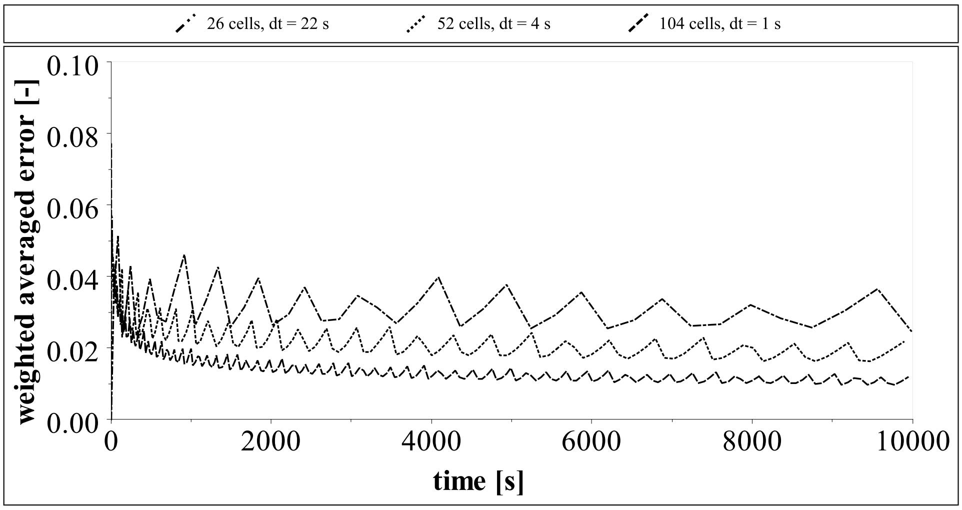

(b) *global pressure fractional flow* formulation

Figure 4.26: Weighted averaged error over time for different number of cells.

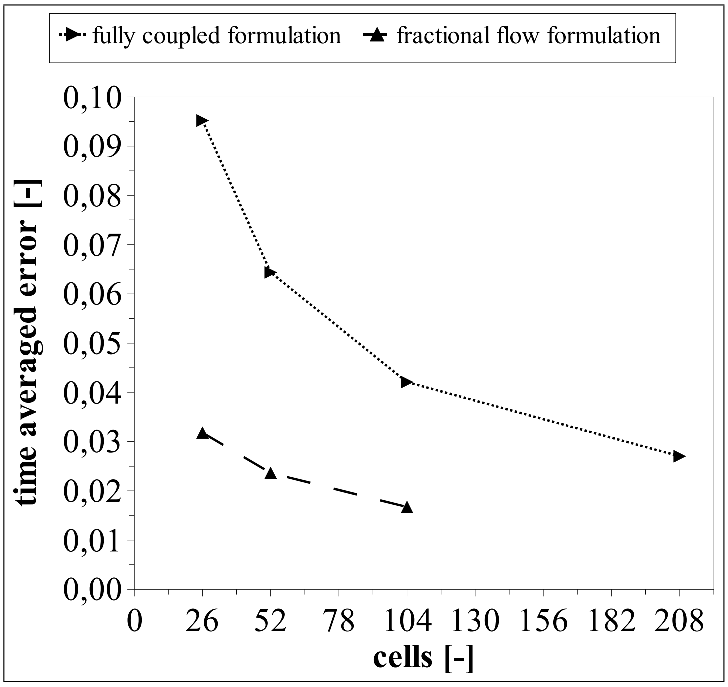

Figure 4.27: Time averaged error of the different formulations over number of cells.

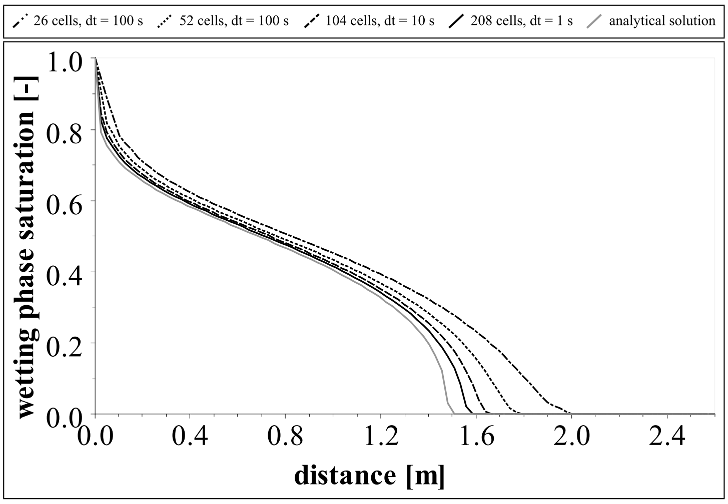

Figure 4.28: Saturation profiles for different number of cells with a constant time step $\Delta t = 100\,s$ at $t = 10000\,s$ (*fully coupled* formulation).

	cells	**26**	**52**	**104**	**208**
FC	$\Delta t = \Delta t(GPFF)$	14.949	90.478	416.110	654.373
	$\Delta t = 100\,s$	4.176	6.444	52.747 ($\Delta t = 10\,s$)	654.373 ($\Delta t = 1\,s$)
GPFF	$\Delta t = \Delta t(GPFF)$	12.945	81.469	362.507	-

Table 4.17: Execution time [s] (*fully coupled* formulation (FC), *classical/global pressure fractional flow* formulation (GPFF)).

	cells	**26**	**52**	**104**
execution time ratio	**GPFF/FC**($\Delta t(GPFF)$)	0.866	0.900	0.871
	GPFF/FC($\Delta t = 100\,s$)	3.100	12.642	6.873 ($\Delta t = 10\,s$)

Table 4.18: Execution time ratios (*fully coupled* formulation (FC), *classical/global pressure fractional flow* formulation (GPFF)).

constant and shows that the *global pressure fractional flow* formulation is around 10 % faster. However, larger time steps are allowed for the *fully coupled* formulation and the execution times needed using a time step $\Delta t = 100\,s$ are considerably shorter than the times needed for the calculations with the *global pressure fractional flow* formulation discussed before (Tab. 4.17). Accordingly, the ratio GPFF/FC($\Delta t = 100\,s$) is always greater than one. Furthermore, it is increasing fast if the element number is increased. The reason is the time step size which remains constant independent on the grid refinement. However, for the finest grids a time step of $\Delta t = 100\,s$ could not be applied due to numerical stability. The time step size of the finest grid could not be raised at all.

In both criteria, accuracy as well as efficiency, the *global pressure fractional flow* formulation shows advantages compared to the *fully coupled* formulation. The largest disadvantage of this formulation is the overestimation of the propagation speed of the wetting phase front. Only for very fine grids the approximation using the *fully coupled* formulation becomes sufficient. Using equal time step sizes the *global pressure fractional flow* formulation is the faster one. However, much larger time steps are allowed for the *fully coupled* formulation. This decreases the execution time far below the time needed by the *global pressure fractional flow.* In the end this advantage is small as much finer grids are needed for the *fully coupled* formulation to achieve comparable approximations.
The *phase pressure fractional flow* formulation could not be discussed at all in this section as it was not able to solve the *McWhorter* problem due to numerical instabilities. The reason might be that compared to the *global pressure fractional flow* formulation the equations of this formulation are stronger coupled for the diffusive problem due to the capillary term in the pressure equation (see Ch. 3). However, still an IMPES scheme is applied. A fully implicit discretisation scheme solving both equations (pressure and saturation equation) simultaneously could improve the numerical stability. The *phase pressure fractional flow* formulation might then combine the advantages of both formulations discussed in this section. This has to be further investigated.

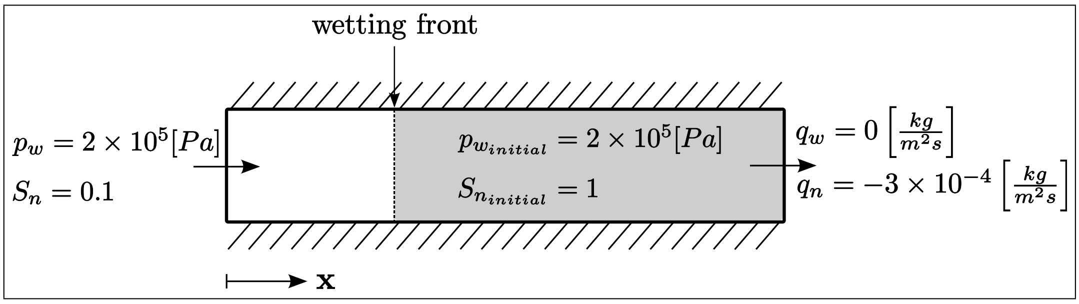

Figure 4.29: *Advection-diffusion* problem with initial and boundary conditions.

4.4 1-D Advection-Diffusion Problem

Combining the processes discussed separately in Chapters 4.1 and 4.3, a *advection-diffusion* problem is set up. It again describes the instationary displacement of a non-wetting fluid by a wetting fluid in an one-dimensional, horizontal system (Fig. 4.29). The following assumptions are made:

- Gravity effects are neglected.
- There exist no sources or sinks.
- The fluids are incompressible and immiscible.
- The fluid viscosities are equal.
- The porous medium is homogeneous.

The system of equations of a *fully coupled* formulation in terms of a p_w-S_n formulation (Eq. (3.6) and (3.7)) can then be simplified as follows:

$$L_w(p_w, S_n) := -\phi \frac{\partial S_n}{\partial t} - \nabla \cdot (\lambda_w \mathbf{K} \nabla p_w) = 0, \tag{4.22}$$

$$L_n(p_w, S_n) := \phi \frac{\partial S_n}{\partial t} - \nabla \cdot (\lambda_n \mathbf{K} (\nabla p_w + \nabla p_c)) = 0. \tag{4.23}$$

Further, the *fractional flow* formulations can be rewritten applying the above assumptions. The equations of the *global pressure fractional flow* formulations are equal to those already derived in Section 4.3 for the *McWhorter* problem (Eq. 4.13 to 4.15).
The pressure equation of the *phase pressure fractional flow* formulation simplifies to:

$$-\nabla \cdot [\lambda_t \mathbf{K} (\nabla p_w + f_n \nabla p_c)] = 0. \tag{4.24}$$

Finally, applying the assumptions to the saturation equation of the *phase pressure fractional flow* formulation leads to

$$\phi \frac{\partial S_w}{\partial t} + \nabla \cdot (f_w \mathbf{v}_{w_{mod}}) = 0. \tag{4.25}$$

4.4.1 Calculations

The numerical simulations were carried out on one dimensional elements. The considered domain has a length of 800 m. The coarsest grid consists of 25 elements, finer grids are constructed by bisecting the elements (Tab. 4.19). As before, the time step size used for the *fractional flow* formulations is determined during the calculation. An automatic time step adaption is implemented using a *Courant-Friedrichs-Lewy* criterion (details, see [6]) for the explicit *Euler* time steps. The average time step of this simulation is then used as constant time step in the simulation applying the *fully coupled* formulation. As different time step sizes result from the different *fractional flow* formulations, the calculations using the *fully coupled* formulation are done twice, where the average time step of both *fractional flow* formulations is used. However, with increasing influence of the capillary effects, the time steps had to be partly decreased compared to the time steps of the corresponding *fractional flow* formulation to achieve numerical stability. The simulation times vary depending on the capillary pressure-saturation function and are chosen in such a manner that the front is not able to reach the outflow boundary (Tab. 4.20).

The initial and boundary conditions are given in Table 4.21. *Dirichlet* boundary conditions are set on the left side of the domain ($x = 0\ m$) and *Neumann* boundary conditions on the right side of the domain ($x = 800\ m$)(Fig. 4.29). It has to be mentioned that the global pressure is no longer equal to the phase pressure if capillary effects occur. It can be related to the wetting phase pressure as

$$\bar{p} = p_w - \int_{S_w}^{1-S_{nr}} f_n \frac{dp_c}{dS_w} dS_w, \tag{4.26}$$

(details, see for example [1]). As shown in Table 4.21, the differences between global pressure and wetting phase pressure at the *Dirichlet* boundary range between 0 and 50 Pa for the considered cases. Initially, the domain is oil saturated. A linear as well as a *Brooks-Corey* relationship are selected. Thus, influences of different capillary pressure relations and relative permeability-saturation relations on the solution can be analysed. The corresponding parameters as well as other porous medium and fluid properties are shown in Table 4.3.

To analyse the character of the propagation processes, a *Peclet* number is calculated which relates advection to diffusion. A local *Peclet* number for twophase flow in porous media can be derived from the saturation equation of the *fractional flow* formulation which has the form of a general transport equation. Thus, as shown in Appendix B the following definition can be formulated:

$$Pe = \frac{\mathbf{v}_t \frac{df_w}{dS_w} \Delta x}{\bar{\lambda} \frac{dp_c}{dS_w}}, \tag{4.27}$$

where Δx is the discretisation length.

As shown in Table 4.19, the calculations of the linear case using the *fully coupled* formulation are done for two different time step sizes. Some results are shown in Figures 4.30 to 4.32. Three different capillary pressure-saturation functions are considered here. It should be noted that the simulation time for $p_{c_{max}} = 100$ is reduced by factor of 10 compared to the simulation times for the smaller $p_{c_{max}}$. It can be observed that for all grids the solutions are time step dependent. The widest difference and thus, most numerical diffusion due to the size of the time step can be observed for $p_{c_{max}} = 1$. The main reason for this is that the time steps

geometry	**length** [m]
	800

discretisation	**linear constitutive relationships**					
	number of cells	Δx [m]	$p_{c_{max}}$ [Pa]	Δt [s]		
				FC	**PPFF (∅)**	**GPFF (∅)**
	25	32	1	see PPFF/ GPFF	6.17×10^6	4.15×10^5
			10		2.40×10^6	8.54×10^4
			100		2.54×10^5	7.70×10^3
	50	16	1	see PPFF/ GPFF	3.09×10^6	1.69×10^5
			10		1.17×10^6	4.01×10^4
			100		1.27×10^5	3.63×10^3
	100	8	1	see PPFF/ GPFF	1.54×10^6	7.63×10^4
			10	1.46×10^5 see GPFF	5.84×10^5	9.74×10^3
			100	1.59×10^4 see GPFF	6.35×10^4	8.82×10^2
			1000	1.61×10^3 see GPFF	6.45×10^3	8.71×10^1
			10000	1.61×10^2 see GPFF	6.45×10^2	8.69
	Brooks-Corey **constitutive relationships**					
	number of cells	Δx [m]	p_d [Pa]	Δt [s]		
				FC	**PPFF (∅)**	**GPFF (∅)**
	25	32	1	see GPFF	1.67×10^4	4.60×10^5
			10		5.97×10^3	1.12×10^5
			100		1.75×10^2	3.07×10^4
	50	16	1	see GPFF	4.24×10^3	1.64×10^5
			10		1.52×10^3	4.95×10^4
			100		1.57×10^2	1.51×10^4
	100	8	1	see GPFF	1.07×10^3	6.33×10^4
			10		3.87×10^2	2.37×10^4
			100		4.00×10^1	3.76×10^3
			1000		3.91	1.56×10^2

Table 4.19: Geometry and discretisation (*fully coupled* formulation (FC), *phase pressure fractional flow* formulation (PPFF), *classical/global pressure fractional flow* formulation (GPFF)).

linear		***Brooks-Corey***	
$\mathbf{p_{cmax}}$	**simulation time**	$\mathbf{p_d}$	**simulation time**
1	4.32×10^7	1	4.32×10^7
10	4.32×10^7	10	4.32×10^7
100	4.32×10^6	100	4.32×10^7
1000	4.32×10^5	1000	8.64×10^5
10000	4.32×10^4	-	-

Table 4.20: Simulation time $[s]$.

	parameter	**value**
boundary conditions	$\mathbf{x = 0\,m}$	
	water pressure $p_w \neq \bar{p}$	$2 \times 10^5 \ [Pa]$
	global pressure	linear
		$200000.01 \ [Pa] \ (p_{c_{max}} = 1)$ $200000.05 \ [Pa] \ (p_{c_{max}} = 10)$ $200000.50 \ [Pa] \ (p_{c_{max}} = 100)$ $200005.00 \ [Pa] \ (p_{c_{max}} = 1000)$ $200050.00 \ [Pa] \ (p_{c_{max}} = 10000)$
		Brooks-Corey
		$200000.00 \ [Pa] \ (p_d = 1)$ $200000.00 \ [Pa] \ (p_d = 10)$ $200000.00 \ [Pa] \ (p_d = 100)$ $200000.04 \ [Pa] \ (p_d = 1000)$
	oil saturation S_n	$0.1 \ [-]$
	$\mathbf{x = 800\,m}$	
	flow rate of water q_w	$0 \ [kg/(m^2 s)]$
	flow rate of oil $q_n = q_t$	$-3 \times 10^{-4} \ [kg/(m^2 s)]$
initial conditions	water pressure $p_w \neq \bar{p}$	s. inflow boundary
	oil saturation S_n	$1.0 \ [-]$

Table 4.21: Initial and boundary conditions.

	parameter	**value**
fluid properties	water density ρ_w	1000 $[kg/m^3]$
	oil density ρ_n	1000 $[kg/m^3]$
	dyn. viscosity water μ_w	0.001 $[kg/(ms)]$
	dyn. viscosity oil μ_n	0.001 $[kg/(ms)]$
solid matrix properties and constitutive relationships	intrinsic permeability $\mathbf{K}$	10^{-7} $[m^2]$
	porosity Φ	0.2 $[-]$
	pore size distr. index λ	2.00 $[-]$
	res. saturation water S_{wr}	0.0 $[-]$
	res. saturation oil S_{nr}	0.0 $[-]$
	rel. permeability $k_r(S_w)$	linear/Brooks-Corey

Table 4.22: Fluid and porous medium properties.

are chosen according to the two *fractional flow* formulations. The time dependence does not decrease due to increasing $p_{c_{max}}$ and thus not due to increasing influence of capillary pressure effects. It decreases because of the decreasing time steps of the *fractional flow* formulations (see Tab. 4.19). To account for the time dependence the results using the smaller time step are always selected for further comparison of the formulations.

Figures 4.33a to 4.35b compare the solution behaviour of the different formulations with regard to different element sizes.
At first, the *fully coupled* formulation is considered (Fig. 4.33a and 4.33b). Both cases, the linear as well as the nonlinear show stronger smearing of the front for the coarser grids, independent of the capillary pressure effects. For the nonlinear case using *Brooks-Corey* constitutive relations, a stronger numerical diffusion can be observed due to the high capillary pressure gradients at small saturations compared to the linear case having a constant gradient. Consistent with the analyses of the advective problem (Sec. 4.1) and the diffusive problem (Sec. 4.3), the numerical diffusion can be reduced by refinement of the grid.
The results using the *phase pressure fractional flow* formulation on different grids are shown in Figures 4.34a and 4.34b. For the nonlinear case, a behaviour comparable to the behaviour of the *fully coupled* formulation can be observed concerning the grid dependence. In contrast, for the linear case, the *phase pressure fractional flow* formulation hardly shows any dependency of the solution on the level of grid refinement. The differences at the left boundary of the domain are negligible because they only appear due to visualisation problems (Fig. 4.34a). It can be concluded that for constant capillary pressure gradients, the numerical diffusion of the *phase pressure fractional flow* formulation is negligible. This does not apply for varying capillary pressure gradients resulting from nonlinear capillary pressure-saturation relations.
Considering the results of the linear case using the *global pressure fractional flow* formulation (Fig. 4.35a), small grid dependence can be observed. However, it is negligible compared to the behaviour of the *fully coupled* formulation. A difference to the other formulations appears for the nonlinear case where the grid dependent numerical diffusion is significantly reduced compared to the other two formulations applying the *global pressure fractional flow* formulation (Fig. 4.35b). Altogether, the *global pressure fractional flow* formulation shows the smallest grid dependence resulting in the least numerical diffusion. This corresponds to

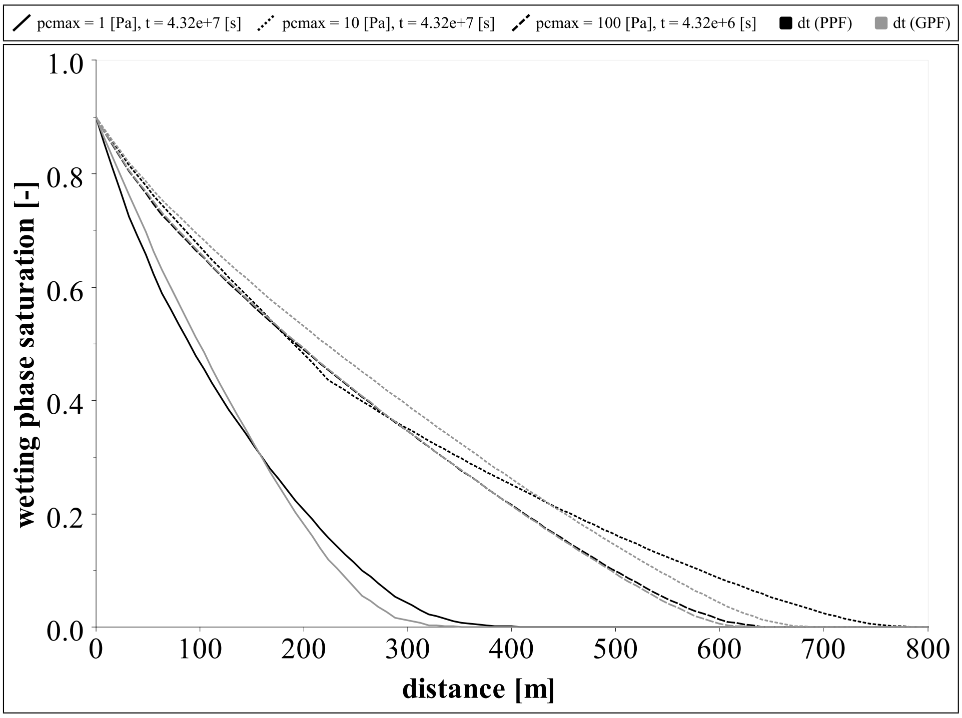

Figure 4.30: Saturation profiles of the linear case using different time step sizes on a grid of 25 elements (*fully coupled* formulation).

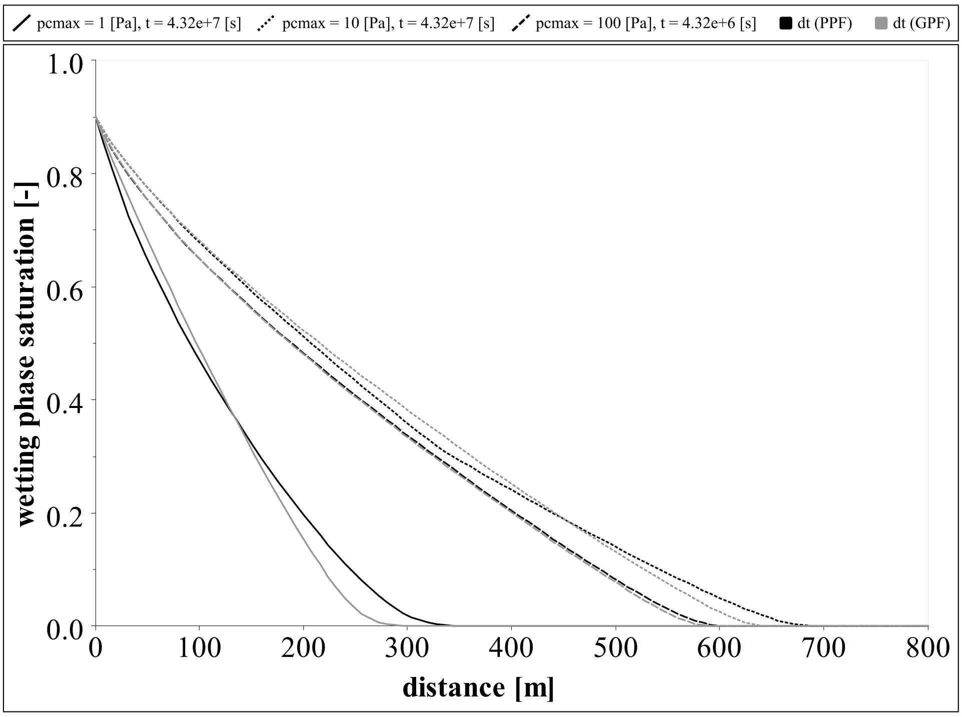

Figure 4.31: Saturation profiles of the linear case using different time step sizes on a grid of 50 elements (*fully coupled* formulation).

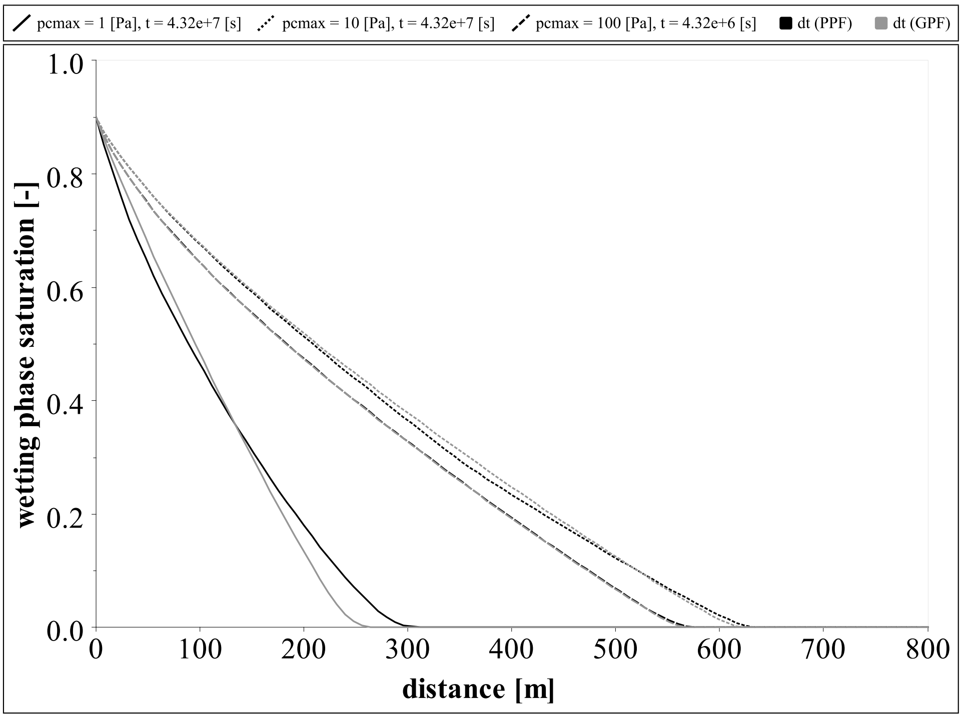

Figure 4.32: Saturation profiles of the linear case using different time step sizes on a grid of 100 elements (*fully coupled* formulation).

the investigation of the diffusive *McWhorter* problem.
To minimise effects of grid dependence, further comparison of the formulations is only done for the calculations on the finest grid.

Figures 4.36a to 4.37b compare the saturation profiles achieved using the different formulations with different linear capillary pressure-saturation functions. As can be observed, the saturation front using the *fully coupled* formulation is slightly faster than the front resulting from the *fractional flow* formulations. Anyhow, the differences of the results provided by the three formulations are almost negligible. As already mentioned in the previous sections the saturation at the left boundary of the domain is equal for both formulations. The differences which can be observed arise from the visualisation of the data, where the cell centred data resulting from the calculations with the *fractional flow* formulation are converted into point data.
Additionally, for $p_{c_{max}} = 1000$ and $p_{c_{max}} = 10000$ the pressure profiles are shown in Figures 4.37a and 4.37b. It can be seen that the global pressure used in the *global pressure fractional flow* formulation does not express the saturation distribution. Furthermore, it is not comparable to the phase pressure, which is solved for in both other formulations, at all. The profile of the wetting phase pressure resulting form the *fully coupled* formulation is comparable to the profile resulting from the *phase pressure fractional flow* formulation. The small difference that can be observed corresponds to the difference observed for the saturation profiles.

A comparison of the three formulations using nonlinear *Brooks-Corey* relationships is shown in Figures 4.38a to 4.39b. As discussed before, the *global pressure fractional flow* formulation introduces less numerical diffusion than the *fully coupled* and the *phase pressure fractional flow* formulation especially, for nonlinear capillary pressure-saturation relationships. Accordingly, it

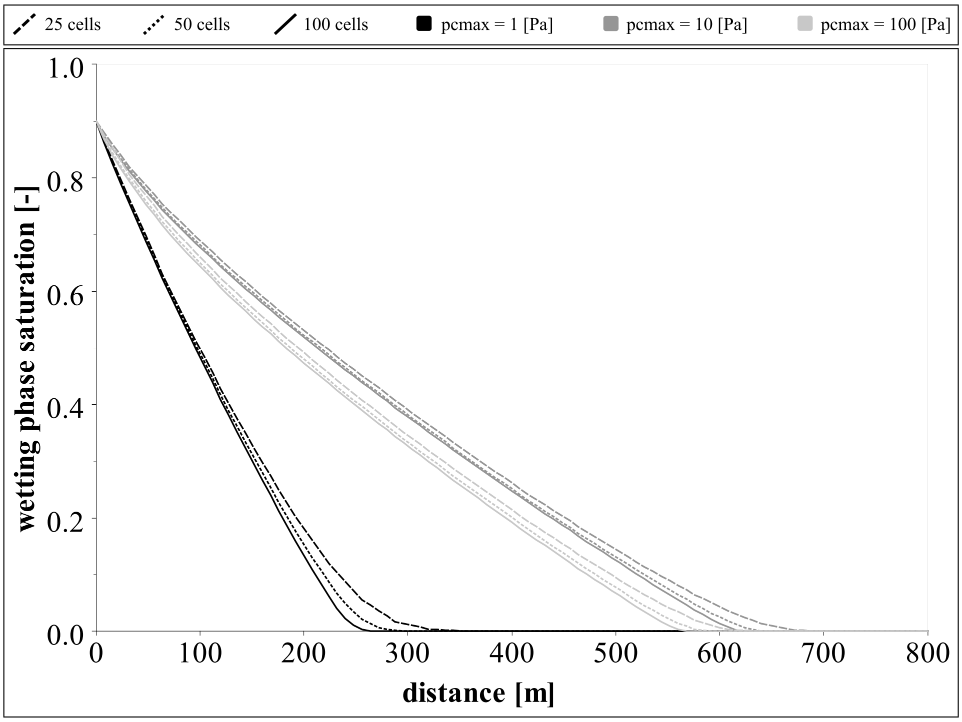

(a) linear

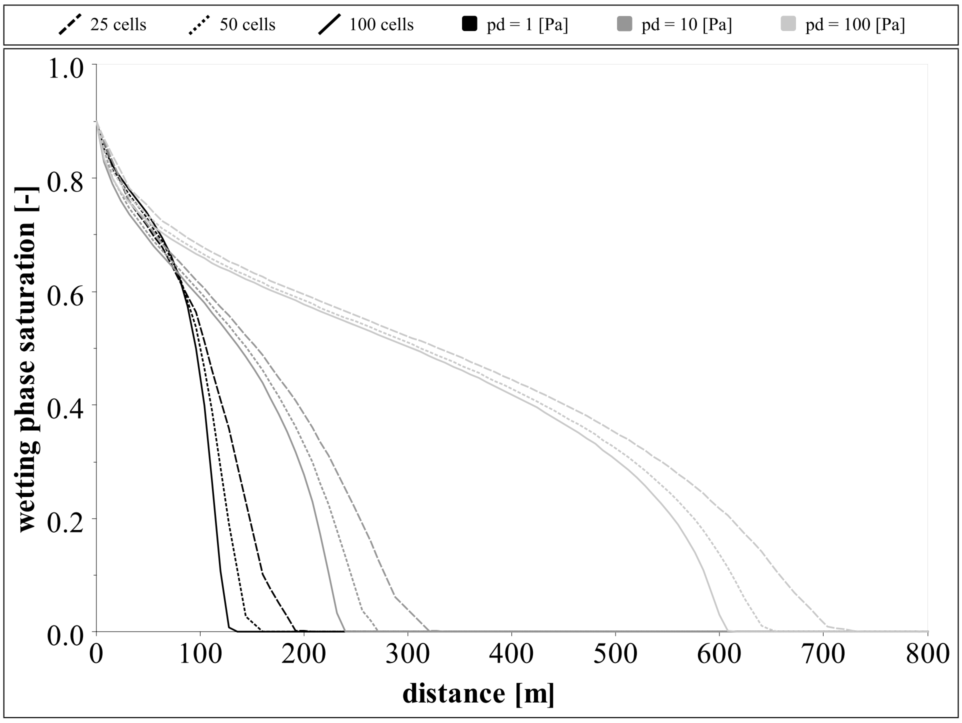

(b) *Brooks-Corey*

Figure 4.33: Saturation profiles using different grids at $t = 500\,d$ ($t(p_{c_{max}} = 100) = 50\,d$, *fully coupled* formulation).

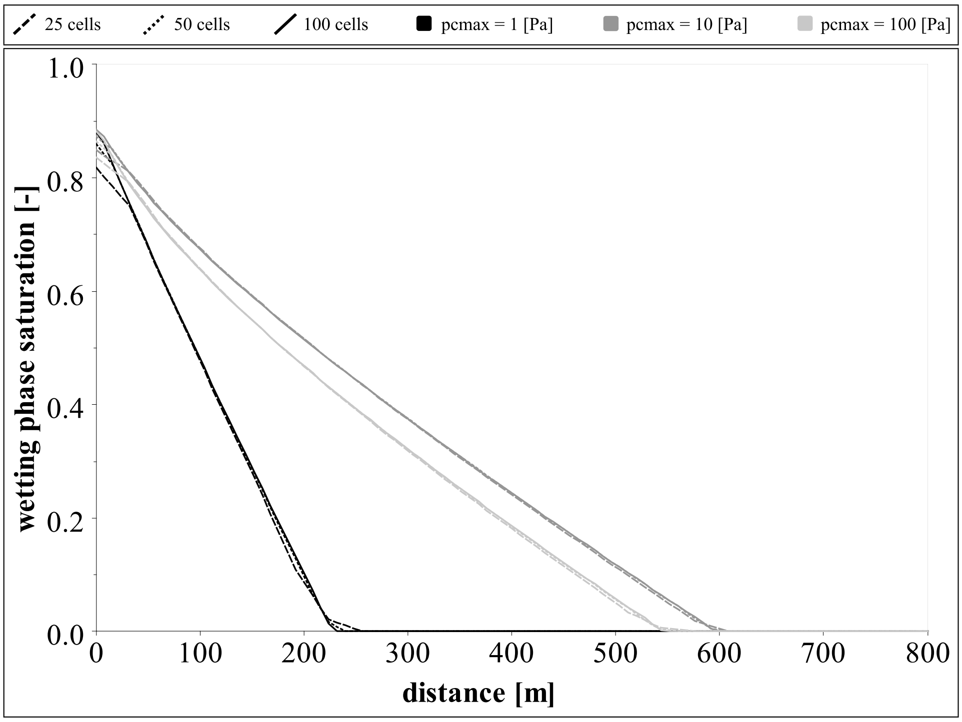

(a) linear

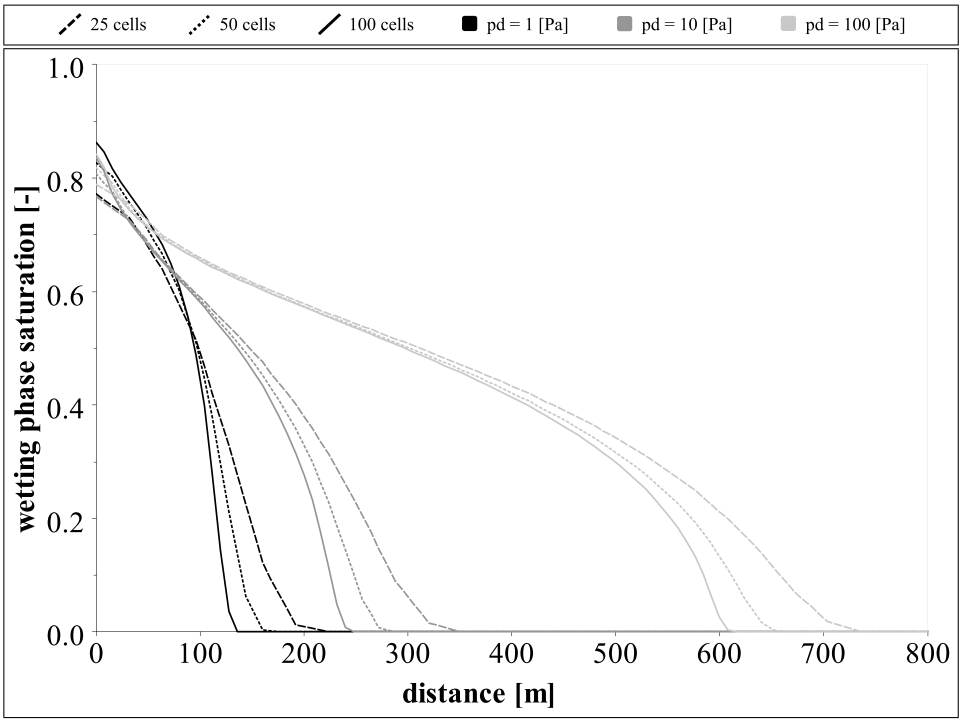

(b) *Brooks-Corey*

Figure 4.34: Saturation profiles using different grids at $t = 500\,d$ ($t(p_{c_{max}} = 100) = 50\,d$, *phase pressure fractional flow* formulation).

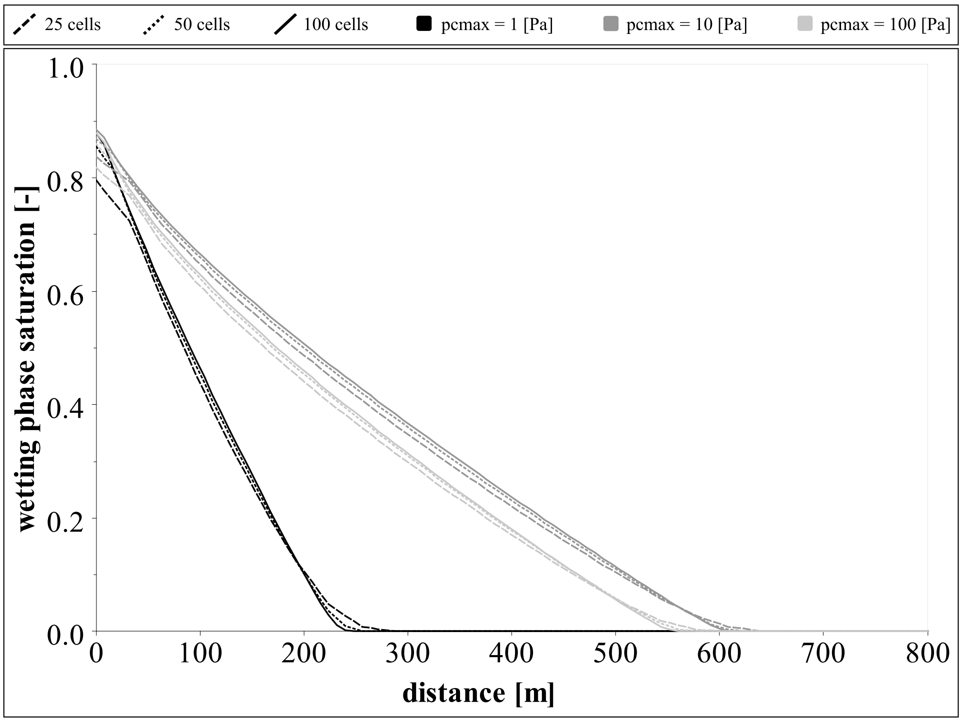

(a) linear

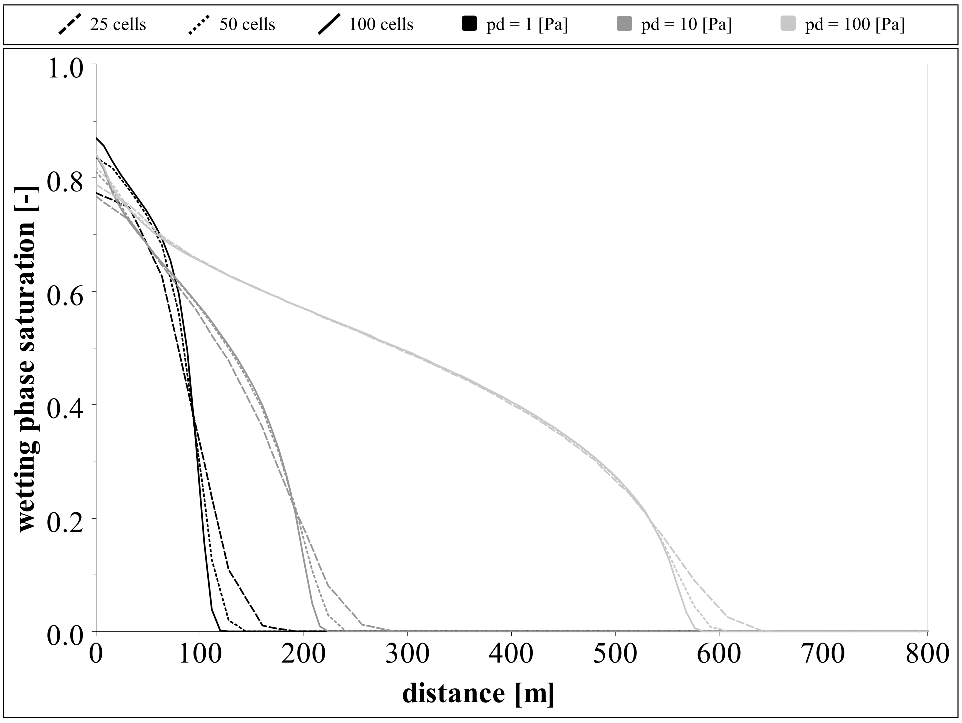

(b) *Brooks-Corey*

Figure 4.35: Saturation profiles using different grids at $t = 500\,d$ ($t(p_{c_{max}} = 100) = 50\,d$, *global pressure fractional flow* formulation).

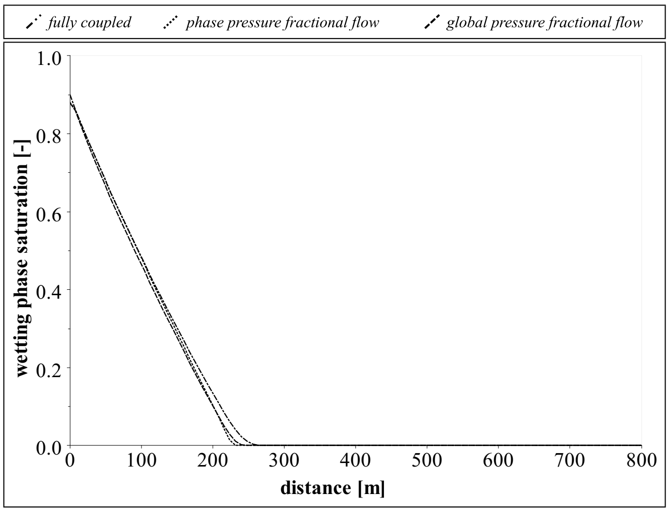

(a) $p_{c_{max}} = 1\,Pa,\, t = 4.32 \times 10^7\ s$

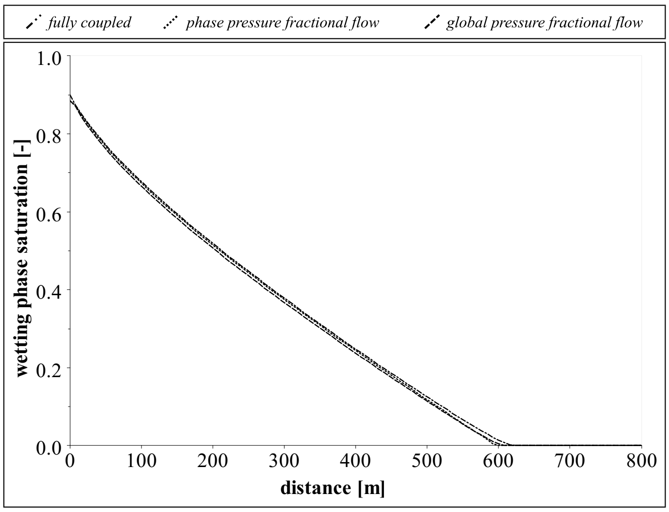

(b) $p_{c_{max}} = 10\,Pa,\, t = 4.32 \times 10^7\ s$

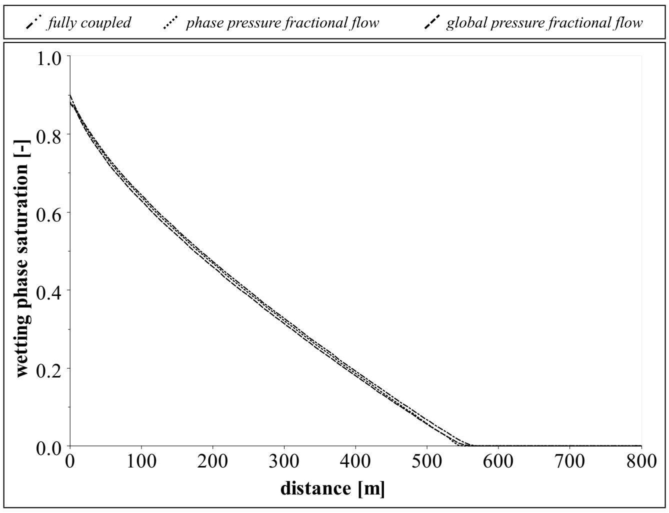

(c) $p_{c_{max}} = 100\,Pa,\, t = 4.32 \times 10^6\ s$

Figure 4.36: Saturation profiles along the domain using the different formulations (linear, 100 cells).

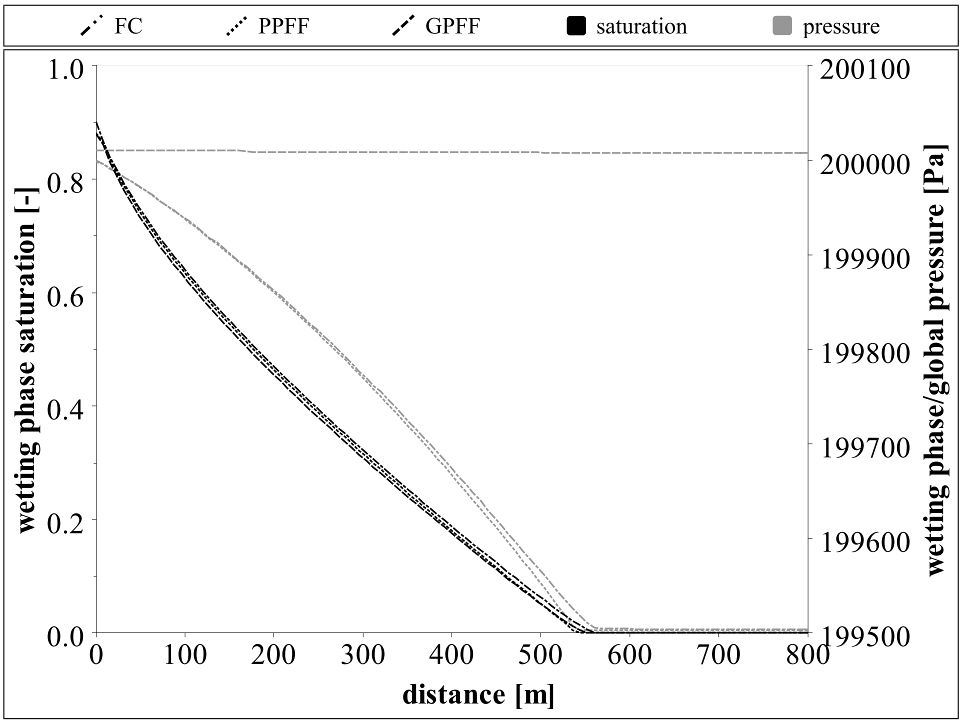

(a) $p_{c_{max}} = 1000\,Pa$, $t = 4.32 \times 10^5\,s$

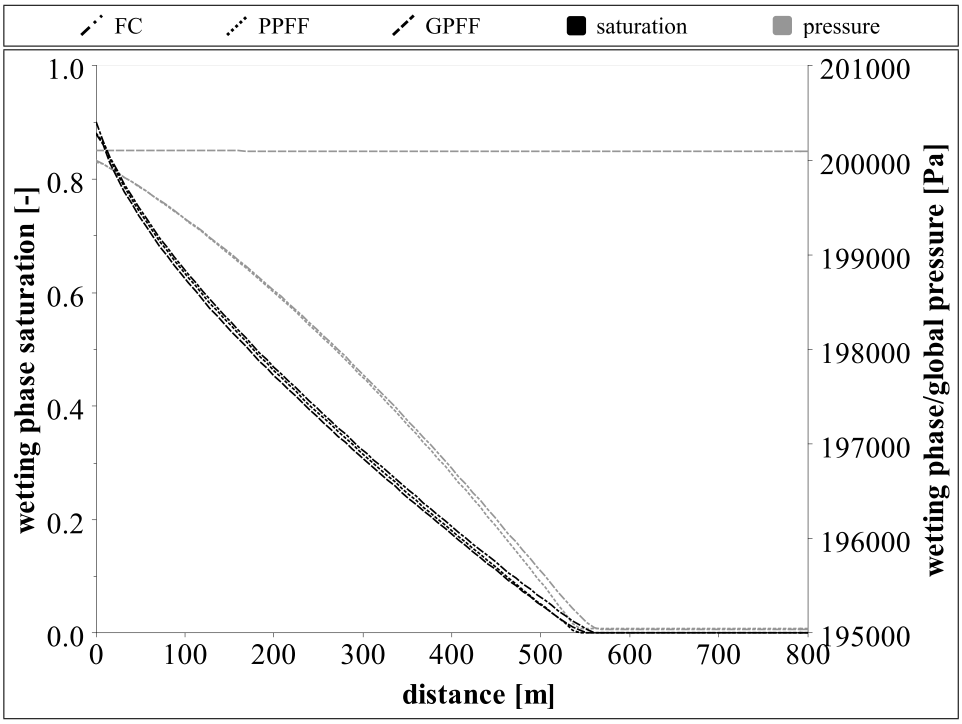

(b) $p_{c_{max}} = 10000\,Pa$, $t = 4.32 \times 10^4\,s$

Figure 4.37: Saturation profiles and pressure profiles along the domain using the different formulations (linear, 100 cells).

can be observed that the movement of the saturation front using the *global pressure fractional flow* formulation is not as fast as the movement of a front resulting from one of the other formulations. The *fully coupled* formulation and the *phase pressure fractional flow* formulation show almost equal saturation profiles for $p_d = 1$ to $p_d = 100$ (Fig. 4.38a to 4.39a). If the capillary pressure effects are further increased, the speed of the wetting phase front calculated using the *fully coupled* formulation is also increased compared to the speed of the front resulting from the *phase pressure fractional flow* formulation (Fig.4.39b). This means that applying the *fully coupled* formulation, the numerical diffusion increases if the influences of the capillary effects become stronger.
As for the linear case, the pressure profiles of the nonlinear case are shown for $p_d = 100$ and $p_d = 1000$ (Fig. 4.39a and 4.39b). Consistent with the observations done concerning the saturation profiles, the wetting phase pressure profiles of the *fully coupled* formulation and of the *phase pressure fractional flow* formulation are almost equal for $p_d = 100$ whereas a difference can be observed for $p_d = 1000$. Thus, the increasing numerical diffusion due to increasing influence of capillary effects is also expressed by the wetting phase pressure distribution. The global pressure resulting from the *global pressure fractional flow* formulation is again not suitable to directly draw conclusions concerning the propagation of the phases and it cannot be directly compared to the wetting phase pressure resulting from the other formulations.

Figures 4.40a and 4.40b show the *Peclet* number which relates advection and diffusion within a transport process plotted over the wetting phase saturation. If the *Peclet* number is small ($Pe \cong 0$), a transport process is diffusion dominated. For large *Peclet* numbers ($Pe \gg 1$), the transport process is advection dominated (details, see [6]).
As can be observed for both cases, linear as well as nonlinear, the *Peclet* number is not constant but varies for different saturations where the linear and the nonlinear *Peclet* curves have a different shape. The main reason is that the capillary pressure gradient is constant in case of a linear capillary pressure-saturation relation whereas it is variable in case of a *Brooks-Corey* capillary pressure-saturation function.
Considering the linear case, the largest *Peclet* numbers occur for small saturations. If the saturation increases, the *Peclet* number decreases. Considering the nonlinear case, a maximum *Peclet* number can be observed which is neither at a saturation of zero nor at a saturation of one. The saturation corresponding to the maximum *Peclet* number is decreasing if the influence of capillary effects is increasing.
With increasing $p_{c_{max}}$ the *Peclet* number of the linear case is decreasing which means that capillary diffusion becomes more important. Especially for the largest value of $p_{c_{max}}$ implying the largest capillary pressure gradient, the process seems to be extensively diffusion dominated. Anyhow, independent on $p_{c_{max}}$, very large *Peclet* numbers can be observed for small saturations. Similarly, increasing p_d, the *Peclet* number of the nonlinear case is decreasing where comparable to the linear case diffusion seems to have large influence, especially for the largest value of p_d applied here. Contrary to the linear case, very small *Peclet* numbers occur for small saturations which means that diffusion is dominant at the front end of the saturation profiles (Fig. 4.38a to 4.39b).
Recapitulating, none of the considered cases is clearly diffusion dominated. However, the discussion of the *Peclet* number shows that the influence of capillary diffusion can become notable.

Finally, the efficiency of the formulations concerning the 1-d-advection-diffusion problem has

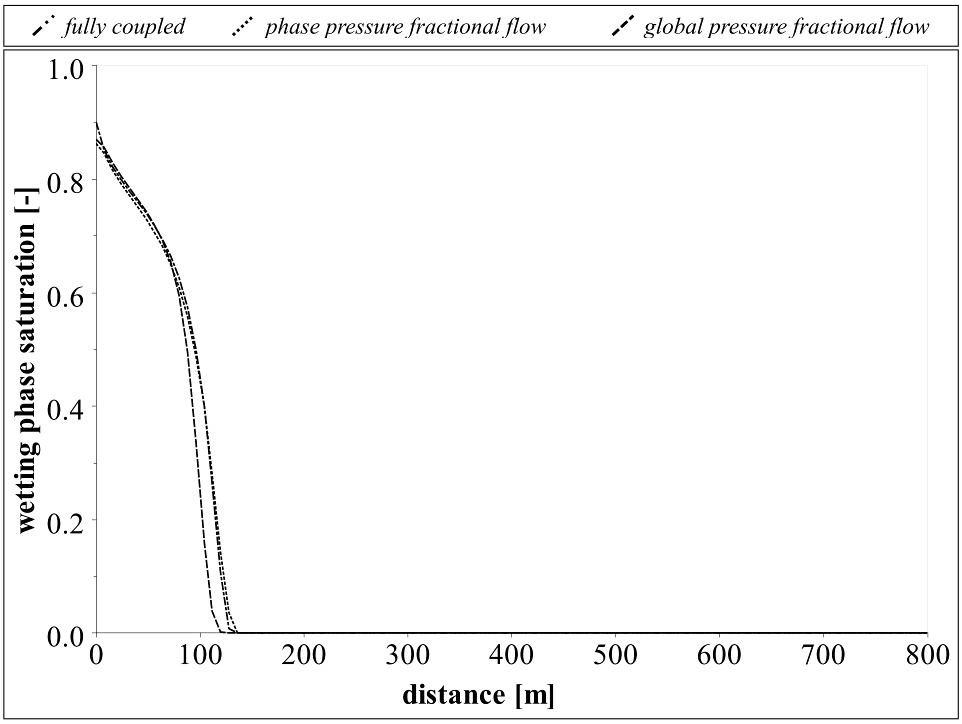

(a) $p_d = 1\ Pa$, $t = 4.32 \times 10^7\ s$

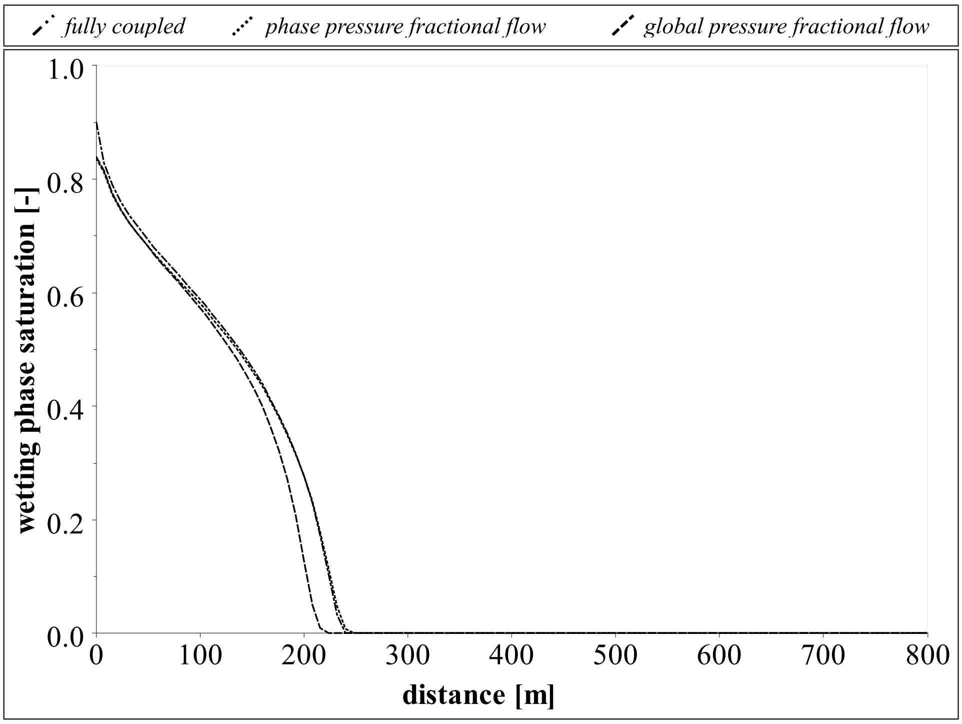

(b) $p_d = 10\ Pa$, $t = 4.32 \times 10^7\ s$

Figure 4.38: Saturation profiles along the domain using the different formulations (*Brooks-Corey*, 100 cells).

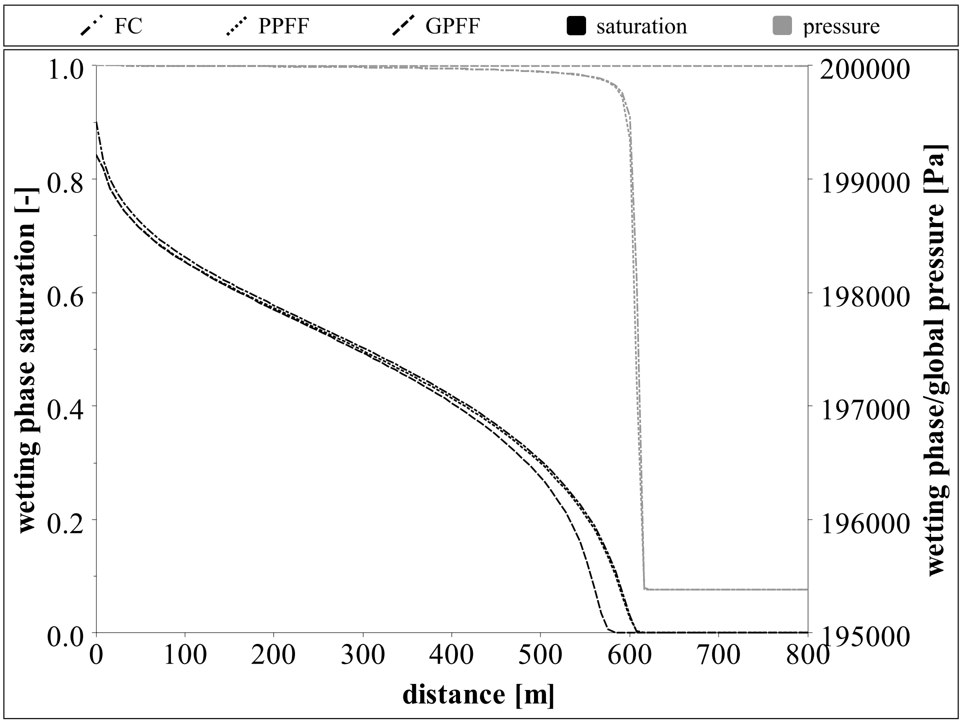

(a) $p_d = 100\ Pa$, $t = 4.32 \times 10^7\ s$

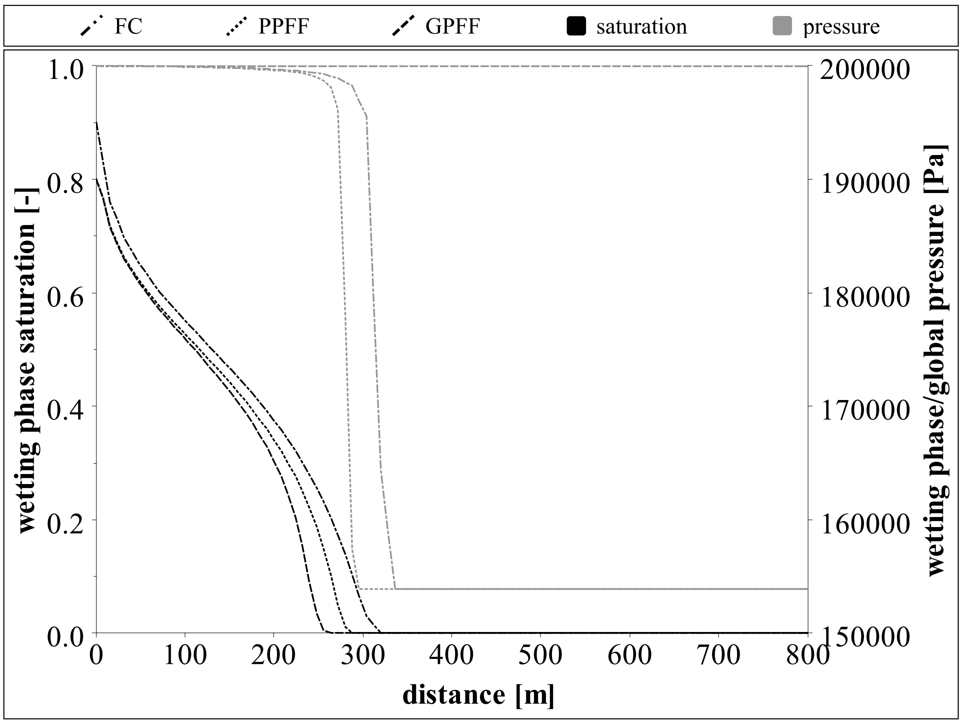

(b) $p_d = 1000\ Pa$, $t = 8.64 \times 10^5\ s$

Figure 4.39: Saturation profiles along the domain using the different formulations (*fully coupled* (FC), *phase pressure fractional flow* (PPFF), *global pressure fractional flow* (GPFF), *Brooks-Corey*, 100 cells).

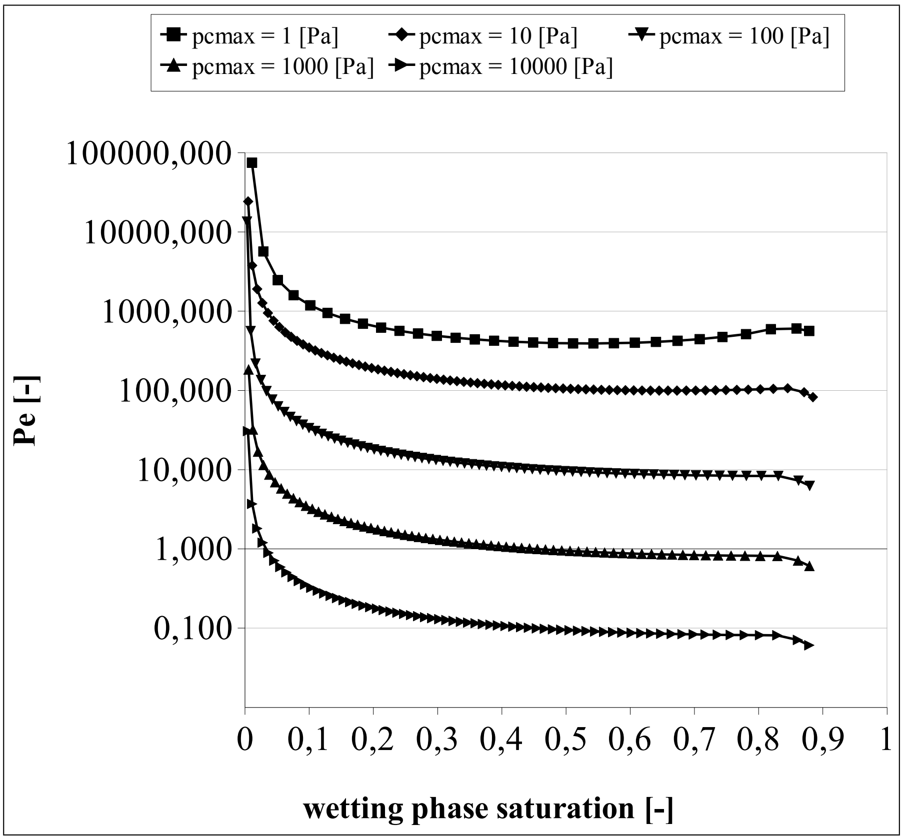

(a) linear

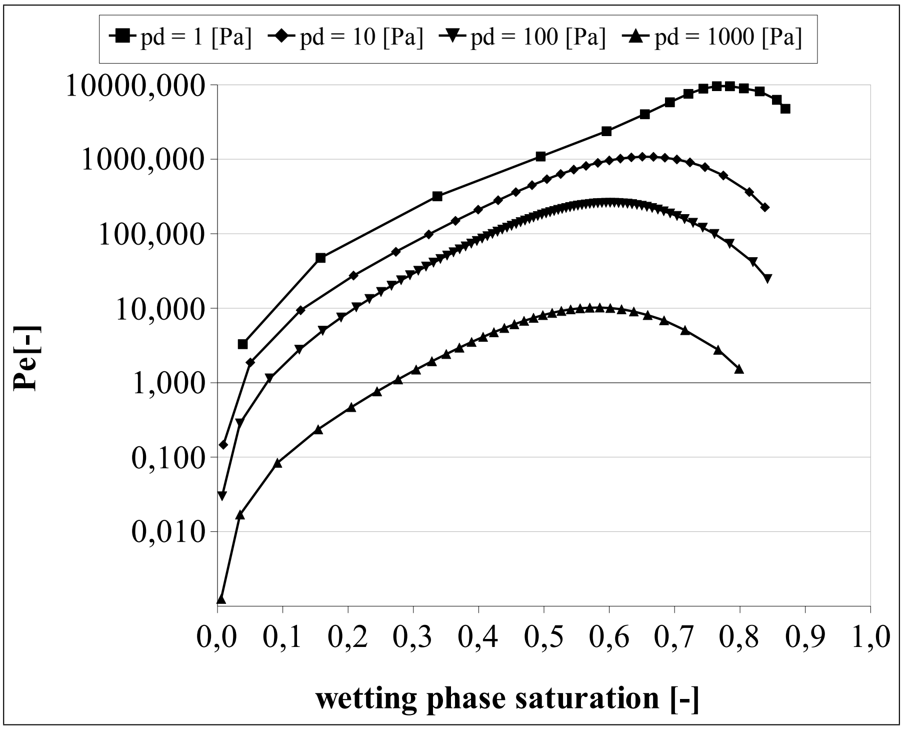

(b) *Brooks-Corey*

Figure 4.40: Peclet number over wetting phase saturation at $t = 500\,d$ (100 cells).

to be looked at. Therefore, the execution times are shown in Table 4.23.
Considering the linear case, both *fractional flow* formulations achieve approximately equal execution times. From $p_{c_{max}} = 100$ to $p_{c_{max}} = 10000$ quasi constant times can be observed. As can be seen in Table 4.20, for $p_{c_{max}} \geq 10$, the simulation times are reduced by a factor 10 every time $p_{c_{max}}$ is further increased. As $p_{c_{max}}$ is also increased by factor 10, this means that the execution time is approximately linearly dependent on the capillary pressure gradient. This has to be noted because the different *fractional flow* formulations differently account for the increasing gradient. As can be seen in Table 4.24, using the *phase pressure fractional flow* formulation, the number of iterations between saturation equation and pressure equation within every time step is considerably increasing with increasing capillary pressure gradient where the time step remains relatively large. Using the *global pressure fractional flow* formulation, the iterations between the equations remain constant, whereas the time step is significantly decreasing with increasing capillary pressure gradient. This behaviour can be expected due to the different ways the capillary pressure terms are brought into the systems of equations of the different *fractional flow* formulations (see Ch. 3).
The *fully coupled* formulation shows much higher execution times especially for higher values of $p_{c_{max}}$ which imply higher capillary pressure gradients. The reason is that small time steps comparable to the time steps of the *global pressure fractional flow* formulation are necessary to reduce numerical diffusion, whereas much larger time steps could be used accounting for the increasing gradient only concerning numerical stability.
In case of a nonlinear capillary pressure-saturation function, the *global pressure fractional flow* formulation shows the smallest execution times. The largest times can be observed for the *phase pressure fractional flow* formulation. The *fully coupled* formulation ranges in between of the *fractional flow* formulations. The time steps using the *global pressure fractional flow* formulation for the nonlinear case are larger than using the formulation for the linear case. The reason might be that the capillary pressure gradient is not constantly high for the *Brooks-Corey* relation but can also be small if the saturations are not too small where the gradient of a linear capillary pressure-saturation relation can be constantly large depending on $p_{c_{max}}$. Furthermore, the time steps are larger than the time steps which result, when applying the *phase pressure fractional flow* formulation. The iterations done within every time step using this formulation are in a constant range, independent on the different nonlinear capillary pressure-saturation relations applied (Tab. 4.24). The same reason as pointed out before concerning the time step sizes of the *global pressure fractional flow* formulation applies here. However, to account for the stronger nonlinear coupling of the equations of the *phase pressure fractional flow* formulation, smaller time steps are necessary.

Concerning the accuracy, both *fractional flow* formulations show advantages compared to the *fully coupled* formulation in case of a linear capillary pressure-saturation function. Especially, the *phase pressure fractional flow* formulation shows almost no grid dependent numerical diffusion. This means that coarser grids can be used with this formulation and thus, the execution time can be further reduced. The *fully coupled* formulation can be faster than the *fractional flow* formulations if large time steps are applied, but as shown this also leads to notable numerical diffusion. Altogether, the *phase pressure fractional flow* formulation provides the best combination of accuracy and efficiency for the linear case.
In case of a nonlinear capillary pressure-saturation relation, the *global pressure fractional flow* formulation shows advantages in both criteria, accuracy as well as efficiency compared to the other formulation. It introduces the least numerical diffusion while the execution times are

	$\mathbf{p_{c_{max}}}$ (linear)/ $\mathbf{p_d}$ (*Brooks-Corey*)	**1**	**10**	**100**	**1000**	**10000**
FC **(Δt of GPFF)**	**linear**	4.460	9.857	20.629	37.330	53.571
	Brooks-Corey	6.284	26.614	335.749	82,229	-
PPFF	**linear**	2.776	10.533	12.361	12.317	12.353
	Brooks-Corey	193.628	429.899	3013,800	658.613	-
GPFF	**linear**	2.524	11.449	12.533	12.661	12.741
	Brooks-Corey	3.824	10.481	71.108	31.374	-

Table 4.23: Execution time [s] (100 cells, *fully coupled* formulation (FC), *phase pressure fractional flow* formulation (PPFF), *classical/global pressure fractional flow* formulation (GPFF)).

***phase pressure fractional flow* formulation**			
cells	$\mathbf{p_{c_{max}}}$ (linear)/ $\mathbf{p_d}$ (*Brooks-Corey*)	**iterations**	
		(linear)	(*Brooks-Corey*)
100	1	36-74	2-17
100	10	50-157	2-18
100	100	65-200	1-17
100	1000	65-200	1-17
100	10000	65-200	-
***classical/global pressure fractional flow* formulation**			
cells	$\mathbf{p_{c_{max}}}$ (linear)/ $\mathbf{p_d}$ (*Brooks-Corey*)	**iterations**	
		(linear)	(*Brooks-Corey*)
100	1-10000	1-2	1-2

Table 4.24: Iteration steps within every timestep of the *fractional flow* formulations using a grid consisting of 100 elements.

still smaller than for the *phase pressure fractional flow* formulation or for the *fully coupled* formulation. Again, the computation speed applying the *fully coupled* formulation can be increased by using larger time steps. However, to achieve execution times comparable to those of the *global pressure fractional flow* formulation, a notable decrease of accuracy due to generation of numerical diffusion has to be accepted.

4.5 Summary

To compare the different kinds of formulations described in Chapter 3, some simple problems were discussed in this chapter where the term formulation includes the mathematical model as well as the numerical method.

The *Buckley-Leverett* problem for which an analytical solution exists was analysed representing a one dimensional advection dominated problem. The *fractional flow* formulation approximated the analytical solution pretty well whereas the *fully coupled* formulation using the box scheme introduced stronger numerical diffusion and thus, it showed a stronger smearing of the front. The main reason is the fully upwinding scheme that was applied for the *fully coupled* formulation. In contrast, in the application of the *fractional flow* formulation upwinding was only used for the advective term of the saturation equation. The diffusive character of the pressure equation was accounted for by central differences. Additionally, the higher order approach of the finite volume method should reduce numerical diffusion.
Concerning the execution times, the *fully coupled* formulation showed advantages because of the better convergence behaviour of the Newton-Raphson iteration method in the nonlinear case, if the element number is increasing.

A two dimensional advection dominated problem was represented by the *Five-spot Waterflood* problem. Like for the *Buckley-Leverett* problem a linear as well as a nonlinear *Brooks-Corey* relative permeability-saturation function was used. Two different configurations of the problem were considered to analyse the grid dependence of the formulations (Fig. 4.13a and 4.13b).
It was shown that both used formulations and corresponding methods (*fully coupled* formulation - box method, *fractional flow* formulation - finite volumes/higher order finite volumes) are mesh dependent concerning the direction of the occurring gradients. Effects of this mesh dependency can be reduced by refinement of the grid.
In general, less numerical diffusion was introduced by the *fully coupled* formulations especially in diagonal direction. One explanation is that the vertex centred box method corresponds to a nine-spot scheme which includes more nodes in diagonal direction than a five-spot scheme corresponding to the finite volume method. Further, it was pointed out that the higher order approach of the finite volume method applied here most likely increases the numerical diffusion if processes which are not parallel to the grid occur.
Considering the results, in the linear case the two formulations showed comparable results concerning the accuracy, but the *fractional flow* formulation was considerably less expansive concerning computational time.
In case of a nonlinear relative permeability-saturation function, the *fully coupled* formulation showed advantages concerning both accuracy and efficiency. It was more efficient in the linearisation of the nonlinear problem and thus, less expansive concerning computational time. Further, it introduced less numerical diffusion than the *fractional flow* formulation.

One dimensional, diffusion dominated flow was investigated by analysing the solution of the *McWhorter* problem. Analogous to the *Buckley-Leverett* problem, an analytical solution exists for the *McWhorter* problem.

Combining accuracy and efficiency, the *global pressure fractional flow* formulation showed advantages compared to the *fully coupled* formulation for the diffusion dominated case. The largest disadvantage of the *fully coupled* formulation was the notable overestimation of the propagation speed of the wetting phase front which can be observed except for very fine grids. This is caused by the fully upwinding scheme that was applied for the *fully coupled* formulation without regard to the kind of process which is simulated. Here, the *global pressure fractional flow* formulation allowed to better account for the character of the process where central differences are used for the diffusion terms in the equations.

The advantage of the *fully coupled* formulation is the smaller dependence on the time step size as an implicit scheme was used. However, this advantage is small. As pointed out before, much finer grids are needed applying the *fully coupled* formulation to achieve sufficient approximations.

The *phase pressure fractional flow* formulation could not be discussed at all concerning the diffusion dominated problem due to numerical instabilities. The reason might be that the IMPES scheme can not sufficiently account for the strong nonlinear coupling of the equations of this formulation which appears for the diffusive problem due to the strong influence of the capillary pressure term in the pressure equation.

Finally, a problem combining both kinds of processes, advection as well as diffusion was considered. Therefore, different capillary pressure-saturation functions were applied where the increasing influence of the capillary diffusion could be measured calculating the *Peclet* number.

None of the considered cases was clearly diffusion dominated. However, for some cases the *Peclet* numbers showed that the influence of capillary diffusion becomes notable.

Applying a linear capillary pressure-saturation function, both *fractional flow* formulations showed advantages compared to the *fully coupled* formulation concerning the accuracy. Especially, the grid dependent numerical diffusion of the *phase pressure fractional flow* formulation is negligible. This means that coarser grids can be used with this formulation and thus, the execution time can be further reduced.

In case of a nonlinear capillary pressure-saturation relation, the *global pressure fractional flow* formulation showed advantages in both criteria, accuracy as well as efficiency compared to the other formulations which corresponds to the investigation of the diffusion dominated *McWhorter* problem. It introduced least numerical diffusion while the execution times are still smaller than those using the other formulations.

The speed of the computation applying the *fully coupled* formulation can be increased by using larger time steps which is possible due to the implicit scheme. However, to achieve execution times comparable to those of the *global pressure fractional flow* formulation a notable decrease of accuracy due to generation of numerical diffusion has to be accepted.

Applying the *phase pressure fractional flow* formulation, problems concerning the numerical convergence behaviour could be observed for the nonlinear case. Very small time steps compared to the other formulations occur here if the influence of the capillary diffusion increases. Reasons have already been pointed out during the investigation of the *McWhorter* problem where even stronger convergence problems occurred using this formulation.

5 Summary and Outlook

In this thesis, different mathematical models for two phase flow in porous media were compared using different numerical methods. The following formulations and methods were investigated:

A *fully coupled* formulation modelling the motion of each phase (by formulating one equation for each phase) was discretized using the box method and an implicit *Euler* scheme. A p_w-S_n as well as a p_n-S_w formulation were applied depending on the problem to solve.
The *global pressure fractional flow* formulation represented by one equation for the global pressure and one saturation equation was discretized in space using a finite volume method for the pressure equation and a higher order finite volume method for the saturation equation. For the time discretisation, a standard IMPES scheme (IMplicit Pressure - Explicit Saturation) was used.
A *phase pressure fractional flow* formulation, where the pressure unknown is one of the phase pressures instead of the unphysical global pressure and the saturation equation is purely advective, was discretized applying the same methods used for the *global pressure fractional flow* formulation.

The models and methods were first discussed and compared theoretically (Ch. 3). Afterwards selected examples representing different flow characters were solved using the different models and methods.
A rough summary of the results is shown in Table 5.1. Evaluation was done with regard to accuracy and efficiency of the methods concerning the different transport processes. However, many different cases including linear as well as nonlinear constitutive relationships are combined here which partly show wide differences. A detailed evaluation and discussion was done in Chapter 4.

The results show that the *fully coupled* formulation was able to solve all the problems. For the one dimensional problems it consistently provided sufficient results concerning the accuracy

	problem type	**advective**		**diffusive**			**advective + diffusive**		
	formulation	**FC**	**FF**	**FC**	**PPFF**	**GPFF**	**FC**	**PPFF**	**GPFF**
1-D	**accuracy**	◦	++	◦	n/a	++	◦	+	++
	efficiency	+	+	+	n/a	+	+	◦	+
2-D	**accuracy**	+	◦	n/a	n/a	n/a	n/a	n/a	n/a
	efficiency	◦	◦	n/a	n/a	n/a	n/a	n/a	n/a

Table 5.1: Rough overview of the results of the investigated problems (++ (very good), + (good), ◦ (sufficient), n/a (not investigated)).

of the approximation as well as the efficiency. Contrary, for the two dimensional problem the best results could be achieved with the *fully coupled* formulation.
The *global pressure fractional flow* formulation achieved the best results with regard to both criteria accuracy and efficiency for all one dimensional problems. However, a major disadvantage of this formulation is the use of the global pressure, which is no physical quantity. As shown by *Binning* and *Celia* [2] additional iterations can be necessary to apply pressure boundary conditions given in terms of the phase pressures which are real physical quantities. This can then strongly affect the efficiency of the formulation.
Partly good results could be achieved applying the *phase pressure fractional flow* formulation. So far, however, it provides no alternative to the other formulations and their corresponding numerical methods.

Outlook

As pointed out in Chapter 3, one big advantage of both *fractional flow* formulations is the separation of the terms representing different transport processes, namely, advection and diffusion. Thus, the *global pressure fractional flow* formulation was able to provide better approximations, introducing less numerical diffusion, compared to the *fully coupled* formulation. Considering the *phase pressure fractional flow* formulation, an even more strict separation of the processes is achieved. All diffusive terms are located in the pressure equation, whereas the saturation equation is purely advective. Except for the linear case of the one dimensional *advection-diffusion* problem this advantage does not show in the results. The reason is that the equations of the *phase pressure fractional flow* formulation are stronger coupled as the equations of the *global pressure fractional flow* formulation. Thus, the IMPES scheme can not provide a sufficient convergence behaviour for the nonlinear case if the influence of the capillary pressure term becomes notable.
To further investigate the applicability of the *phase pressure fractional flow* formulation, the stronger coupling has to be accounted for. Thus, comparable to the *fully coupled* formulation, an implicit scheme linearising the system of equations using a *Newton-Raphson* iteration scheme should be applied and tested.
Second, it should be taken a closer look at the capillary pressure term. Although upwinding is only applied for the advective saturation equation, the solution of the *advection-diffusion* problem showed an influence of numerical diffusion comparable to the *fully coupled* formulation in the nonlinear case. Combining this observation with the results from the advection dominated problem, the conclusion can be made that the reason is the capillary pressure term. One first step to be done is to apply the methods used in the *global pressure fractional flow* formulation for the capillary pressure term. This means that this term should be reformulated accordingly for the *phase pressure fractional flow* formulation. Further, the saturation slope used to estimate the values at the interfaces of an element implemented for the saturation equation should also be used to estimate the saturation dependent values like the capillary pressure derivative in the pressure equation.
In a further step different discretisation methods like for example mimetic finite differences could be tested which directly model the according velocity needed for the saturation equation.
To improve the *fully coupled* formulation and decrease the numerical diffusion appearing there, especially in case of an *advection-diffusion* problem, a differencing scheme which accounts for the character of the transport process could be investigated. A *Peclet* criterion could be used

to estimate the influence of capillary diffusion in order to switch the differencing method to account for a diffusion dominated process if the influence is notable.

Concerning the mesh dependency in the two dimensional case, it was pointed out that the upwind method should be improved to account for diagonal flow. A method for vertex centred formulations is described by *Helmig* [6]. Considering the higher order finite volume method, especially the way of determining the slopes should account for the direction of the flow. This has to be further investigated to minimise numerical cross diffusion and to achieve better results with regard to mesh dependency on the direction of occurring gradients.

A Derivation of the Pressure Equation

The pressure equations of a multiphase flow system in porous media can be derived from the mass balance equation

$$\frac{\partial(\phi\rho_\alpha S_\alpha)}{\partial t} + \nabla\cdot(\rho_\alpha \mathbf{v}_\alpha) - \rho_\alpha q_\alpha = 0, \tag{A.1}$$

where ϕ is the porosity of the porous medium and ρ_α the density, S_α the saturation, $\mathbf{v}_\alpha$ the velocity, and q_α the source/sink term corresponding to fluid phase α. Division by ρ_α yields

$$\frac{1}{\rho_\alpha}\left[\frac{\partial(\phi\rho_\alpha S_\alpha)}{\partial t} + \nabla(\rho_\alpha \mathbf{v}_\alpha)\right] - q_\alpha = 0. \tag{A.2}$$

Summing up the equations of the phases α of Equation (A.2), one obtains the following equation:

$$\sum_\alpha \left\{\frac{1}{\rho_\alpha}\left[\frac{\partial(\phi\rho_\alpha S_\alpha)}{\partial t} + \nabla(\rho_\alpha \mathbf{v}_\alpha)\right] - q_\alpha\right\} = 0. \tag{A.3}$$

Applying the product rule, Equation (A.3) can be rewritten as

$$\sum_\alpha \left\{\frac{1}{\rho_\alpha}\left[\rho_\alpha S_\alpha\frac{\partial\phi}{\partial t} + \phi S_\alpha\frac{\partial\rho_\alpha}{\partial t} + \phi\rho_\alpha\frac{\partial S_\alpha}{\partial t} + \rho_\alpha\nabla\cdot\mathbf{v}_\alpha + \mathbf{v}_\alpha\cdot\nabla\rho_\alpha\right] - q_\alpha\right\} = 0. \tag{A.4}$$

From the closure relation $\sum_\alpha S_\alpha = 1$ it yields that

$$\sum_\alpha \phi\frac{\partial S_\alpha}{\partial t} = 0. \tag{A.5}$$

Thus, Equation (A.4) can be reformulated as

$$\sum_\alpha S_\alpha\frac{\partial\phi}{\partial t} + \sum_\alpha \nabla\cdot\mathbf{v}_\alpha + \sum_\alpha \frac{1}{\rho_\alpha}\left[\phi S_\alpha\frac{\partial\rho_\alpha}{\partial t} + \mathbf{v}_\alpha\cdot\nabla\rho_\alpha\right] - \sum_\alpha q_\alpha = 0. \tag{A.6}$$

Furthermore, a total velocity v_t can be defined as

$$\mathbf{v}_t = \sum_\alpha \mathbf{v}_\alpha. \tag{A.7}$$

From Equation (A.7), we have

$$\nabla\cdot\mathbf{v}_t = \nabla\cdot\sum_\alpha \mathbf{v}_\alpha = \sum_\alpha \nabla\cdot\mathbf{v}_\alpha. \tag{A.8}$$

Inserting Equation (A.8) into Equation (A.6) yields a general multiphase pressure equation

$$\sum_\alpha S_\alpha\frac{\partial\phi}{\partial t} + \nabla\cdot\mathbf{v}_t + \sum_\alpha \frac{1}{\rho_\alpha}\left[\phi S_\alpha\frac{\partial\rho_\alpha}{\partial t} + \mathbf{v}_\alpha\cdot\nabla\rho_\alpha\right] - \sum_\alpha q_\alpha = 0. \tag{A.9}$$

With the definition of the *Darcy* velocity for multiphase systems

$$\mathbf{v}_\alpha = -\frac{k_{r_\alpha}}{\mu_\alpha}\mathbf{K}(\nabla p_\alpha - \rho_\alpha \mathbf{g}), \tag{A.10}$$

where k_{r_α} is the relative permeability, $\mathbf{K}$ the fluid independent intrinsic permeability, μ_α the dynamic fluid viscosity, p_α the pressure of phase α, and $\mathbf{g}$ the gravity vector, acting in vertical direction, the total velocity can be calculated as

$$\mathbf{v}_t = \sum_\alpha \mathbf{v}_\alpha = \sum_\alpha -\frac{k_{r_\alpha}}{\mu_\alpha}\mathbf{K}(\nabla p_\alpha - \rho_\alpha \mathbf{g}). \tag{A.11}$$

Furthermore, the mobility of a phase α

$$\lambda_\alpha = \frac{k_{r_\alpha}}{\mu_\alpha} \tag{A.12}$$

and the fractional flow function corresponding to phase α

$$f_\alpha = \frac{\lambda_\alpha}{\lambda_t}, \tag{A.13}$$

where $\lambda_t = \sum_\alpha \lambda_\alpha$ is the total mobility, can be introduced. From (A.13) we have

$$\lambda_\alpha = f_\alpha \lambda_t. \tag{A.14}$$

Inserting Equations (A.12), (A.13) and (A.14) into Equation (A.11) yields

$$\mathbf{v}_t = -\lambda_t \mathbf{K}\left[\sum_\alpha f_\alpha \nabla p_\alpha - \sum_\alpha f_\alpha \rho_\alpha \mathbf{g}\right]. \tag{A.15}$$

With the formulation of the total velocity given in Equation (A.15) the pressure equation (Eq. (A.6))can be finally rewritten as

$$\begin{aligned}\sum_\alpha S_\alpha \frac{\partial \phi}{\partial t} - \nabla \cdot \left\{\lambda_t \mathbf{K}\left[\sum_\alpha f_\alpha \nabla p_\alpha - \sum_\alpha f_\alpha \rho_\alpha \mathbf{g}\right]\right\} \\ + \sum_\alpha \frac{1}{\rho_\alpha}\left[\phi S_\alpha \frac{\partial \rho_\alpha}{\partial t} + \mathbf{v}_\alpha \cdot \nabla \rho_\alpha\right] - \sum_\alpha q_\alpha = 0.\end{aligned} \tag{A.16}$$

Assuming isothermal conditions, incompressible fluids, and no mass transfer between the phases ($\rho_\alpha(\mathbf{x}, t) = const.$), and a porosity which does not change with time ($\frac{\partial \phi}{\partial t} = 0$), the derived pressure equation can be simplified to

$$\nabla \cdot \mathbf{v}_t - \sum_\alpha q_\alpha = -\nabla \cdot \left\{\lambda_t \mathbf{K}\left[\sum_\alpha f_\alpha \nabla p_\alpha - \sum_\alpha f_\alpha \rho_\alpha \mathbf{g}\right]\right\} - \sum_\alpha q_\alpha = 0. \tag{A.17}$$

B Derivation of the Peclet Number

To find a dimensionless saturation equation, the following formulation as derived in Chapter 3.2 is considered,

$$\phi \frac{\partial S_w}{\partial t} + \mathbf{v}_t \frac{d\, f_w}{d\, S_w} \nabla S_w + \nabla \cdot \left[\bar{\lambda} \mathbf{K} \frac{d\, p_c}{d\, S_w} \nabla S_w \right] = 0, \tag{B.1}$$

where gravitational effects as well as source/sink terms are neglected. We have that ϕ is the porosity of the porous medium, S_w the saturation of the wetting phase, $\mathbf{v}_t$ the total velocity, $\mathbf{K}$ the fluid independent intrinsic permeability and p_c the capillary pressure. The fractional flow function corresponding to the wetting phase f_w is defined as $f_w = \frac{\lambda_w}{\lambda_t}$, where λ_w is the mobility of the wetting phase and $\lambda_t = \lambda_w + \lambda_n$ is the total mobility. Moreover, λ_n is the mobility of the non-wetting phase, and $\bar{\lambda}$ can be calculated as $\bar{\lambda} = f_w \lambda_n$.

Using a characteristic length x_{ch}, a characteristic velocity v_{ch}, and a characteristic density ρ_{ch}, the following dimensionless quantities are defined:

$$\begin{aligned}
\mathbf{V}_t &= \frac{\mathbf{v}_t}{v_{ch}} && \Rightarrow && \mathbf{v}_t = \mathbf{V}_t\, v_{ch} \\
T &= \frac{t\, v_{ch}}{x_{ch}} && \Rightarrow && t = \frac{T\, x_{ch}}{v_{ch}} \\
X &= \frac{x}{x_{ch}} && \Rightarrow && x = X\, x_{ch} \\
P_c &= \frac{p_c}{\rho_{ch}\, v_{ch}^2} && \Rightarrow && p_c = P_c\, \rho_{ch}\, v_{ch}^2 \\
\bar{\Lambda} &= \bar{\lambda}\, \rho_{ch}\, v_{ch}\, x_{ch} && \Rightarrow && \bar{\lambda} = \frac{\bar{\Lambda}}{\rho_{ch}\, v_{ch}\, x_{ch}}
\end{aligned} \tag{B.2}$$

Inserting Equation (B.2) into Equation (B.1) yields the following dimensionless saturation equation

$$\frac{v_{ch}}{x_{ch}} \phi \frac{\partial S_w}{\partial T} + \frac{v_{ch}}{x_{ch}} \mathbf{V}_t \frac{d\, f_w}{d\, S_w} \nabla S_w + \frac{v_{ch}}{x_{ch}^3} \nabla \cdot \left[\bar{\Lambda} \mathbf{K} \frac{d\, P_c}{d\, S_w} \nabla S_w \right] = 0, \tag{B.3}$$

which can be further rewritten as

$$\underbrace{\phi \frac{\partial S_w}{\partial T}}_{\text{accumulation term}} + \underbrace{\mathbf{V}_t \frac{d\, f_w}{d\, S_w} \nabla S_w}_{\text{advective term}} + \underbrace{\frac{1}{x_{ch}^2} \nabla \cdot \left[\bar{\Lambda} \mathbf{K} \frac{d\, P_c}{d\, S_w} \nabla S_w \right]}_{\text{diffusive term}} = 0. \tag{B.4}$$

A *Peclet* number relates the influence of advective processes to the influence of diffusive processes. Thus, from Equation (B.4) a *Peclet* number can be defined as

$$Pe = \frac{\mathbf{V}_t \frac{d\, f_w}{d\, S_w}}{\frac{1}{x_{ch}^2} \bar{\Lambda} \mathbf{K} \frac{d\, P_c}{d\, S_w}}. \tag{B.5}$$

Inserting Equation (B.2) again yields

$$Pe = \frac{\mathbf{v}_t \frac{d\, f_w}{d\, S_w} x_{ch}}{\bar{\lambda} \mathbf{K} \frac{d\, p_c}{d\, S_w}}. \tag{B.6}$$

Here, the discretisation length Δx is chosen to be the characteristic length. Thus, a grid dependent *Peclet* number can finally be calculated as

$$Pe = \frac{\mathbf{v}_t \frac{d f_w}{d S_w} \Delta x}{\bar{\lambda} \mathbf{K} \frac{d p_c}{d S_w}}. \tag{B.7}$$

Bibliography

[1] P. Bastian. *Numerical Computation of Multiphase FLows in Porous Media.* Habilitation. Christian-Albrechts-Universität Kiel, 1999.

[2] P. Binning and M. A. Celia. Practical implementation of the fractional flow approach to multi-phase flow simulation. *Advances in Water Resources*, Vol. 22(5):461–478, 1999.

[3] S. E. Buckley and M. C. Leverett. Mechanism of fluid displacement in sands. *Transactions of the AIME*, Vol. 146:107 – 116, 1942.

[4] Robert Eymard, Thierry Gallouët, and Raphaèle Herbin. Finite volume methods. In *Handbook of numerical analysis, Vol. VII*, pages 713–1020. North-Holland, Amsterdam, 2000.

[5] R. Fucíka, J. Mikyskaa, M. Benesa, and T. H. Illangasekareb. An improved semi-analytical solution for verification of numerical models of two-phase flow in porous media. *Vadose Zone Journal*, Vol. 6:93–104, 2007.

[6] R. Helmig. *Multiphase Flow and Transport Processes in the Subsurface.* Springer, 1997.

[7] H. Hoteit and A. Firoozabadi. Numerical modeling of two-phase flow in heterogenous permeable media with different capillarity pressures. *to appear in Advances in Water Resources.*

[8] http://www.dune-project.de. *DUNE-website.*

[9] D. B. McWhorter and D. K. Sunada. Exact integral solution for two-phase flow. *Water Resources Research*, Vol. 26(3):399–413, 1990.

[10] A. Scheidegger. The physics of flow through porous media. In *University of Toronto Press.* Toronto and Buffalo, 3rd edition, 1974.

Published Preprints

http://www.nupus.uni-stuttgart.de/publications

2007/1 Cao, Y. / Eikemo, B. / Helmig, R.: Fractional Flow Formulation for Two-phase Flow in Porous Media

2008/1 Helmig, R. / Weiss, A. / Wohlmuth, B.: Variational inequalities for modeling flow in heterogeneous porous media with entry pressure

2008/2 Cao, Y. / Helmig, R. / Wohlmuth, B.: Convergence study and comparison of the multipoint flux approximation L-method

2008/3 van Duijn, C.J. / Pop, I.S. / Niessner, J. / Hassanizadeh, S.M.: Philip’s redistribution problem revisited: the role of fluid-fluid interfacial areas

2008/4 Niessner, J. / Hassanizadeh, S.M.: Modeling kinetic interphase mass transfer for two-phase flow in porous media including fluid–fluid interfacial area

2008/5 Niessner, J. / Hassanizadeh, S.M.: A Model for Two-Phase Flow in Porous Media Including Fluid–Fluid Interfacial Area

2008/6 Cao, Y. / Helmig, R. / Wohlmuth, B.: Geometrical interpretation of the multipoint flux approximation L-method

2008/7 Vervoort, R.W. / van der Zee, S.E.A.T.M.: Simulating the effect of capillary flux on the soil water balance in a stochastic ecohydrological framework

2008/8 Niessner, J. / Hassanizadeh, S.M.: Two-phase flow and transport in porous media including fluid–fluid interfacial area

2008/9 Haslauer, C.P. / Bárdossy, A, / Sudicky, E.A.: Geostatistical Analysis of Hydraulic Conductivity Fields Using Copulas

2008/10 Wolff, M.: Comparison of Mathematical and Numerical Models for Twophase Flow in Porous Media